

[illegible]

UNLIMITED DISTRIBUTION



National Defence
Research and
Development Branch

Défense nationale
Bureau de recherche
et développement

DREA CR/95/406

STRETCH ZONE WIDTH MEASUREMENT OF SIDE-GROOVED HSLA 80 FRACTURE SPECIMENS

by
K. MacKay - M.W. Chernuka

MARTEC LIMITED
1888 Brunswick Street, Suite 400
Halifax, Nova Scotia, Canada
B3J 3J8

CONTRACTOR REPORT

Prepared for

Defence
Research
Establishment
Atlantic



Centre de
Recherches pour la
Défense
Atlantique

Canada

THIS IS AN UNEDITED REPORT ON SCIENTIFIC OR TECHNICAL WORK
CONTRACTED BY THE DEFENCE RESEARCH ESTABLISHMENT ATLANTIC OF
THE RESEARCH AND DEVELOPMENT BRANCH OF THE DEPARTMENT OF
NATIONAL DEFENCE, CANADA.

THE CONTENTS OF THE REPORT ARE THE RESPONSIBILITY OF THE
CONTRACTOR, AND DO NOT NECESSARILY REFLECT THE OFFICIAL POLICIES
OF THE DEPARTMENT OF NATIONAL DEFENCE.

PLEASE DIRECT ENQUIRIES TO:

THE CHIEF,
DEFENCE RESEARCH ESTABLISHMENT ATLANTIC,
P.O. BOX 1012,
DARTMOUTH, NOVA SCOTIA, CANADA
B2Y 3Z7



National Defence
Research and
Development Branch

Défense nationale
Bureau de recherche
et développement

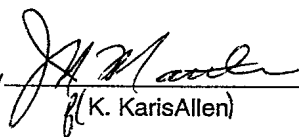
DREA CR/95/406

STRETCH ZONE WIDTH MEASUREMENT OF SIDE-GROOVED HSLA 80 FRACTURE SPECIMENS

by
K. MacKay - M.W. Chernuka

MARTEC LIMITED
1888 Brunswick Street, Suite 400
Halifax, Nova Scotia, Canada
B3J 3J8

Scientific Authority


(K. KarisAllen)

October 1994

W7707-4-2878/01-OSC
Contract Number

CONTRACTOR REPORT

Prepared for

Defence
Research
Establishment
Atlantic



Centre de
Recherches pour la
Défense
Atlantique



TABLE OF CONTENTS

Abstract
List of Tables
List of Figures

1. INTRODUCTION 1.1

2. EXPERIMENTAL PROCEDURE 2.1

3. RESULTS AND DISCUSSION 3.1

 3.1 Stretch Zone Width Measurement Errors 3.1

 3.2 Stretch Zone Width Variability 3.1

 3.3 Stretch Zone Width Variation with Temperature 3.2

 3.4 Stretch Zone Width Variation with Loading Rate 3.2

4. CONCLUSIONS 4.1

REFERENCES

APPENDIX A: SEM MICROGRAPHS OF STRETCH ZONES

LIST OF TABLES

TABLE 3.1: Summary of SZW Measurements

LIST OF FIGURES

FIGURE 1.1: Model of a stretch zone.

FIGURE 1.2: The relationship between J and stretch zone width.

FIGURE 2.1: Location of stretch zone width measurements made on the fracture surfaces.

FIGURE 3.1: Stretch zone width variation along the crack front for specimen 10 which exhibited ductile tearing after the stretch zone.

FIGURE 3.2: Stretch zone width variation along the crack front for specimen 13 which exhibited ductile tearing after the stretch zone.

FIGURE 3.3: Stretch zone width variation along the crack front for specimen 15 which exhibited ductile tearing after the stretch zone.

FIGURE 3.4: Stretch zone width variation along the crack front for specimen 25 which exhibited ductile tearing after the stretch zone.

FIGURE 3.5: Stretch zone width variation along the crack front for specimen 26 which exhibited ductile tearing after the stretch zone.

FIGURE 3.6: Stretch zone width variation along the crack front for specimen 3 which exhibited ductile tearing after the stretch zone.

FIGURE 3.7: Stretch zone width variation along the crack front for specimen 16 which exhibited cleavage fracture after the stretch zone.

FIGURE 3.8: Stretch zone width variation along the crack front for specimen 2 which exhibited cleavage fracture after the stretch zone.

FIGURE 3.9: Stretch zone width variation along the crack front for specimen 27 which exhibited cleavage fracture after the stretch zone.

FIGURE 3.10: Stretch zone width variation along the crack front for specimen 31 which exhibited cleavage fracture after the stretch zone.

FIGURE 3.11: Stretch zone width variation along the crack front for specimen 32 which exhibited cleavage fracture after the stretch zone.

FIGURE 3.12: Stretch zone width variation along the crack front for specimen 33 which exhibited cleavage fracture after the stretch zone.

FIGURE 3.13: SEM micrographs of fracture surfaces showing
a) ductile tearing after the stretch zone
b) cleavage fracture after the stretch zone.

FIGURE 3.14: Stretch zone width variation with temperature for specimens tested with a 0.02 mm/s crosshead rate.

FIGURE 3.15: Stretch zone width variation with temperature for specimens tested with a 0.2 mm/s crosshead rate.

FIGURE 3.16: Stretch zone width variation with temperature for specimens tested with a 1.75 mm/s crosshead rate.

FIGURE 3.17: Stretch zone width variation with temperature for specimens tested with 2 mm/s crosshead rate.

LIST OF FIGURES - Continued

- FIGURE 3.18: Stretch zone width variation with temperature for specimens tested with a 2710 mm/s crosshead rate.
- FIGURE 3.19: Stretch zone width variation with loading rate for specimens tested between -32°C and -30°C .
- FIGURE 3.20: Stretch zone width variation with loading rate for specimens tested between -22°C and -20°C .
- FIGURE 3.21: Stretch zone width variation with loading rate for specimens tested at -15°C .
- FIGURE 3.22: Stretch zone width variation with loading rate for specimens tested at -10°C .
- FIGURE 3.23: Stretch zone width variation with loading rate for specimens tested between -5°C and 22°C .

ABSTRACT

Stereoscopic imaging with a scanning electron microscope was used to measure stretch zone width on the fracture surfaces of side grooved HSLA 80 SENB fracture specimens which were tested over a range of temperatures (-42°C to 22°C) and loading rates (0.01 to 2710 mm/s). The data were examined to determine the relationship between stretch zone width and temperature at constant loading rate, and the relationship between stretch zone width and loading rate at constant temperature. Measurement error, the limited number of data points, and intrinsic variability collectively limit the confidence with which trends could be determined. For loading rates below 2 mm/s, the stretch zone width increased with temperature until a limiting temperature of -20°C was reached. Beyond this temperature the variation in stretch zone was less than the measurement error. At a loading rate of 2710 mm/s, the stretch zone width appeared to increase linearly with temperature over the range of -5°C to 15°C . The variation in stretch zone width with loading rate was less than the measurement error over the range of 0.01 to 60 mm/s. There appeared to be a decrease in stretch zone width when the loading rate was increased to 2710 mm/s. For specimens which exhibited stable crack growth after blunting, the stretch zone width was greater in the central region of the specimen than at the edges. For specimens which exhibited unstable (brittle) crack extension immediately after the stretch zone, the stretch zone width was essentially uniform across the specimen.

RÉSUMÉ

On a utilisé l'imagerie stéréoscopique avec un microscope électronique à balayage pour mesurer la largeur de la zone d'allongement sur les surfaces de rupture d'éprouvettes d'acier haute résistance faiblement allié (HSLA) 80 SENB qui ont été testées sur une plage de températures (-42°C à 22°C) et de vitesses de chargement (0,01 à 2710 mm/s). On a examiné les données afin de déterminer la relation entre la largeur de la zone d'allongement et la température à vitesse de chargement constante, et la relation entre la largeur de la zone d'allongement et la vitesse de chargement à température constante. Les erreurs de mesure, le nombre limité de points de données et la variabilité intrinsèque contribuent ensemble à limiter le degré de confiance avec lequel les tendances pourraient être déterminées. Aux vitesses de chargement inférieures à 2 mm/s, la largeur de la zone d'allongement augmentait avec la température jusqu'à de cette température limite de -20°C soit atteinte. Au-delà de cette température, la variation de largeur de la zone d'allongement était moins importante que l'erreur sur la mesure. À une vitesse de chargement de 2710 mm/s, la largeur de la zone d'allongement semblait augmenter de façon linéaire en fonction de la température sur la plage de -5°C à 15°C . La variation de la largeur de la zone d'allongement en fonction de la vitesse de chargement était moins importante que l'erreur sur la mesure sur la plage de 0,01 à 60 mm/s. Il semblait se produire une réduction de la largeur de la zone d'allongement lorsque la vitesse de chargement était augmentée jusqu'à 2710 mm/s. Dans les cas des éprouvettes qui présentaient une propagation stable des fissures après émoussement, la largeur de la zone d'allongement était plus grande dans la région centrale de l'éprouvette que sur les bords. Dans le cas des éprouvettes qui présentaient une propagation instable (fragile) des fissures immédiatement après la zone d'allongement, la largeur de la zone d'allongement était à toute fin pratique uniforme sur toute la largeur de l'éprouvette.

1. INTRODUCTION

A series of fracture toughness tests was conducted on side-grooved HSLA 80 steel SENB specimens using a range of test temperatures and loading rates. This report describes the stretch zones found on the fracture surfaces of these specimens, identifies the critical CTOD and J values which were determined from stretch zone width measurements, and identifies trends in toughness data with respect to test temperature and loading rate.

The fracture toughness of a material can be determined based on the measurement of a fracture surface feature called the stretch zone. A stretch zone is formed during crack tip blunting from deformed grains that were originally part of the fatigue surface [1]. A model of a stretch zone is sketched in Figure 1.1 [2]. The stretch zone can be identified on a fracture surface as the region on the fatigue surface between the points where yielding initiates and stable tearing initiates. Figure 1.2 shows the relationship between the J integral and stretch zone width. Since the stretch zone is fully formed at the initiation of tearing, the critical J and COD values can be determined by stretch zone width. For plane strain conditions, J_c can be calculated from stretch zone width using the following [3]:

$$J_c = 2m \sigma_y \text{SZW} \quad (1.1)$$

where σ_y is the flow stress (equal to the average of the yield stress and the ultimate tensile strength), SZW is the average stretch zone width, and m is a factor between one and two.. For SENB fracture specimens with $a/W = 0.5$, the value of m is approximately two.

From the model depicted in Figure 1.1, the critical plastic crack tip opening displacement (CTOD_{cp}) is simply twice the stretch zone width:

$$\text{CTOD}_{cp} = 2 \text{SZW} \quad (1.2)$$

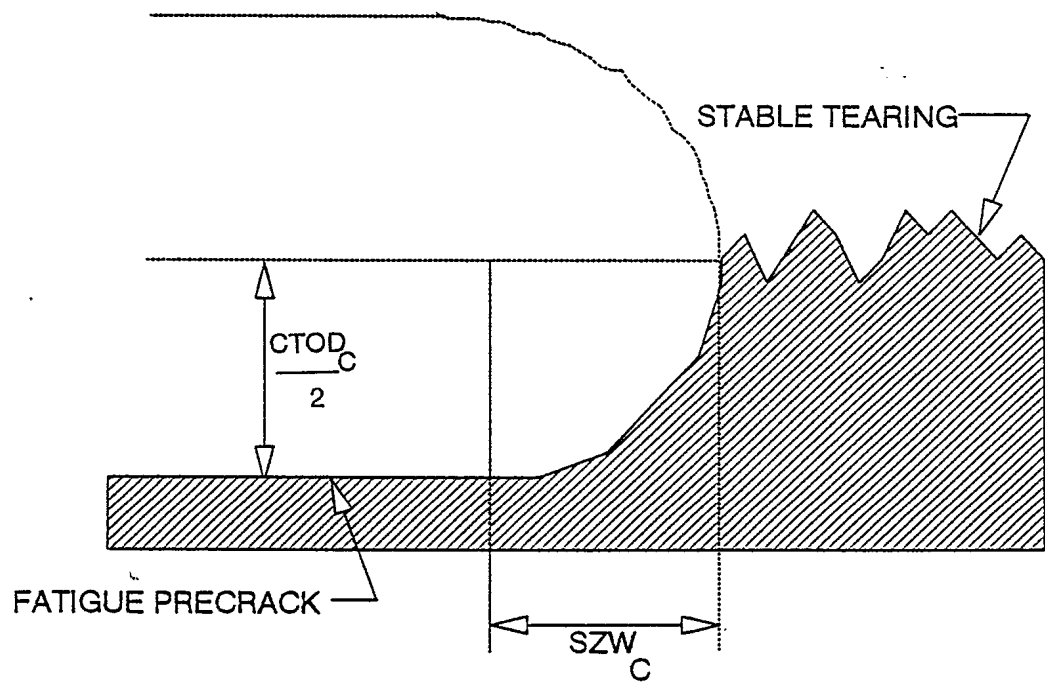


FIGURE 1.1: Model of a stretch zone.

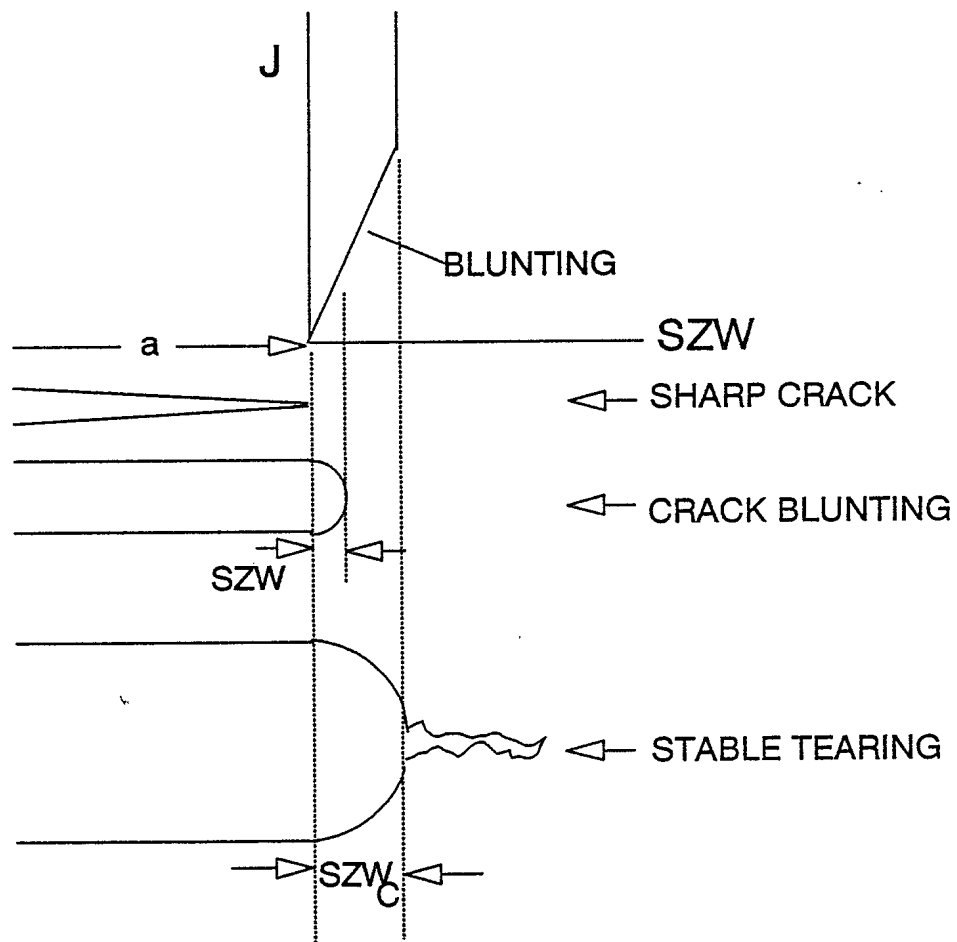


FIGURE 1.2: The relationship between J and stretch zone width.

2. EXPERIMENTAL PROCEDURE

The fracture surfaces were cleaned in order to remove rust and other debris. Replica stripping was used to remove most of the rust and debris from the fracture surfaces. Cellulose acetate tape was softened in acetone for six seconds and then applied to the fracture surface. The tape was allowed to dry for 10 minutes and was then peeled off. This was repeated until debris was no longer picked up by the tape. In instances where some tape may have remained on the fracture surface, the specimens were cleaned in acetone with the aid of an ultrasonic bath.

Examination of the stretch zones on the fracture surfaces were made using a scanning electron microscope. Stretch zone width measurements were made at four positions along the fatigue crack front as shown in Figure 2.1. The two outside measurements were taken 0.005 W (0.25 mm) from the side grooves and the two central measurements were taken at 2.5 mm from the centre (the two central positions correspond to positions four and six using the ASTM E813 nine point crack length measurement system). Stereoscopic images were taken of the stretch zone at each of these four positions. This was accomplished by taking SEM images of the stretch zone at -6° , $+6^\circ$ and 0° relative to a plane normal to the incident electron beam. The stretch zone was oriented so that it was parallel to the tilt axis of the SEM stage. The first image was focused by adjusting the lens current of the SEM which is normal operating procedure. The other two images taken at the same location were focused by adjusting the height of the specimen stage. This ensured that the three images were taken at the same magnification [4]. Projection distortions were minimized by using magnifications in excess of 100 times, where projection distortion is negligible, and by placing the stretch zone on the optic axis, where projection distortion is the smallest [4]. The stretch zone images were examined using a mirror stereoscope with the image taken at -6° placed on the left and the image taken at $+6^\circ$ placed on the right. The stereoscope presents a three-dimensional image of the stretch zone which allows the beginning and end of the stretch zone to be identified on the image taken at 0° . Once the limits of the stretch zone are identified, 10 equally spaced stretch zone width measurements are made across the image taken at 0 degrees. Since the images were recorded at the four positions described above, 40 stretch zone width measurements were made on each specimen.

Blank

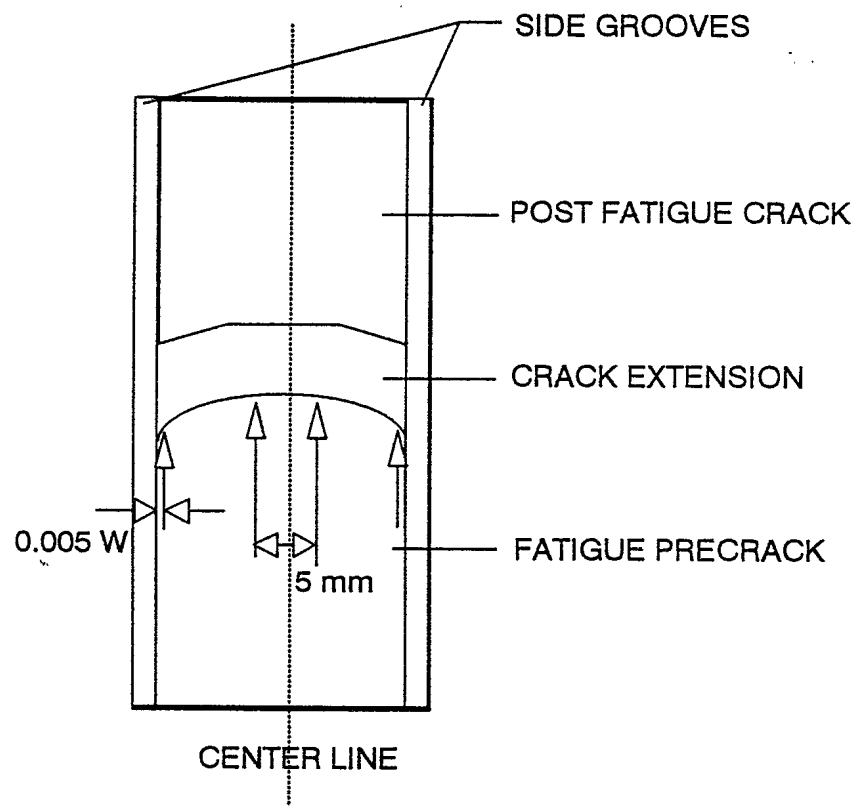


FIGURE 2.1: Location of stretch zone width measurements made on the fracture surfaces.

Blank

3. RESULTS AND DISCUSSION

A summary of the results are given in Table 3.1 including the calculated values of J_c and $CTOD_{cp}$ from SZW. J_c and $CTOD_{cp}$ were calculated from average SZW using Equations 1.1 and 1.2, respectively.

3.1 Stretch Zone Width Measurement Errors

Systematic errors in stretch zone width measurement are insignificant except for SEM magnification error which was determined to be $\pm 5\%$ based on a standard grid. The magnification error is expected to be the same for all measurements. In addition to the systematic errors, there is also some uncertainty in the stretch zone width measurements because of the difficulty in determining where the stretch zone begins and ends. The error in stretch zone width from all causes was estimated to be less than 20% of the average stretch zone width.

3.2 Stretch Zone Width Variability

The stretch zones exhibited two types of intrinsic variability. The first type comes from the variation in stretch zone width in each image. The variation of the 10 points measured across an image resulted in a standard deviation that was less than 25% of the local average for the majority of the images. However, several positions showed standard deviations as high as 34% to 37%. The bars shown in Figures 3.1 through 3.12 indicate the minimum and maximum stretch zone width for the 10 points measured on each image. The second type of intrinsic variability comes from stretch zone width variation across the fatigue crack front. For specimens that exhibited stable tearing after blunting, the stretch zone width is greater in the centre of the specimen than at the edges. Figures 3.1 through 3.6 show typical curves of stretch zone width measured along the fatigue crack front for specimens tested at a variety of temperatures and loading rates. For specimens that exhibited unstable (brittle) crack extension after blunting (specimens 2, 16, 27, 31, 32, 33), the stretch zone width is essentially uniform across the fatigue crack front. Figures 3.7 through 3.12 show the stretch zone width measured along the fatigue crack front for the specimens which underwent unstable crack extension. Figure 3.13 shows SEM micrographs of specimens which show stable crack growth after the stretch zone and

3.2

unstable crack extension after the stretch zone. Appendix A contains SEM micrographs of the stretch zones from all the fracture surfaces examined.

3.3 Stretch Zone Width Variation with Temperature

Figures 3.14 through 3.18 show the variation in stretch zone width with temperature for a variety of loading rates. The bars in these figures indicate the minimum and maximum stretch zone width measured on the fracture surface. For the lowest loading rate (0.02 mm/s), the variation in stretch zone width between each temperature is less than the measurement error. For the lower loading rates, there is a general increase in fracture toughness with temperature until a limiting temperature is reached at approximately -20°C . Above this temperature limit, the variation in stretch zone width is less than the measurement error. This trend can be explained by the test temperature passing from the materials transition temperature range to the upper shelf temperature range. However, as the loading rate increases, the relationship between stretch zone width and temperature appears to become linear. Figure 3.18 shows that stretch zone width increases linearly with temperature at a loading rates of 2710 mm/s. It should be noted that the difference in stretch zone width between each temperature in Figure 3.18 is greater than the measurement error. It is difficult to tell whether this trend is real (or an artifact of the measurement error/scatter) due to the measurement error and the limited number of data points for the higher loading rate.

3.4 Stretch Zone Width Variation with Loading Rate

Figures 3.19 through 3.23 show the variation in stretch zone width with loading rate for a given temperature range. The temperature ranges are kept small (1 to 2°C) for the colder temperatures. The specimens tested above -5°C are plotted together as the material is then well into the upper shelf temperature range for static loading rates as discussed earlier. For the specimens tested at or below -5°C , the variation in stretch zone width with loading rate is less than the measurement error. However, the loading rates used at these colder temperatures did not exceed 60 mm/s. For the specimens tested above -5°C , the difference in stretch zone width for specimens below 60 mm/s and those at 2710 mm/s is greater than the measurement errors/scatter in stretch zone width. Thus, there appears to be a small decrease in stretch zone width for loading rates of 2710 mm/s for these

specimens. It should be noted that the three specimens loaded at 2710 mm/s exhibited unstable crack extension after stretch zone formation.

3.4

TABLE 3.1: Summary of SZW Measurements							
Specimen Number	Average SZW	Minimum SZW	Maximum SZW	Temperature (°C)	Crosshead Rate (m/s)	J _c (kJ/m ²)	CTOD _c μm
1	158	73	309	-42	0.02	593	316
2	71	32	95	-30	0.2	266	141
3	198	88	369	-30	0.02	746	397
4	223	115	359	-20	0.2	839	446
5	187	70	275	-20	0.02	701	373
6	205	67	460	-20	0.02	770	410
7	225	96	440	-10	0.2	844	449
8	245	120	368	-10	2	919	489
9	182	103	266	-10	20	683	364
10	184	102	319	-15	2	690	367
11	188	42	431	1	20	706	376
12	232	109	331	-15	0.2	873	465
13	226	141	285	1	60	848	451
14	221	85	386	-15	0.2	830	442
15	183	66	350	-15	0.02	686	365
16	104	57	138	-22	2	392	209
20	208	76	370	-32	0.04	781	416
21	178	104	271	-32	0.175	670	357
22	158	74	291	-31	1.75	594	316
23	191	89	358	-22	0.4	718	382
24	157	63	236	-20	1.75	590	314
25	169	66	342	22	0.01	634	338
26	156	109	216	-30	17.5	584	311
27	29	3	61	-41	1.75	109	58
31	73	55	107	-5	2710	273	145
32	148	83	199	15	2710	557	297
33	111	68	149	5	2710	415	221

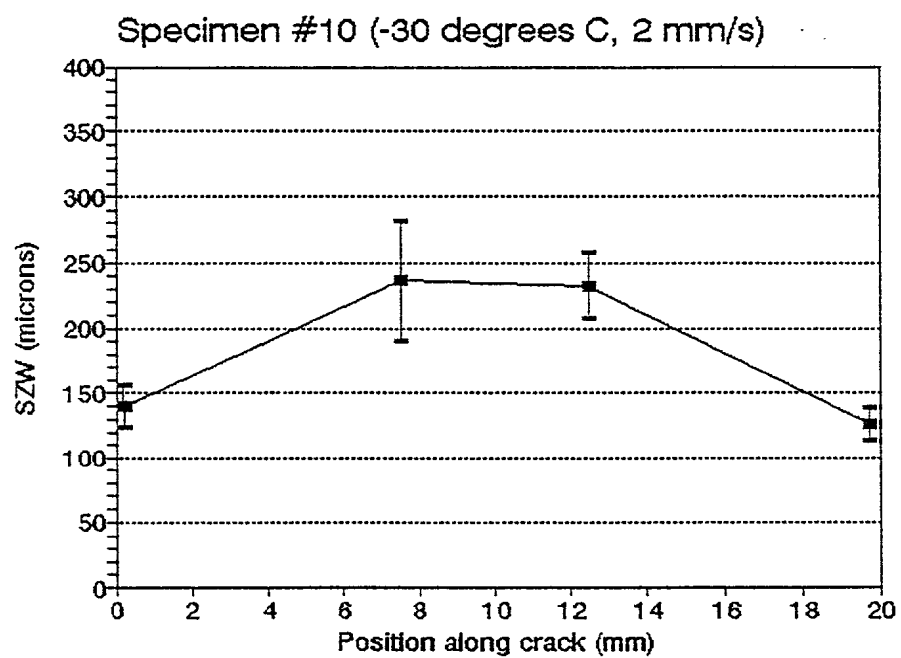


FIGURE 3.1: Stretch zone width variation along the crack front for specimen 10 which exhibited ductile tearing after the stretch zone.

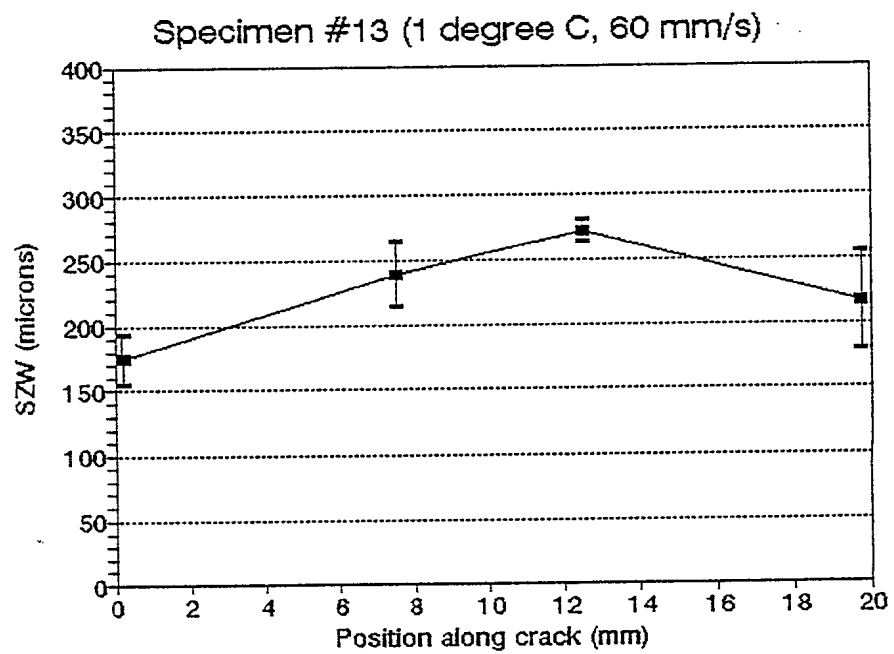


FIGURE 3.2: Stretch zone width variation along the crack front for specimen 13 which exhibited ductile tearing after the stretch zone.

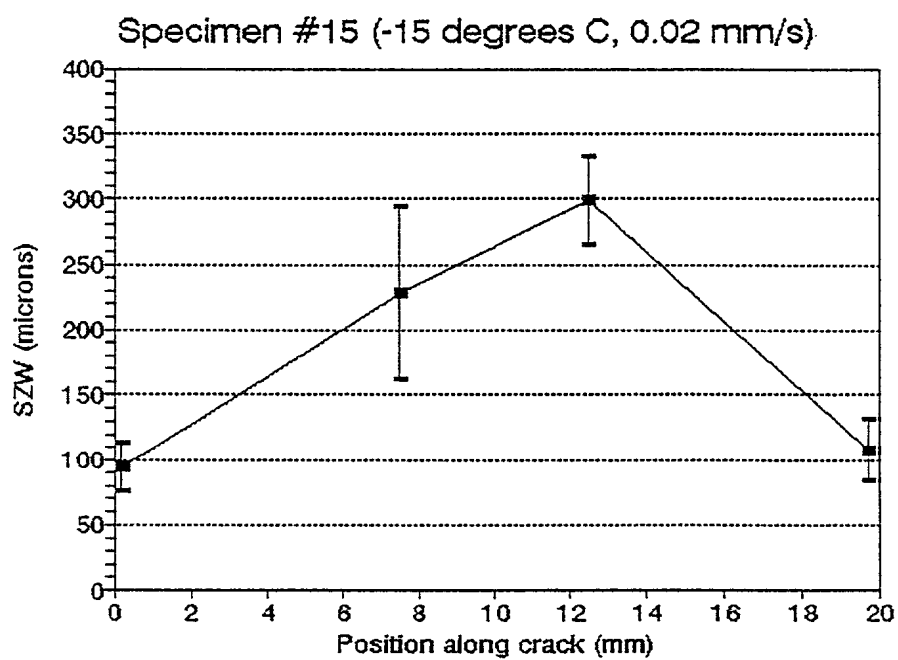


FIGURE 3.3: Stretch zone width variation along the crack front for specimen 15 which exhibited ductile tearing after the stretch zone.

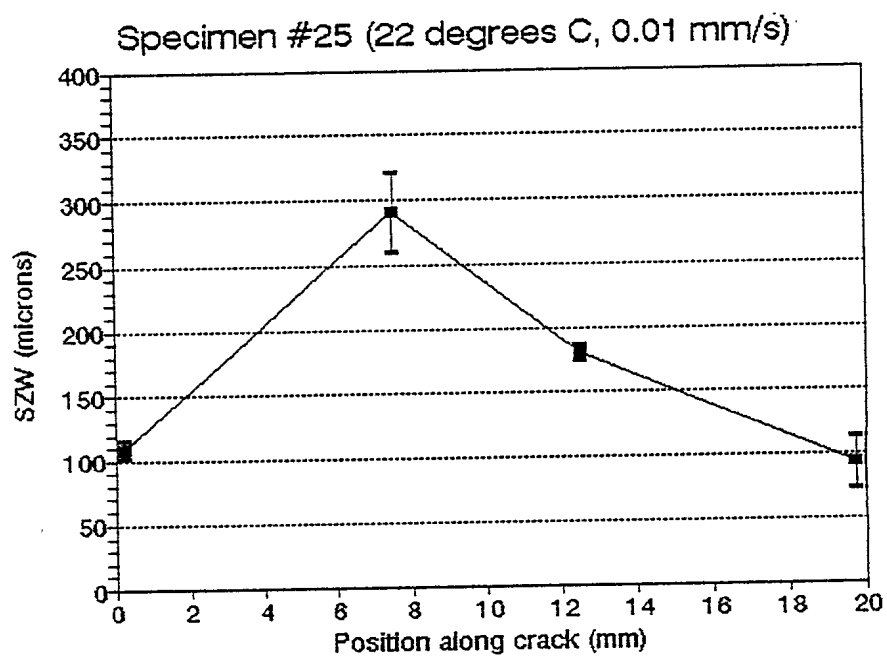


FIGURE 3.4: Stretch zone width variation along the crack front for specimen 25 which exhibited ductile tearing after the stretch zone.

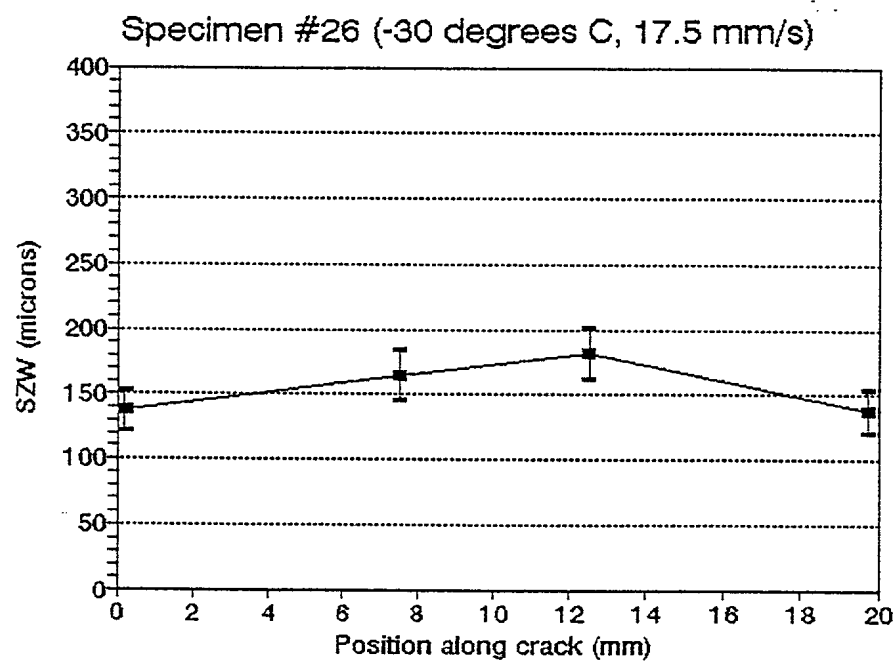


FIGURE 3.5: Stretch zone width variation along the crack front for specimen 26 which exhibited ductile tearing after the stretch zone.

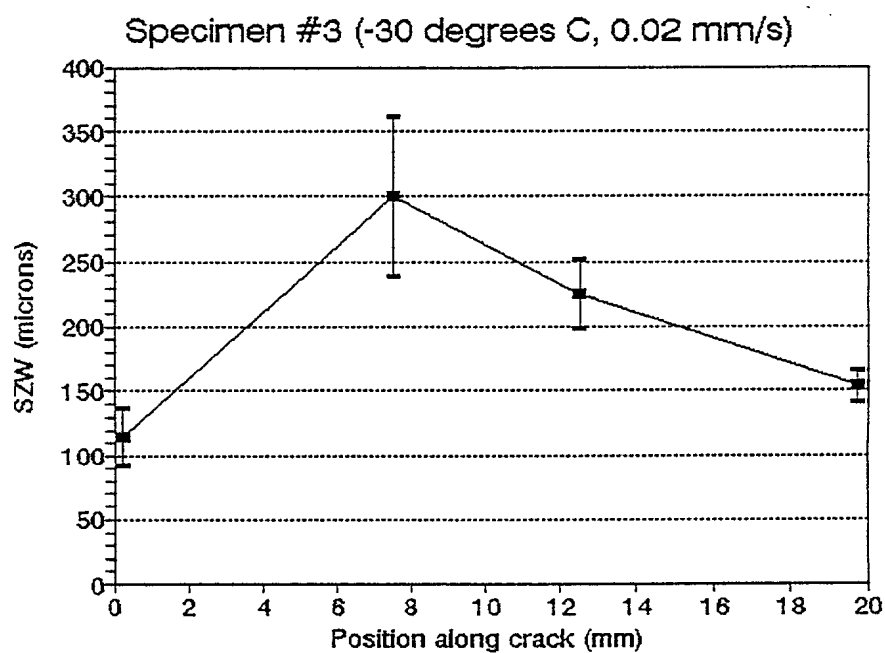


FIGURE 3.6: Stretch zone width variation along the crack front for specimen 3 which exhibited ductile tearing after the stretch zone.

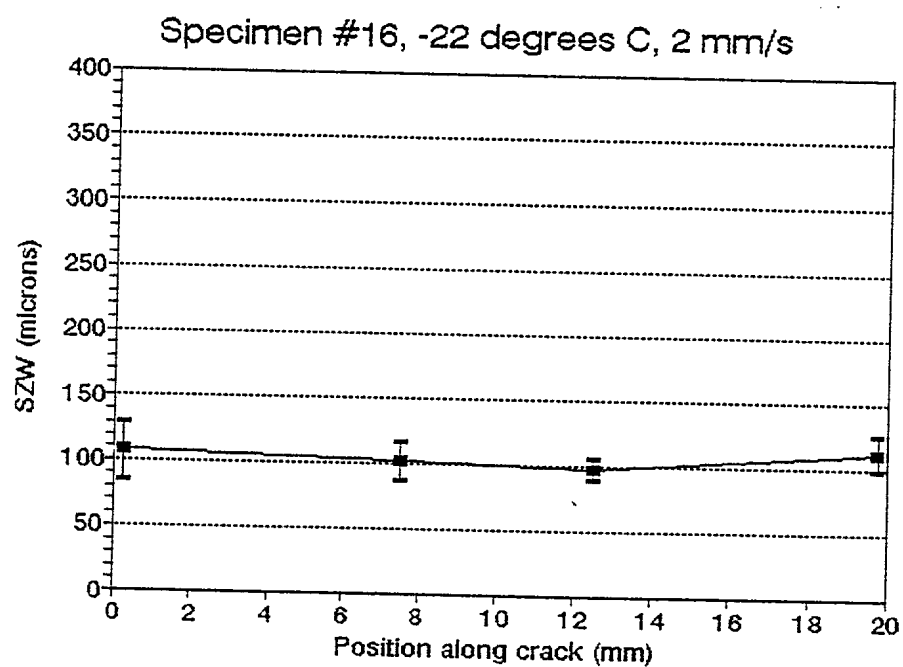


FIGURE 3.7: Stretch zone width variation along the crack front for specimen 16 which exhibited cleavage fracture after the stretch zone.

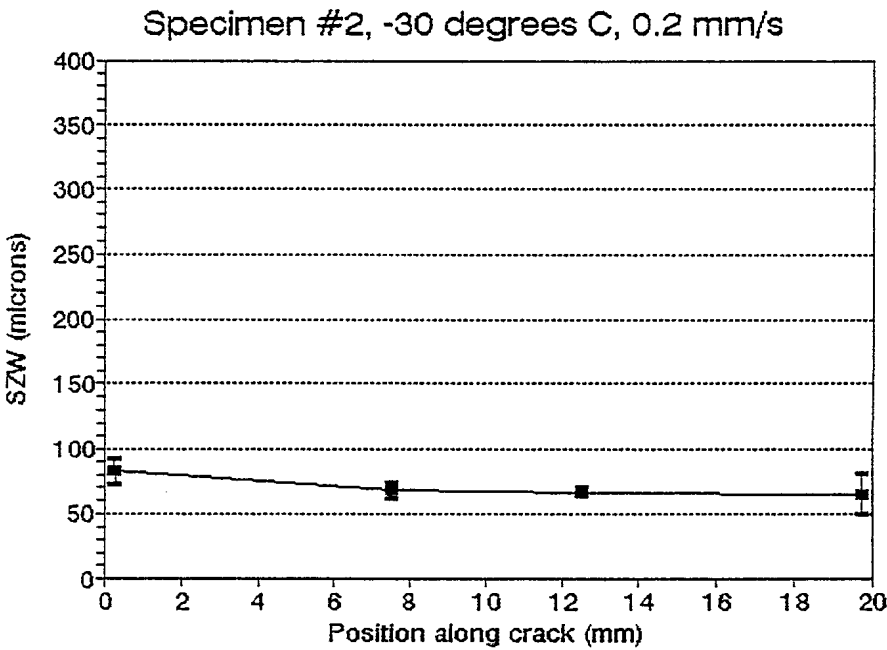


FIGURE 3.8: Stretch zone width variation along the crack front for specimen 2 which exhibited cleavage fracture after the stretch zone.

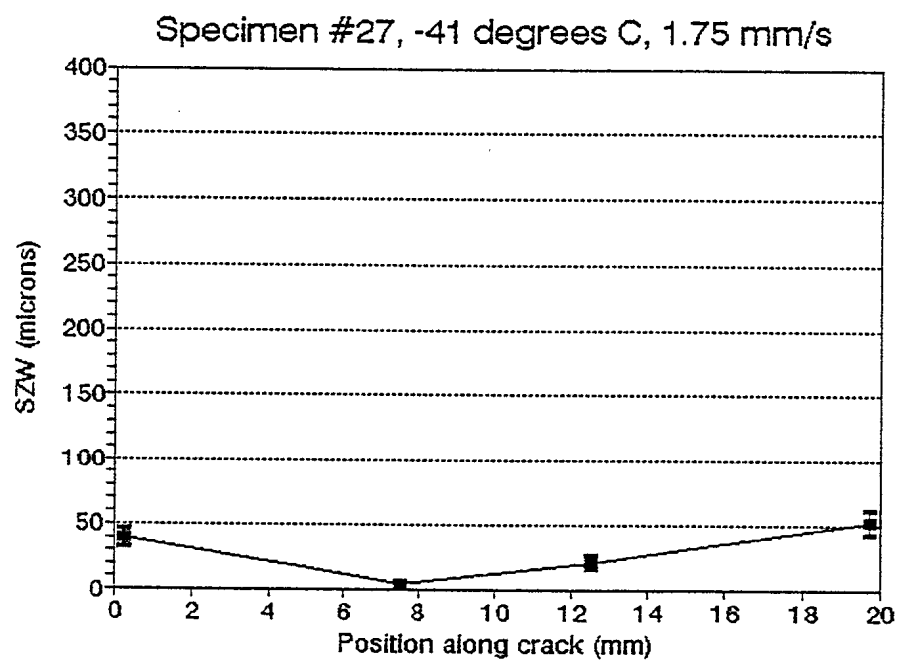


FIGURE 3.9: Stretch zone width variation along the crack front for specimen 27 which exhibited cleavage fracture after the stretch zone.

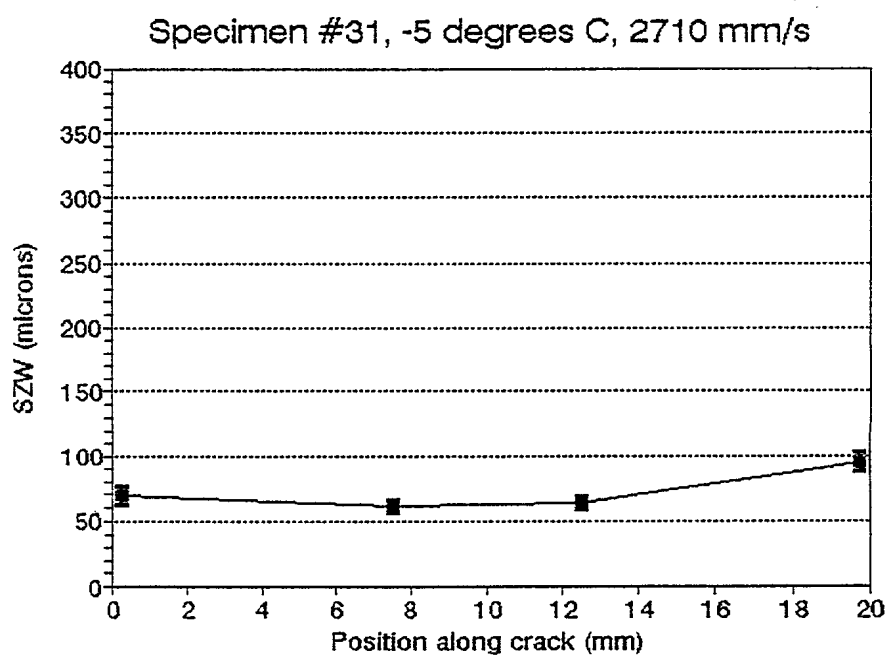


FIGURE 3.10: Stretch zone width variation along the crack front for specimen 31 which exhibited cleavage fracture after the stretch zone.

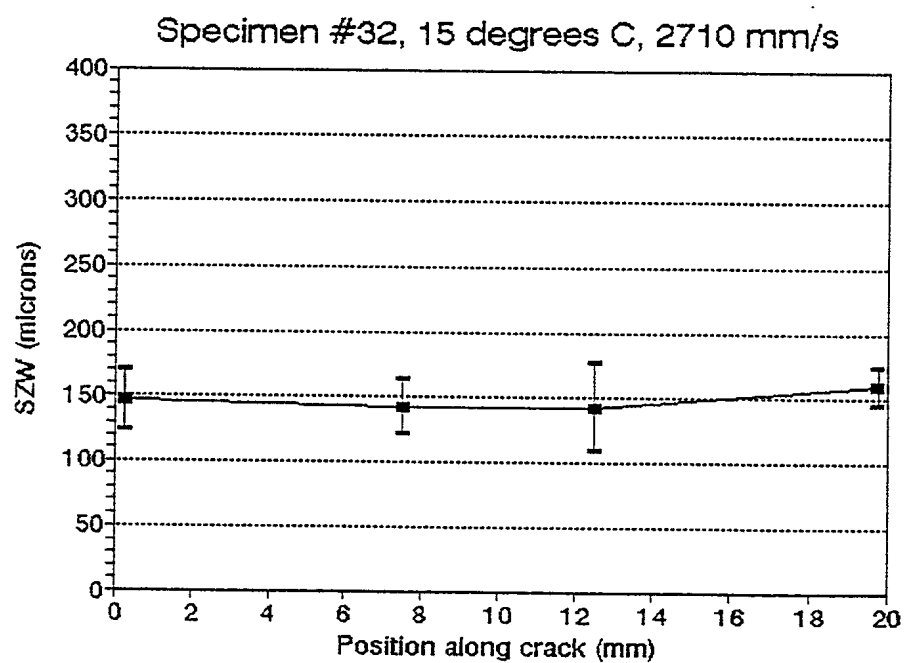


FIGURE 3.11: Stretch zone width variation along the crack front for specimen 32 which exhibited cleavage fracture after the stretch zone.

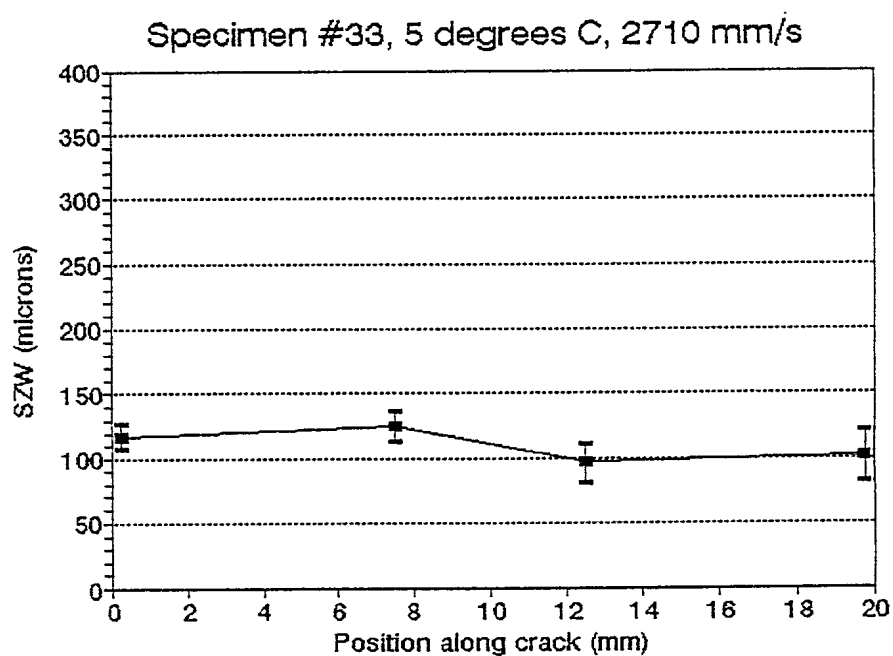


FIGURE 3.12: Stretch zone width variation along the crack front for specimen 33 which exhibited cleavage fracture after the stretch zone.

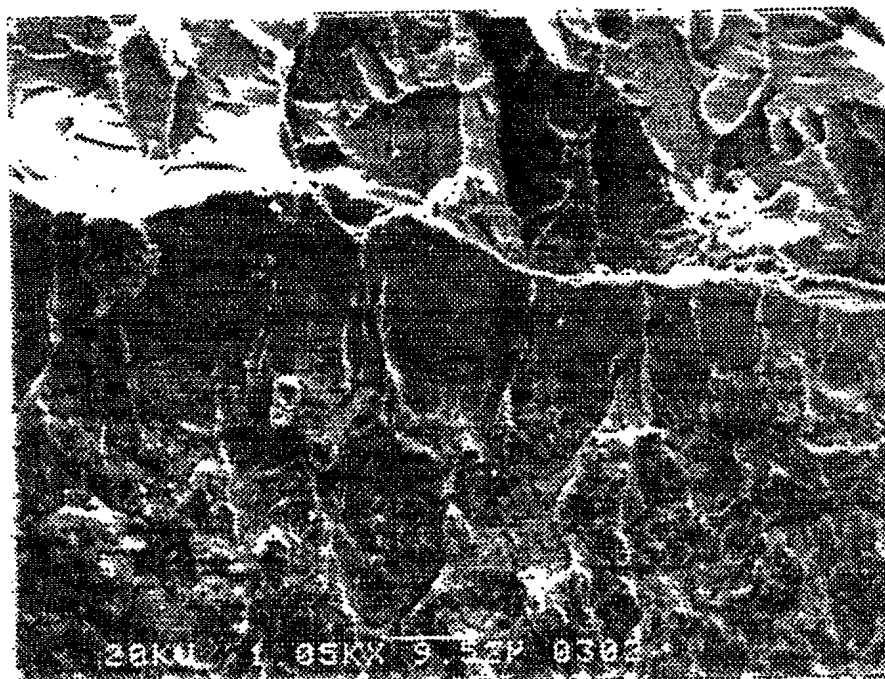
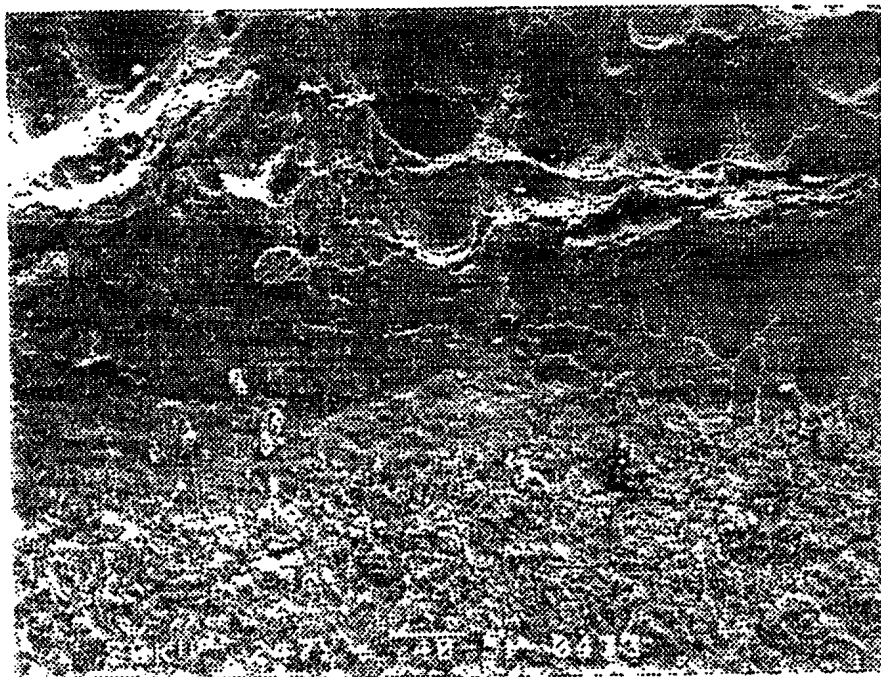


FIGURE 3.13: SEM micrographs of fracture surfaces showing
a) ductile tearing after the stretch zone (Specimen 23, 247X)
and b) cleavage fracture after the stretch zone (Specimen 27, 1050X).

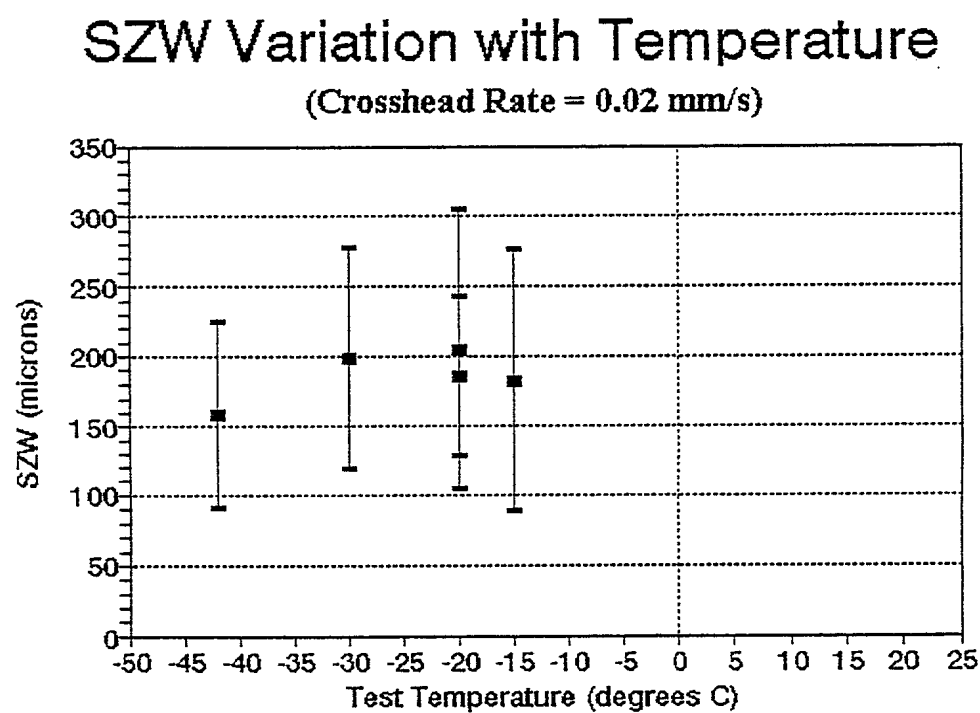


FIGURE 3.14: Stretch zone width variation with temperature for specimens tested with a 0.02 mm/s crosshead rate.

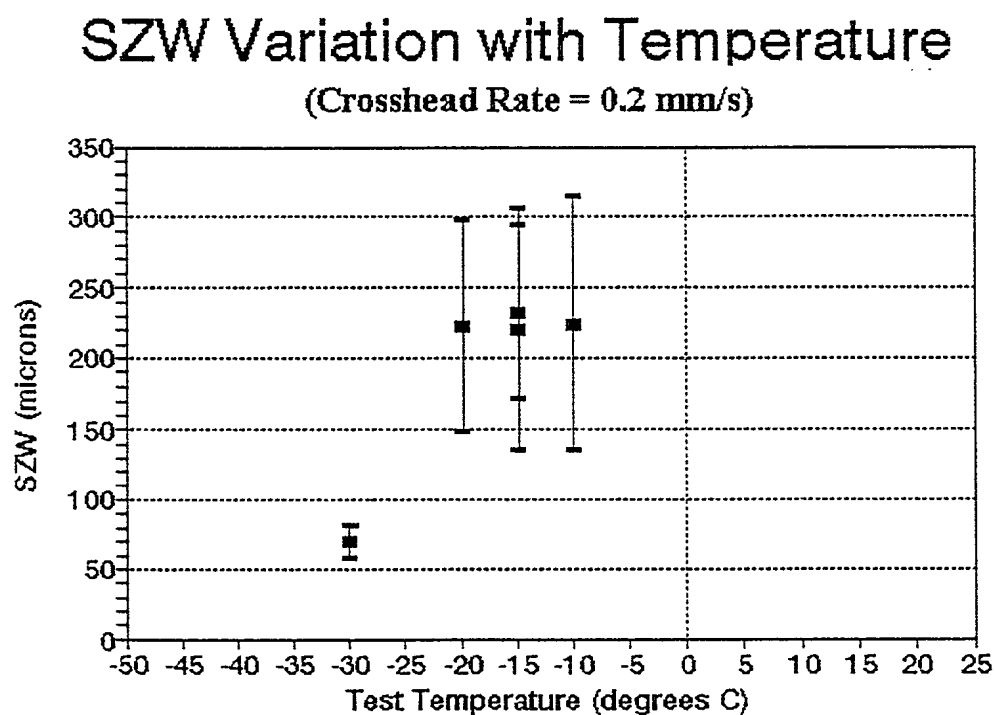


FIGURE 3.15: Stretch zone width variation with temperature for specimens tested with a 0.2 mm/s crosshead rate.

SZW Variation with Temperature

(Crosshead Rate = 1.75 mm/s)

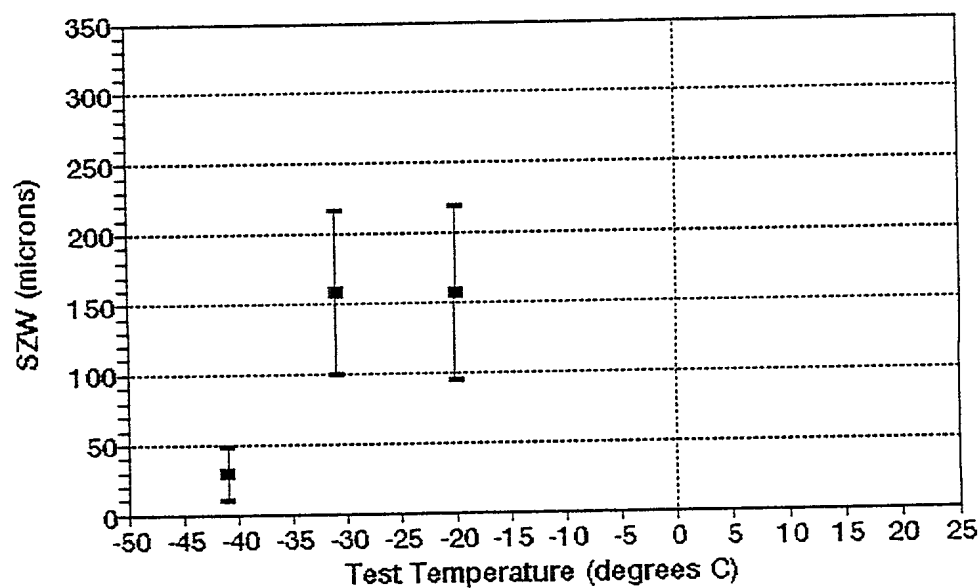


FIGURE 3.16: Stretch zone width variation with temperature for specimens tested with a 1.75 mm/s crosshead rate.

SZW Variation with Temperature

(Crosshead Rate = 2 mm/s)

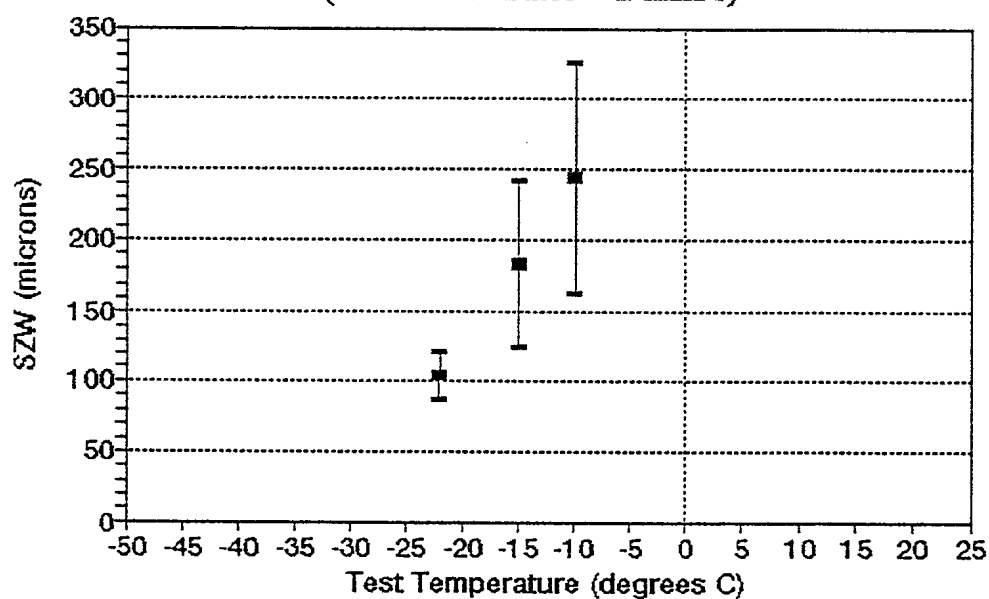


FIGURE 3.17: Stretch zone width variation with temperature for specimens tested with 2 mm/s crosshead rate.

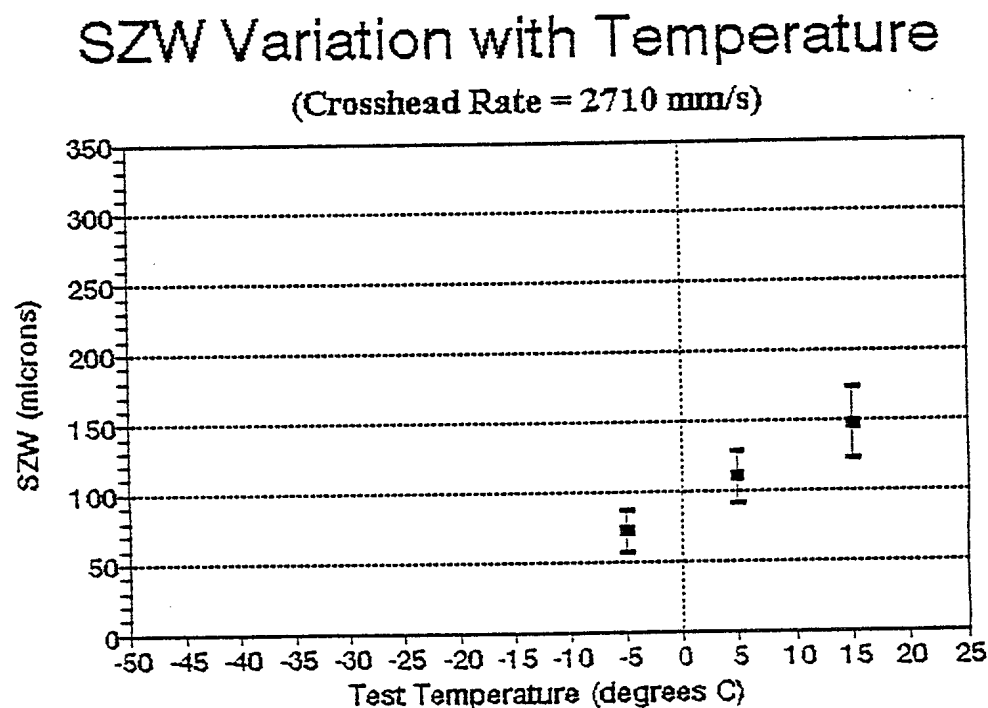


FIGURE 3.18: Stretch zone width variation with temperature for specimens tested with a 2710 mm/s crosshead rate

SZW Variation with Crosshead Rate

(Temperature = -32 to -30 degrees C)

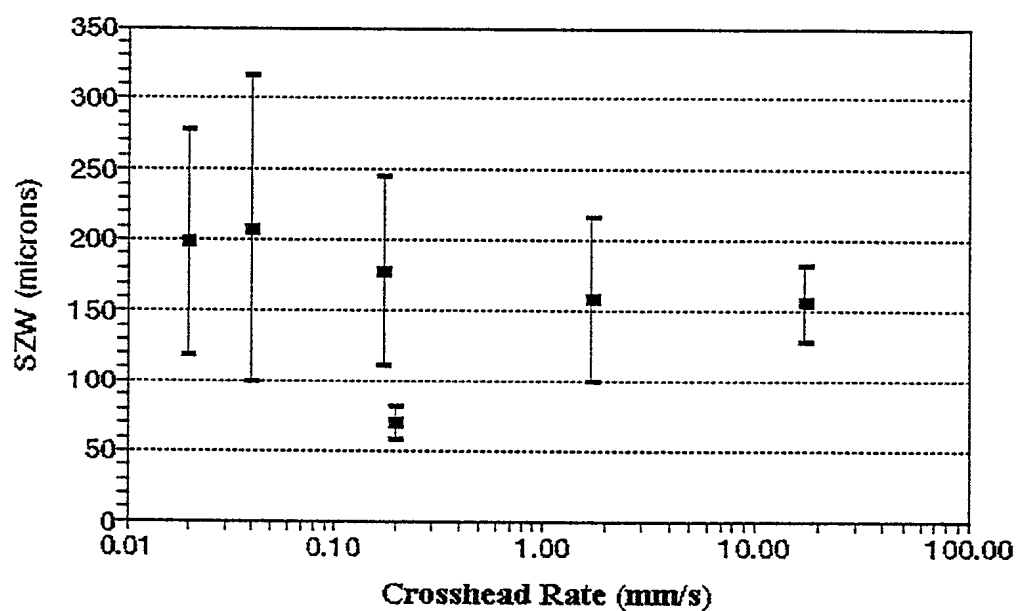


FIGURE 3.19: Stretch zone width variation with loading rate for specimens tested between -32°C and -30°C.

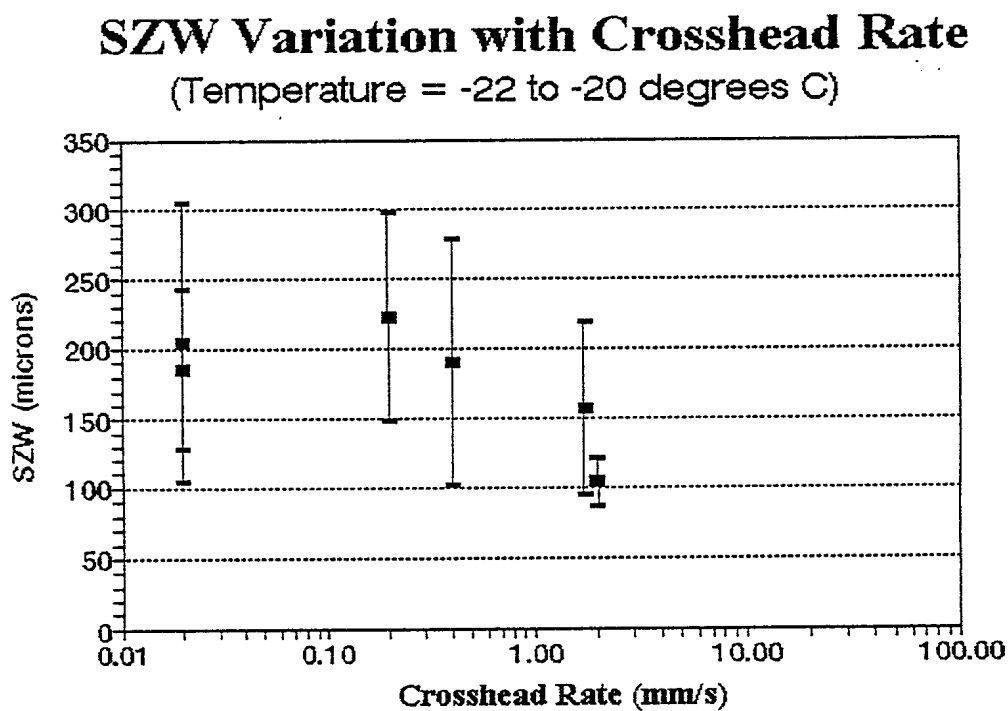


FIGURE 3.20: Stretch zone width variation with loading rate for specimens tested between -22°C and -20°C.

SZW Variation with Crosshead Rate

(Temperature = -15 degrees C)

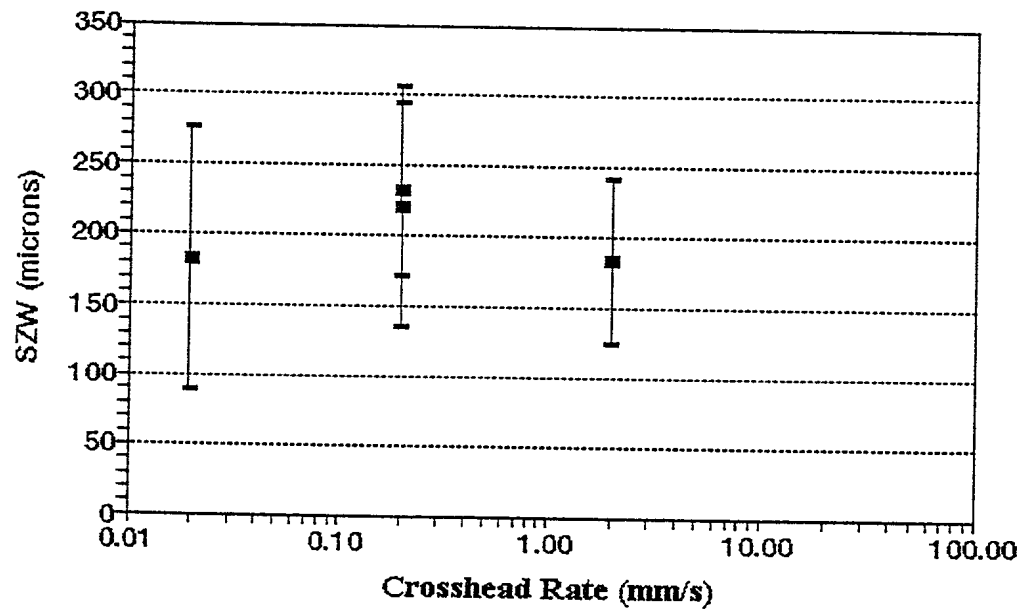


FIGURE 3.21: Stretch zone width variation with loading rate for specimens tested at -15°C.

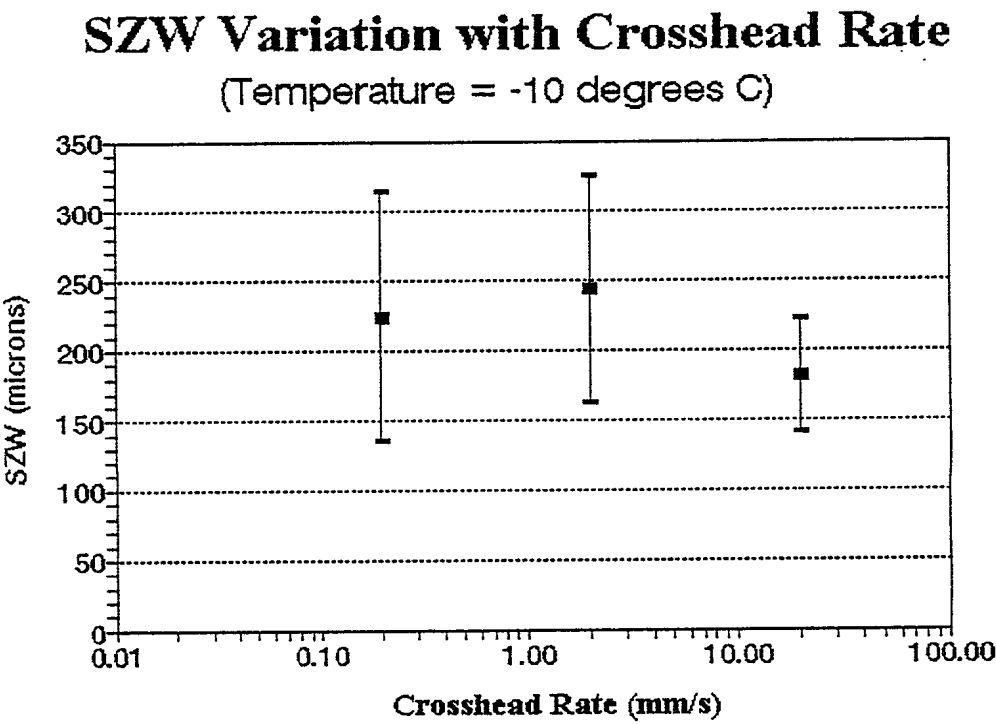


FIGURE 3.22: Stretch zone width variation with loading rate for specimens tested at -10°C.

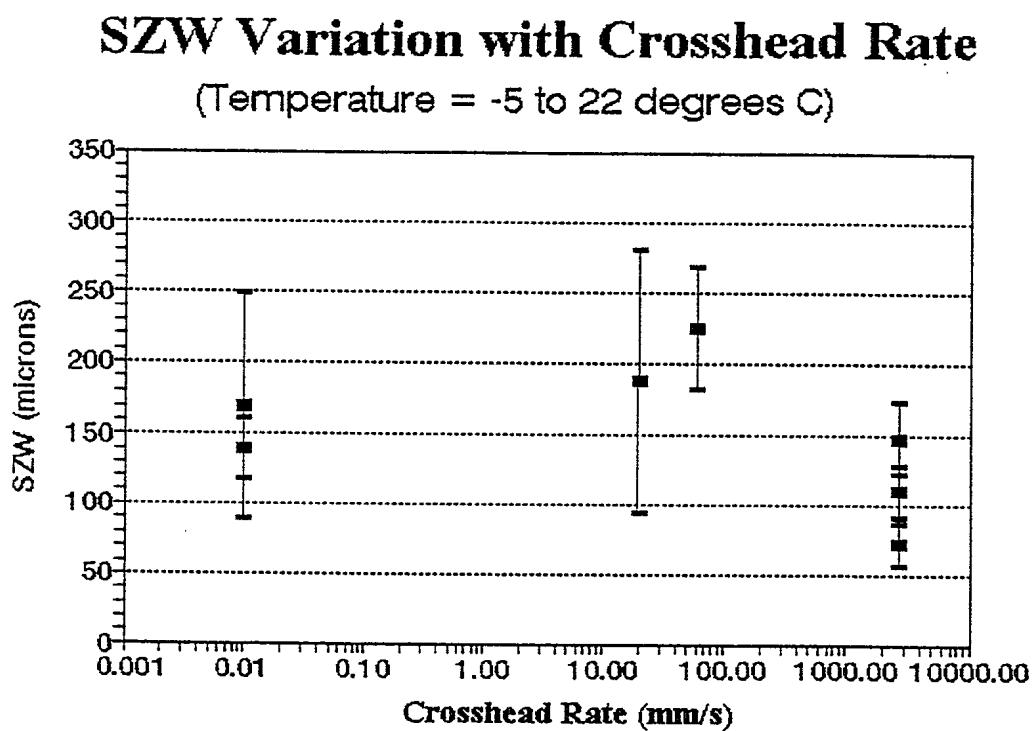


FIGURE 3.23: Stretch zone width variation with loading rate for specimens tested between -5°C and 22°C.

BLANK

4. CONCLUSIONS

For loading rates below 2 mm/s there is a increase in stretch zone width with temperature until the upper shelf temperature range is reached at -20°C . Above -20°C the average stretch zone width does not vary by more than the measurement error. At 2710 mm/s the stretch zone width increases linearly with temperature between -5°C and 15°C .

For specimens tested below -5°C , the variation in stretch zone width with loading rate, at constant temperature, is less than the measurement error over the range of loading rates tested (0.01 - 60 mm/s). For temperatures above -5°C specimens tested at loading rates of 2710 mm/s show a decrease in stretch zone width compared to those tested at loading rates below 60 mm/s.

Blank

REFERENCES

1. L.G. Lao and J.D. Embury, Engineering Fracture Mechanics, No. 30, p. 177-190, 1988.
2. P. Nguyen-Duy and S. Bayard, Journal Engineering Materials Technology, No. 55, p 103, 1981.
3. O. Kolendnik and H.P. Stuwe, International Journal of Fracture, No. 33, p. R63-R66, 1985.
4. J.I. Goldstein, D.E. Newbury, P. Echlin, D.C. Joy, C. Fiori, and E. Lifshin, Scanning Electron Microscopy and X-Ray Microanalysis, Plenum Press, New York, Chapter 4, 1981.

BLANK

APPENDIX A:

SEM MICROGRAPHS OF STRETCH ZONES

Blank

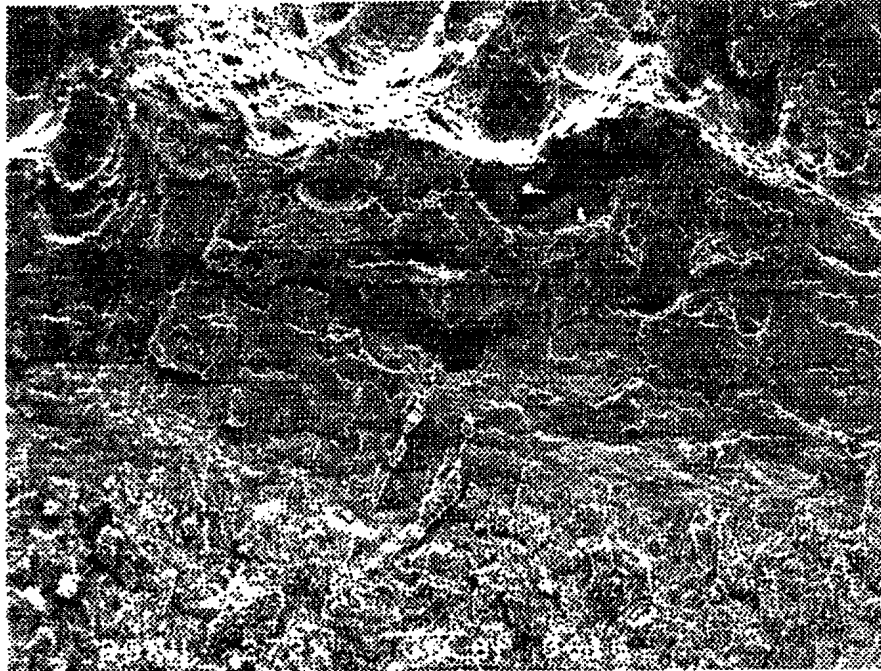


FIGURE A.1: Specimen 1, Position 1 (272 X).

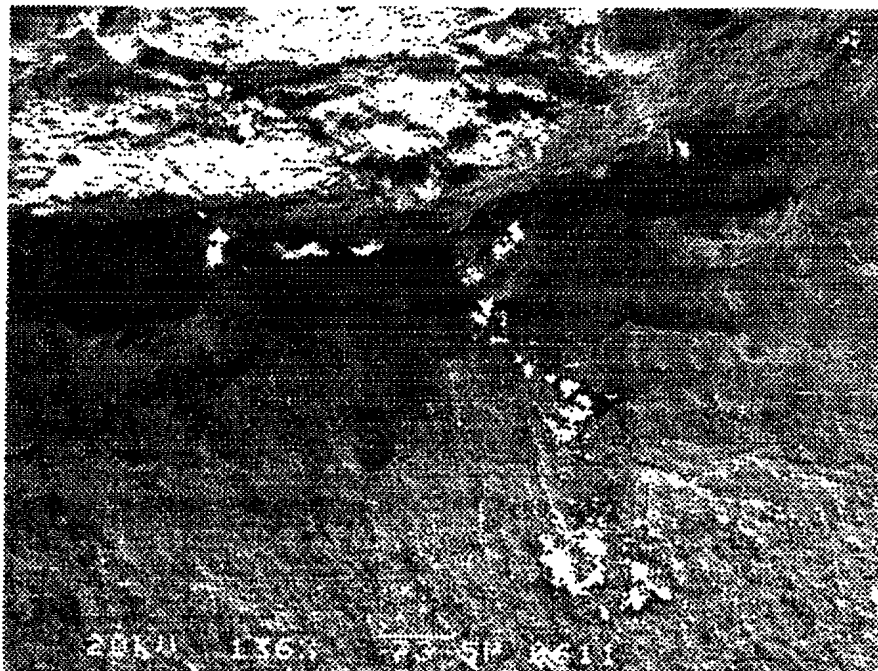


FIGURE A.2: Specimen 1, Position 2 (136 X).

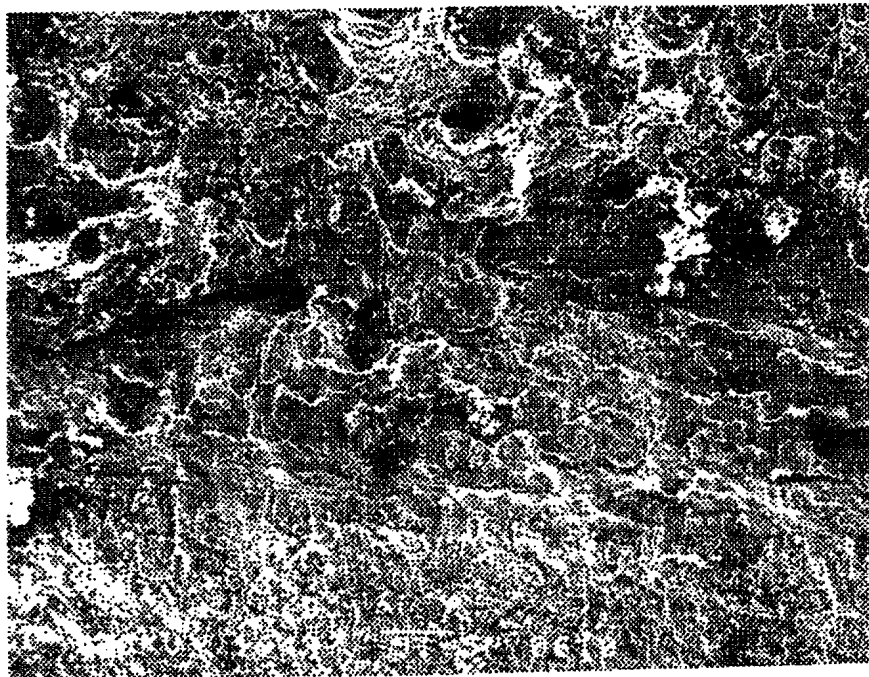


FIGURE A.3: Specimen 1, Position 3 (194 X).

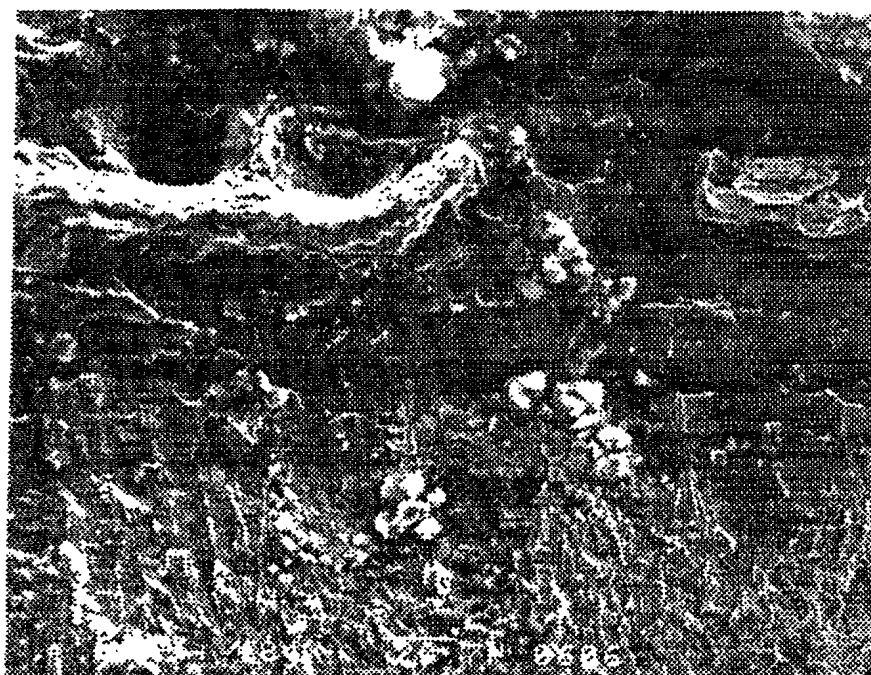


FIGURE A.4: Specimen 1, Position 4 (484 X).

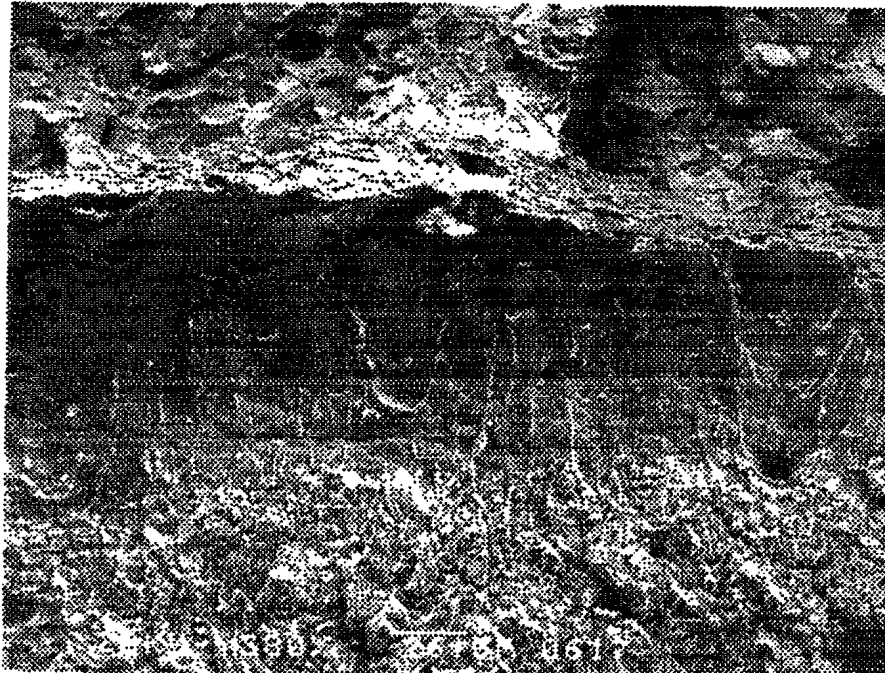


FIGURE A.5: Specimen 2, Position 1 (380 X).

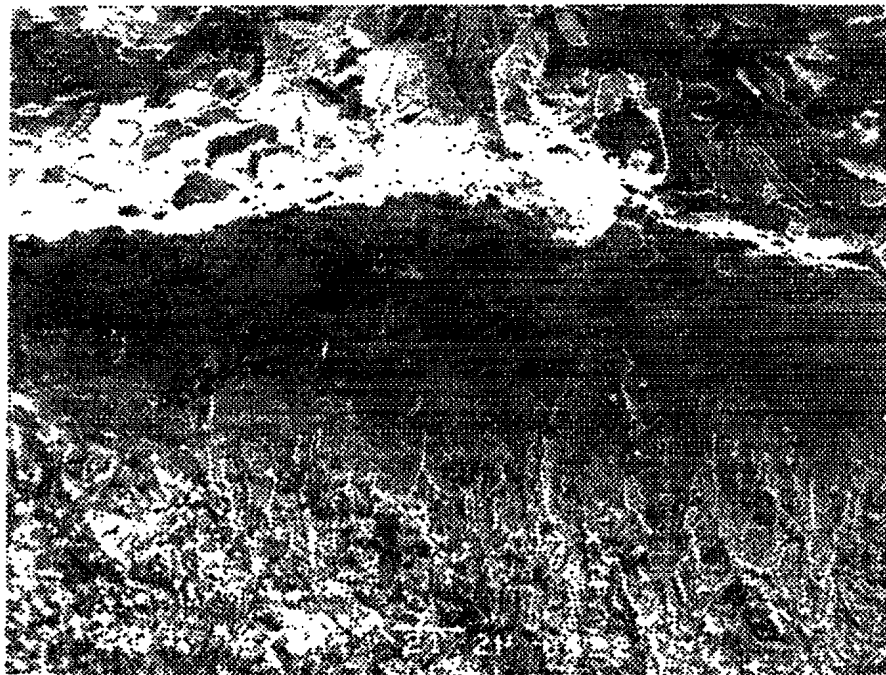


FIGURE A.6: Specimen 2, Position 2 (472 X).

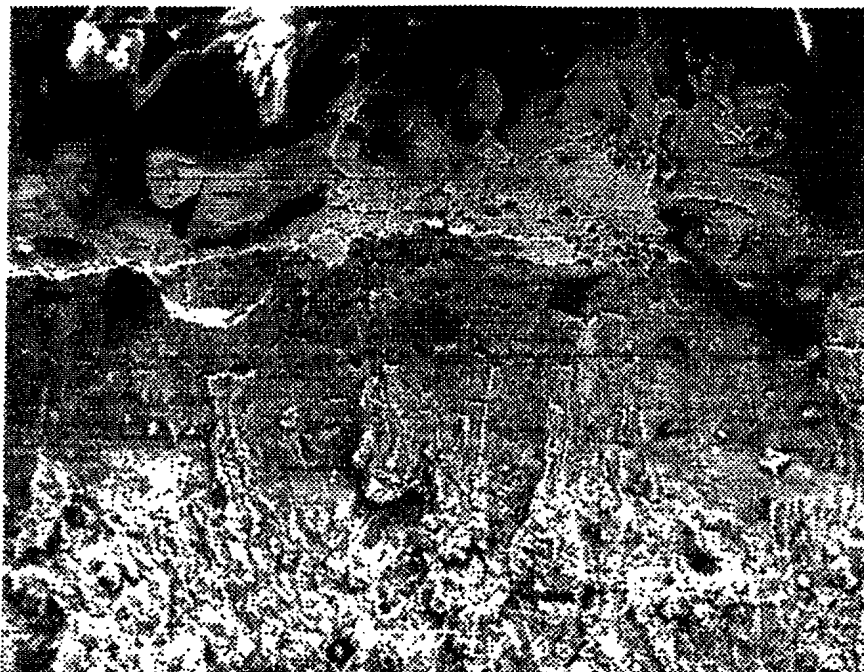


FIGURE A.7: Specimen 2, Position 3 (473 X).

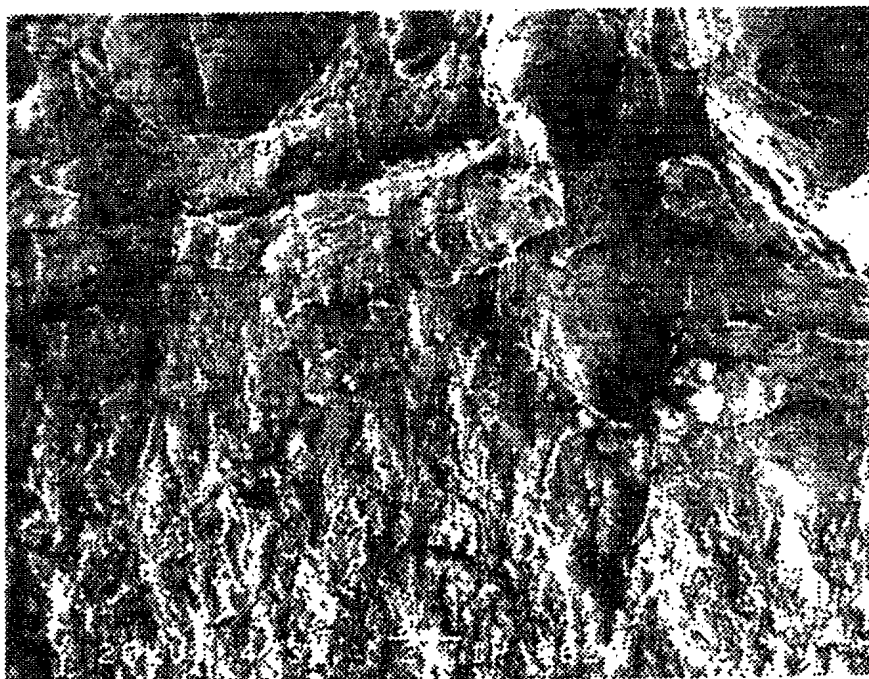


FIGURE A.8: Specimen 2, Position 4 (473 X).

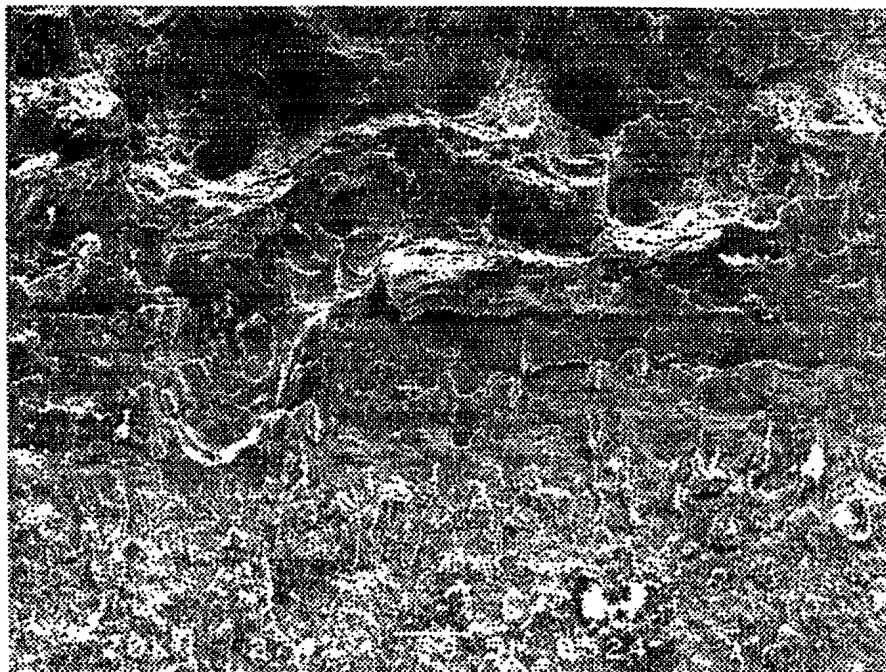


FIGURE A.9: Specimen 3, Position 1 (274 X).

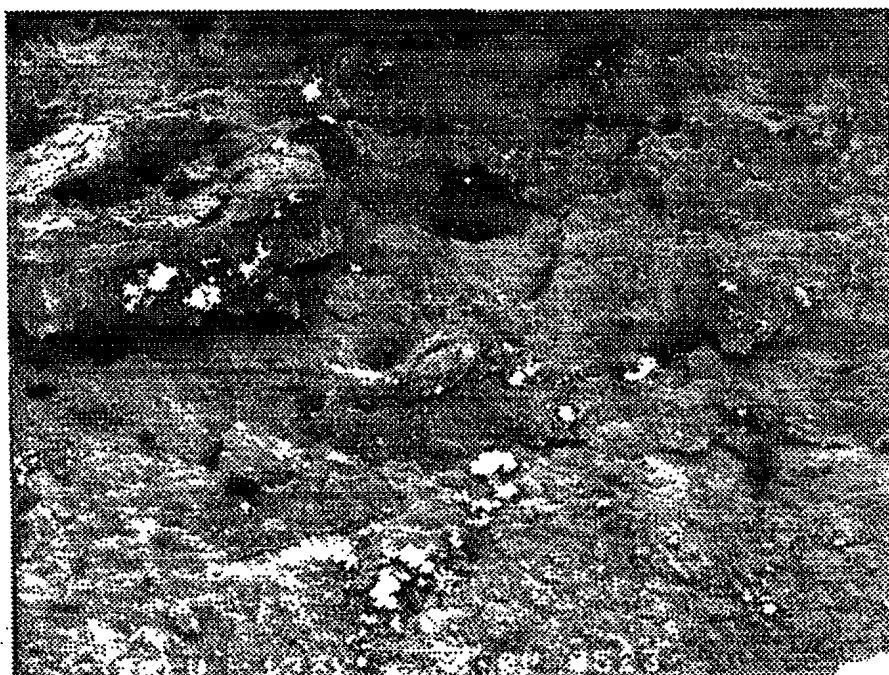


FIGURE A.10: Specimen 3, Position 2 (137 X).

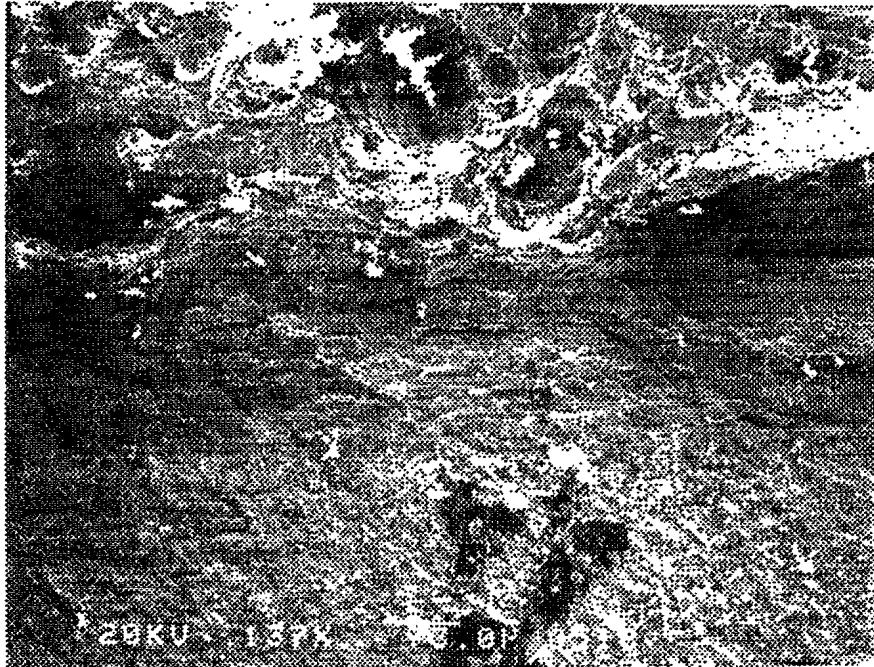


FIGURE A.11: Specimen 3, Position 3 (137 X).

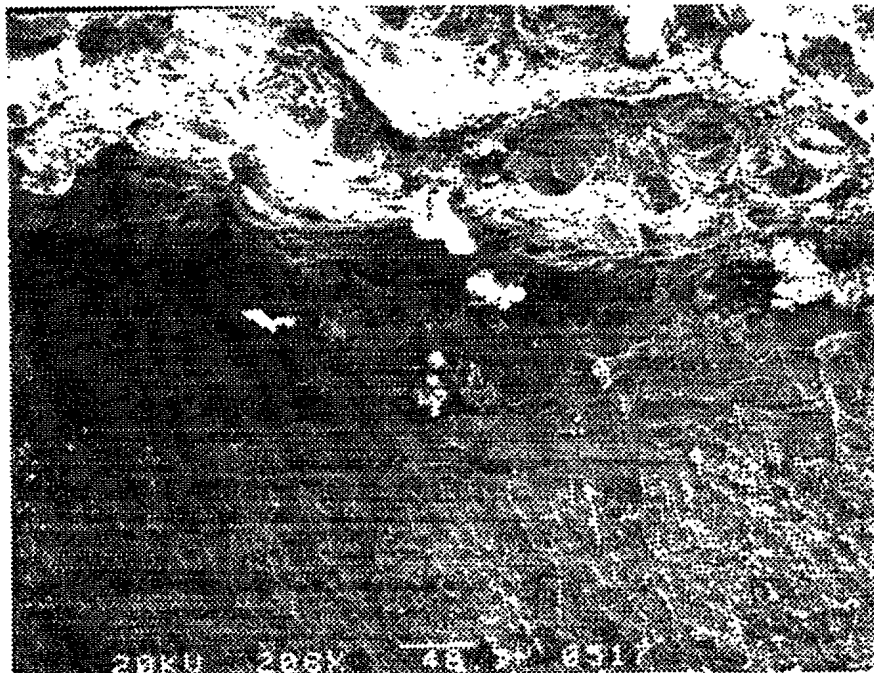


FIGURE A.12: Specimen 3, Position 4 (208 X).

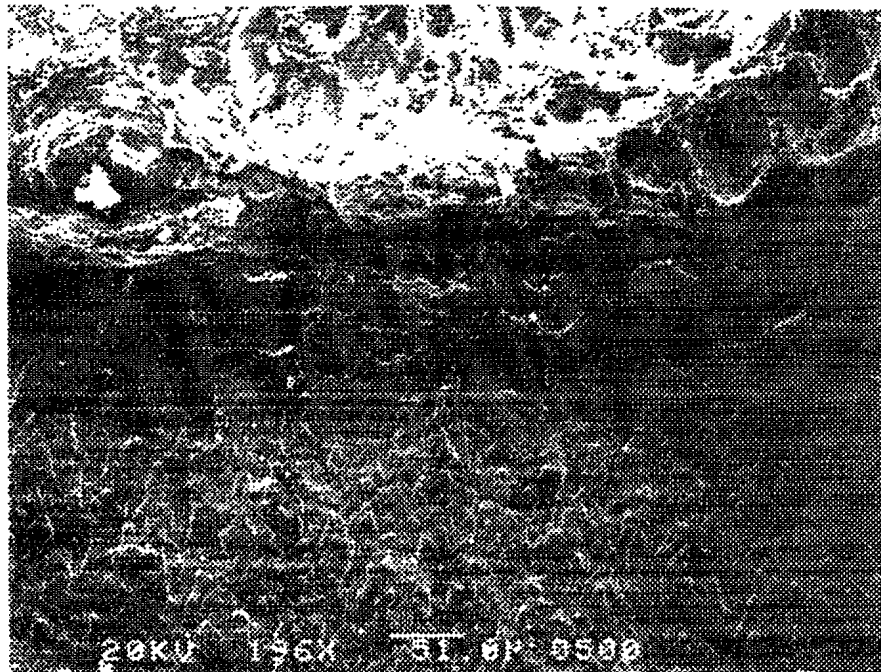


FIGURE A.13: Specimen 4, Position 1 (196 X).

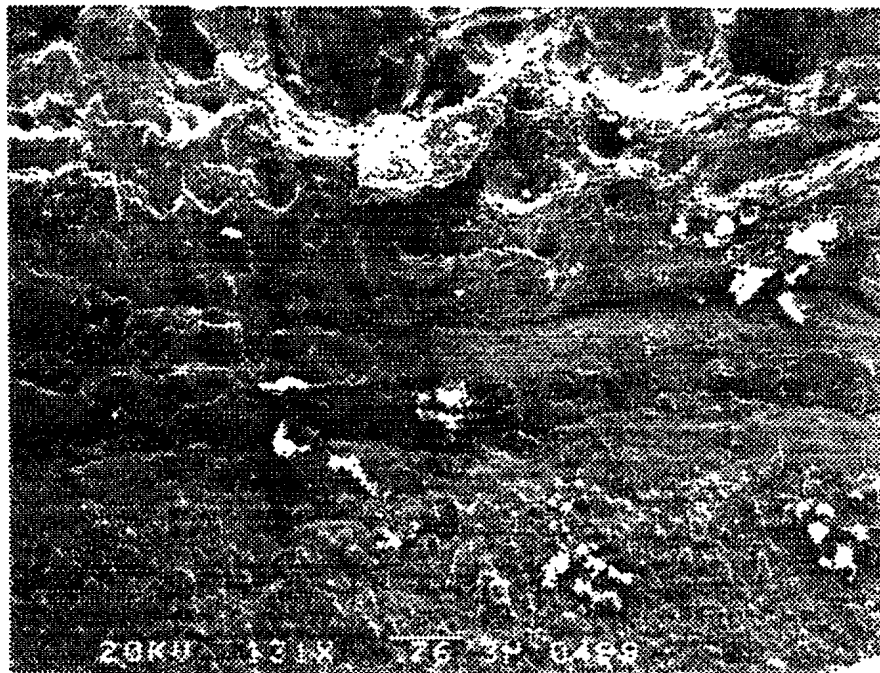


FIGURE A.14: Specimen 4, Position 2 (131 X).

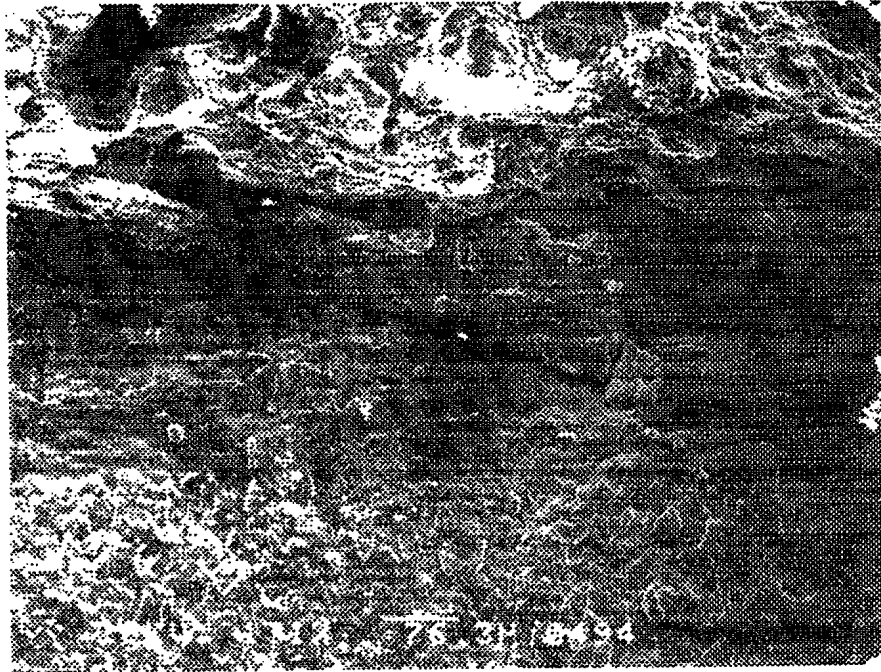


FIGURE A.15: Specimen 4, Position 3 (131 X).

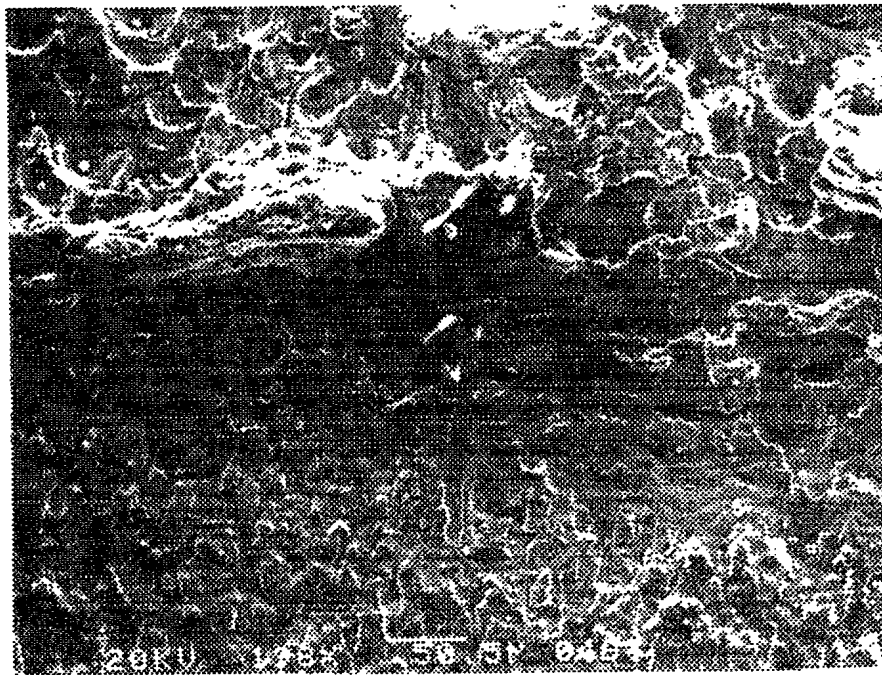


FIGURE A.16: Specimen 4, Position 4 (199 X).

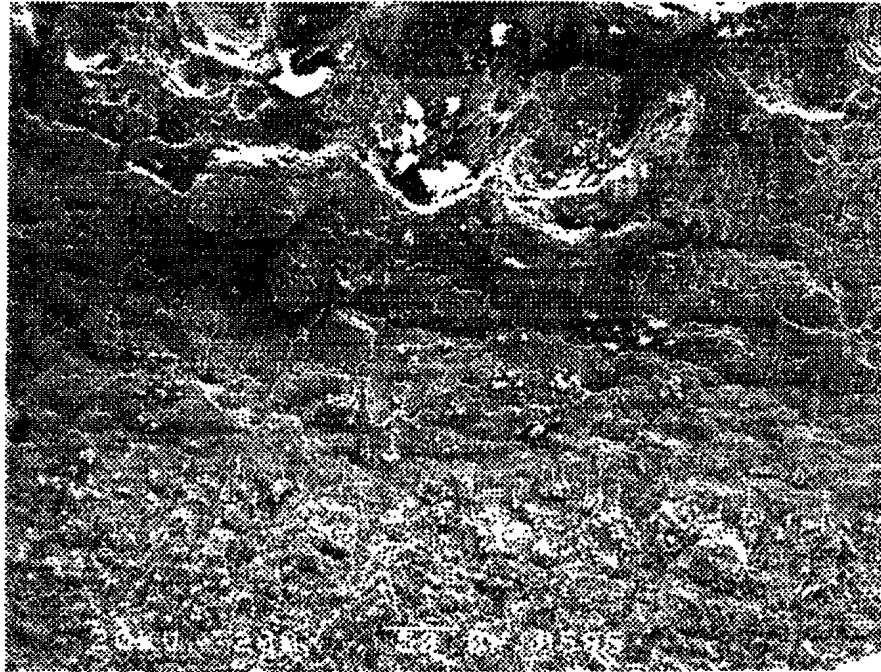


FIGURE A.17: Specimen 5, Position 1 (200 X).



FIGURE A.18: Specimen 5, Position 2 (149 X).

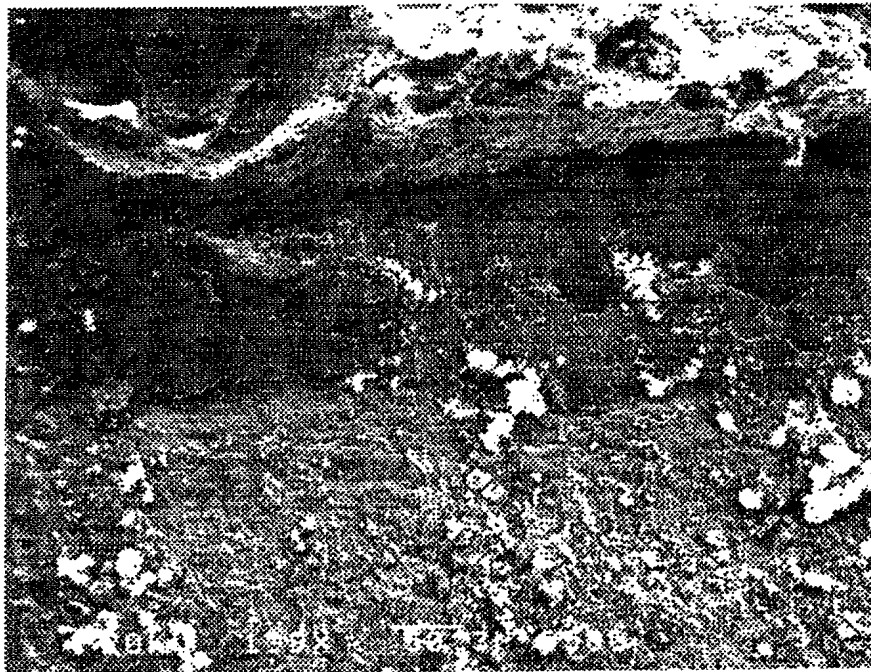


FIGURE A.19: Specimen 5, Position 3 (199 X).

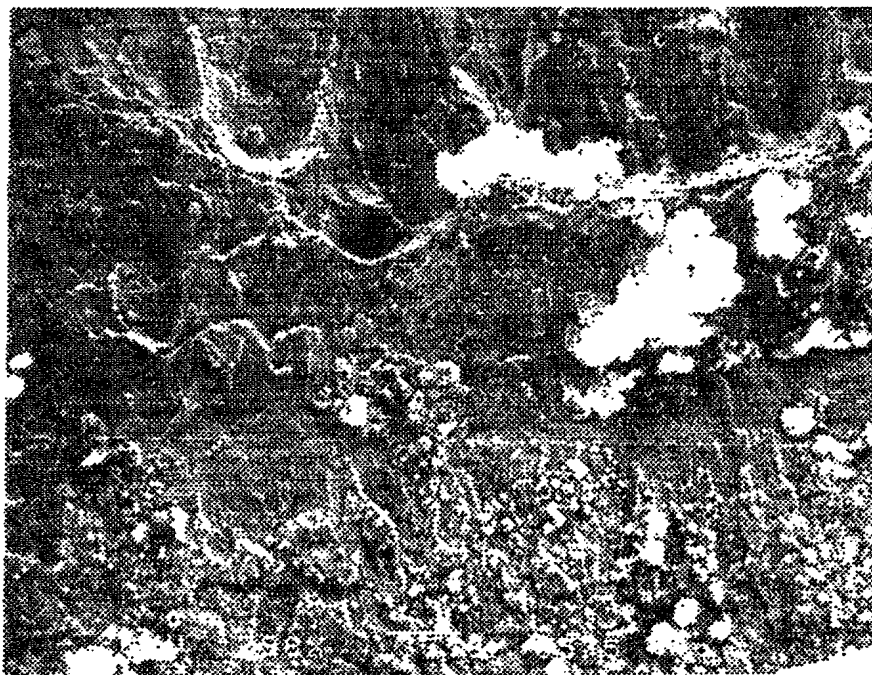


FIGURE A.20: Specimen 5, Position 4 (298 X).

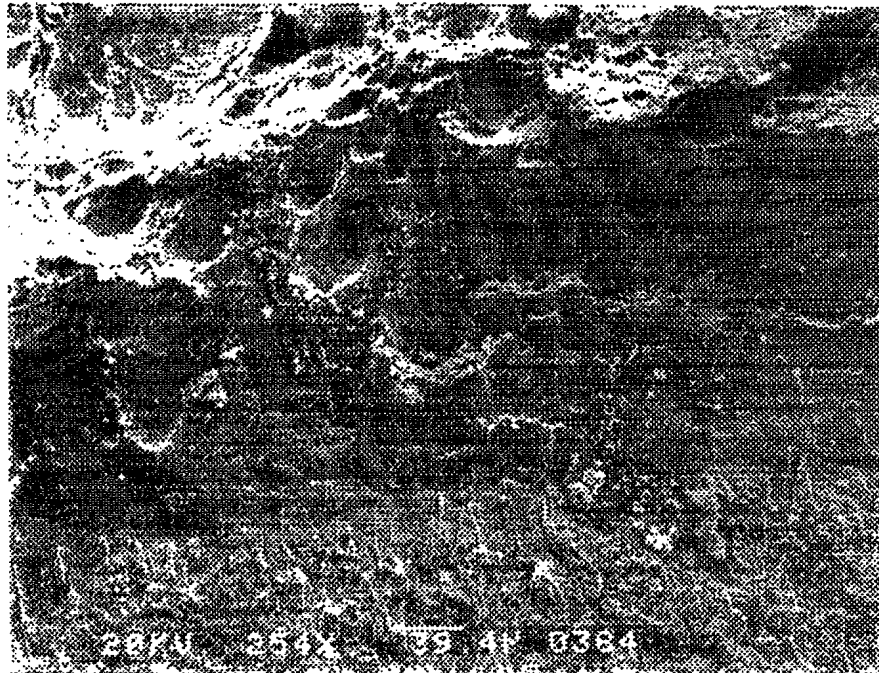


FIGURE A.21: Specimen 6, Position 1 (254 X).

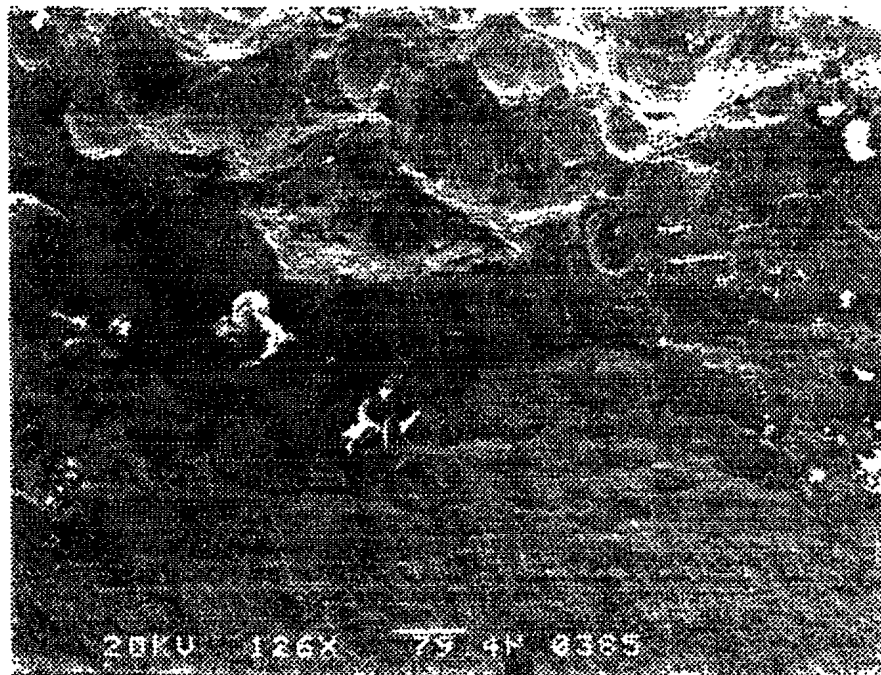


FIGURE A.22: Specimen 6, Position 2 (126 X).

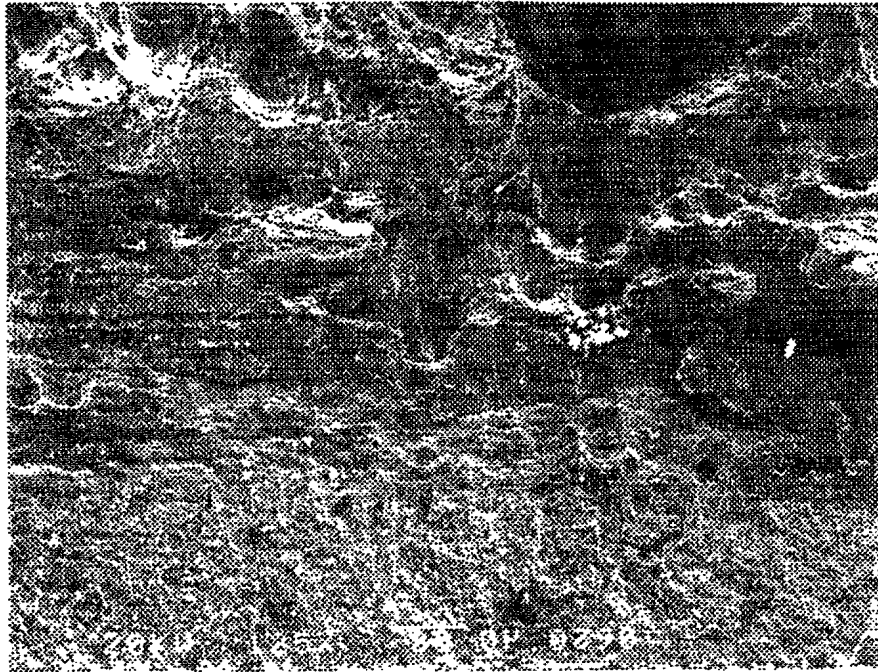


FIGURE A.23: Specimen 6, Position 3 (125 X).

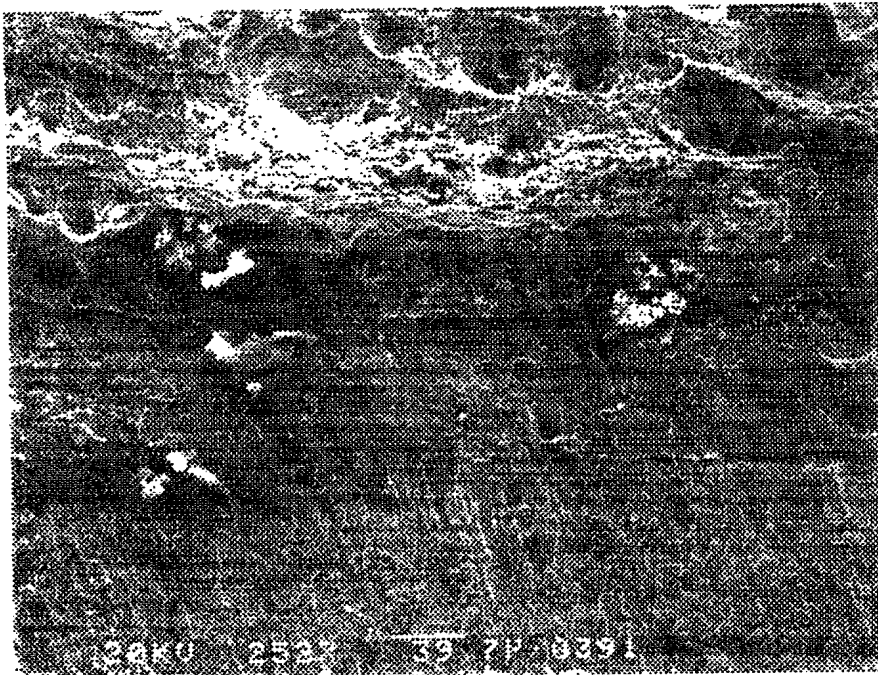


FIGURE A.24: Specimen 6, Position 4 (252 X).



FIGURE A.25: Specimen 7, Position 1 (167 X).

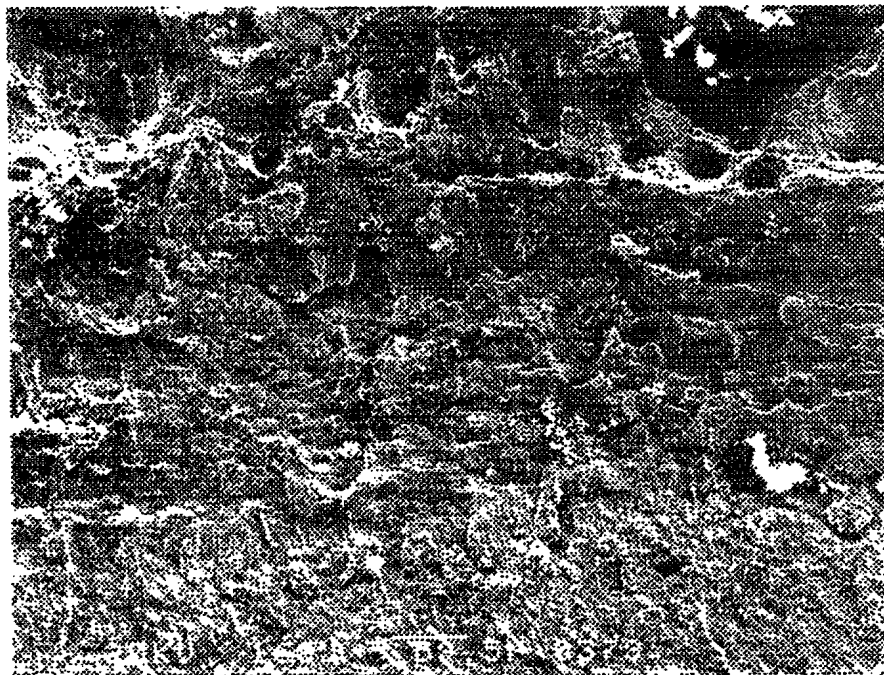


FIGURE A.26: Specimen 7, Position 2 (168 X).



FIGURE A.27: Specimen 7, Position 3 (126 X).



FIGURE A.28: Specimen 7, Position 4 (305 X).

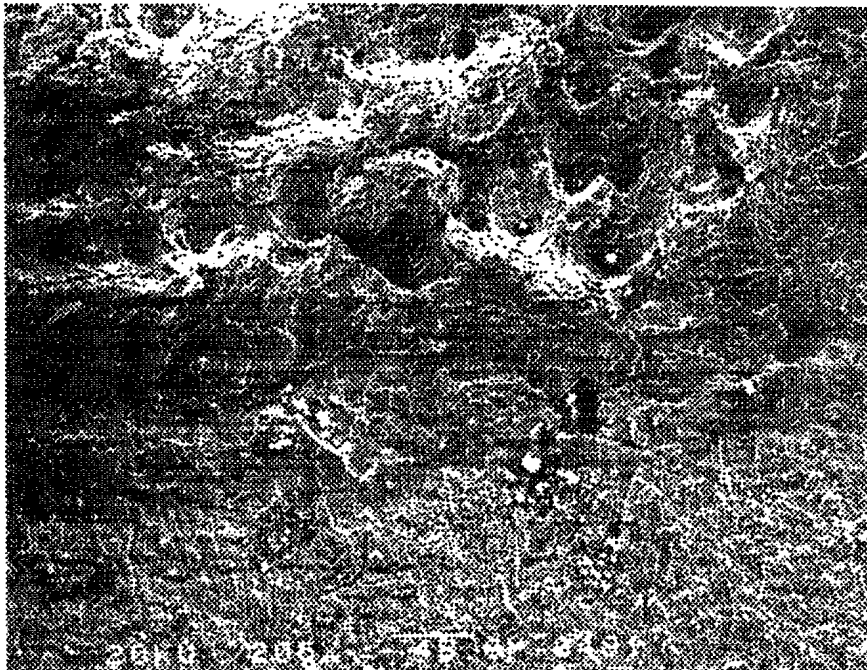


FIGURE A.29: Specimen 8, Position 1 (205 X).

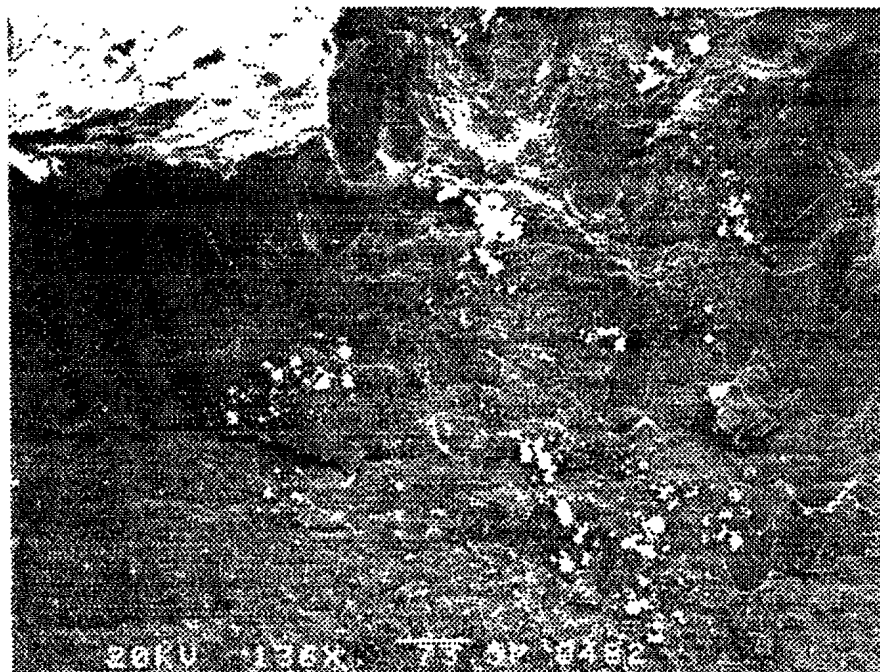


FIGURE A.30: Specimen 8, Position 2 (136 X).

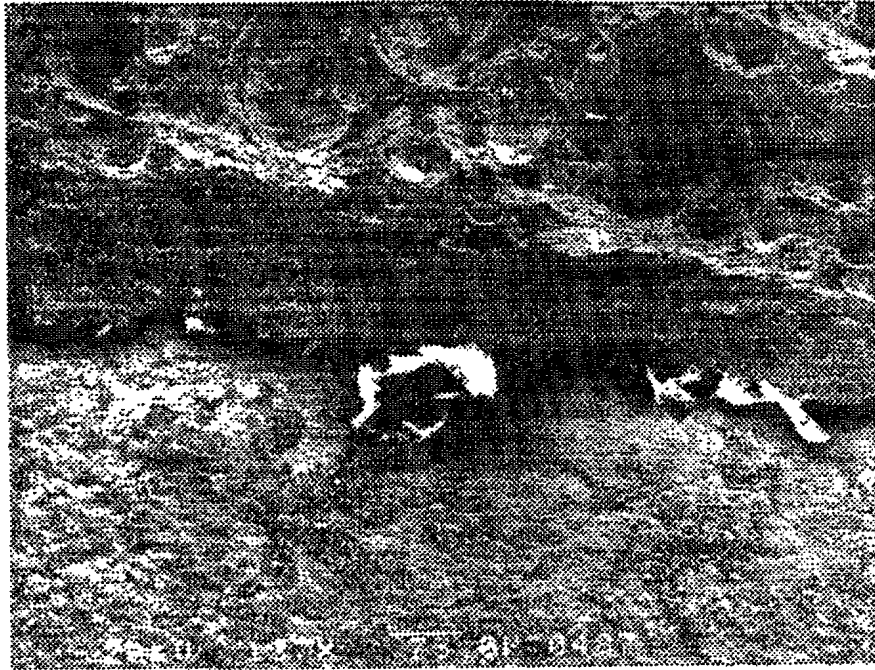


FIGURE A.31: Specimen 8, Position 3 (137 X).

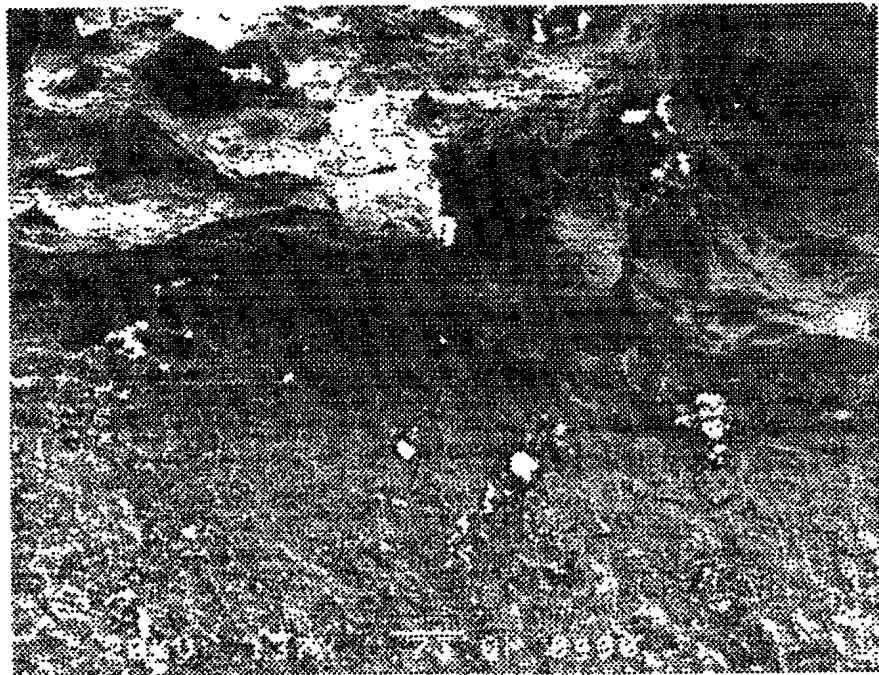


FIGURE A.32: Specimen 8, Position 4 (137 X).

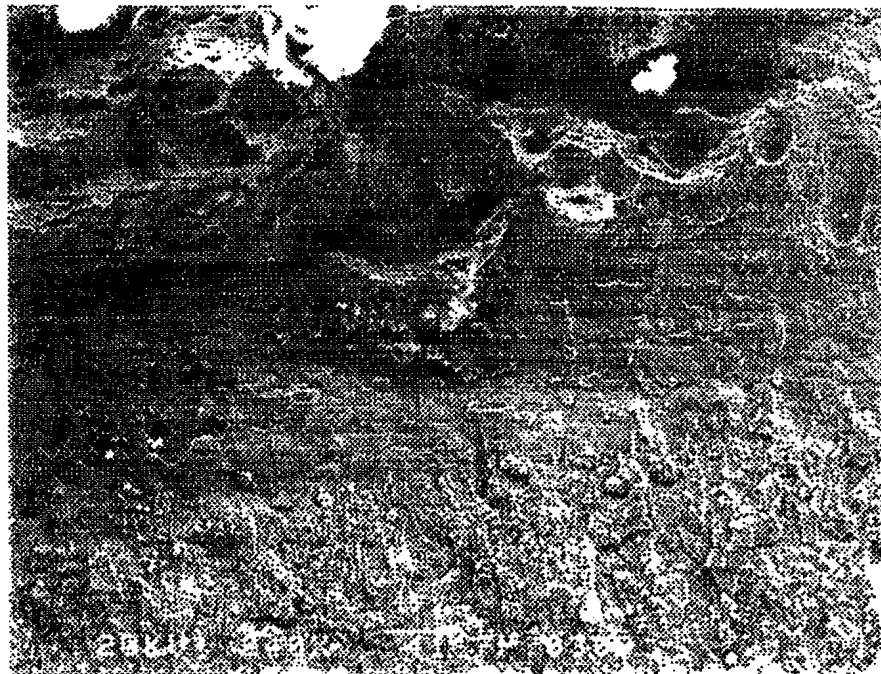


FIGURE A.33: Specimen 9, Position 1 (241 X).

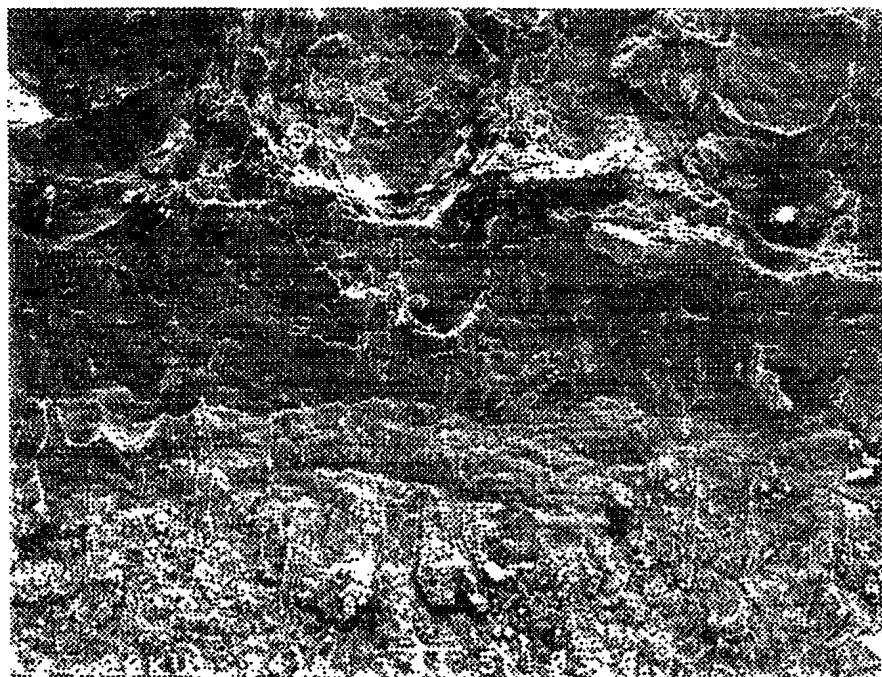


FIGURE A.34: Specimen 9, Position 2 (241 X).

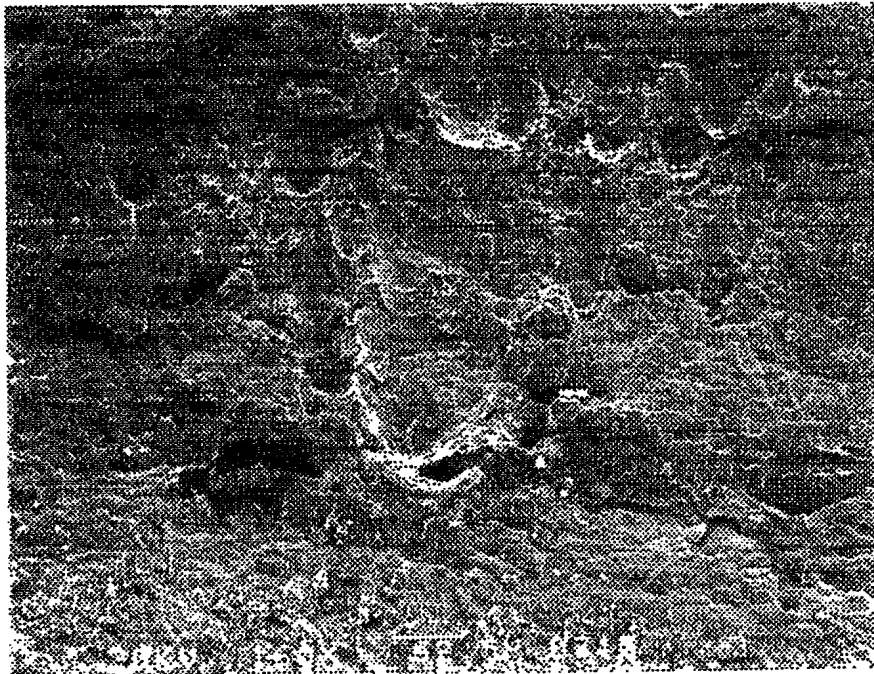


FIGURE A.35: Specimen 9, Position 3 (160 X).

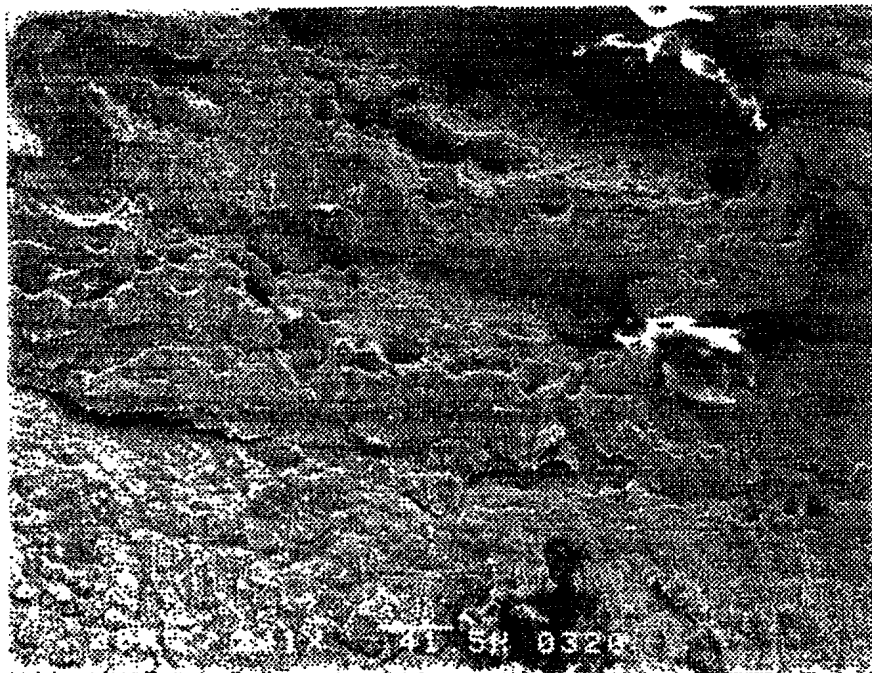


FIGURE A.36: Specimen 9, Position 4 (241 X).

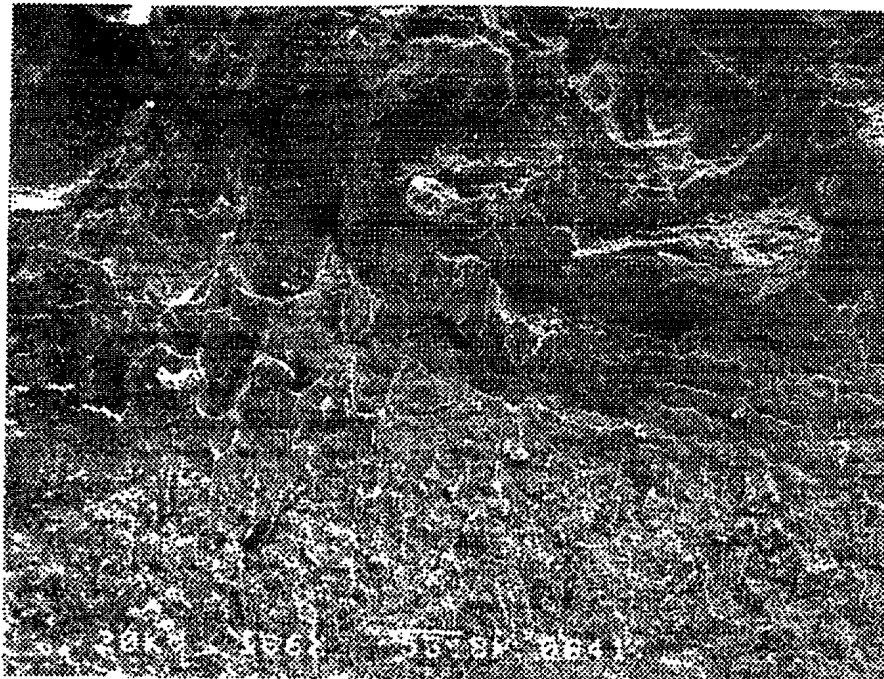


FIGURE A.37: Specimen 10, Position 1 (186 X).

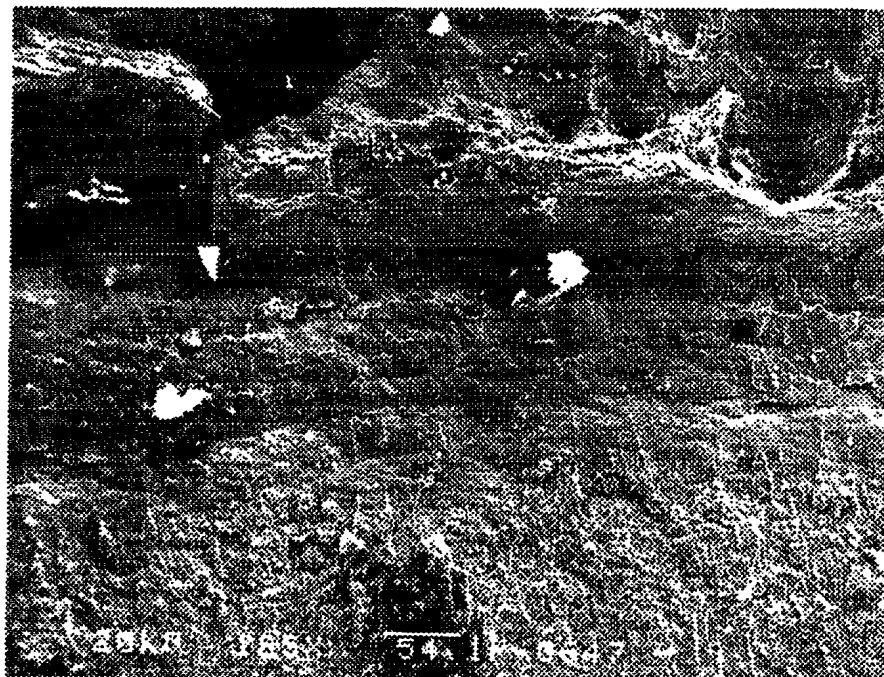


FIGURE A.38: Specimen 10, Position 2 (185 X).

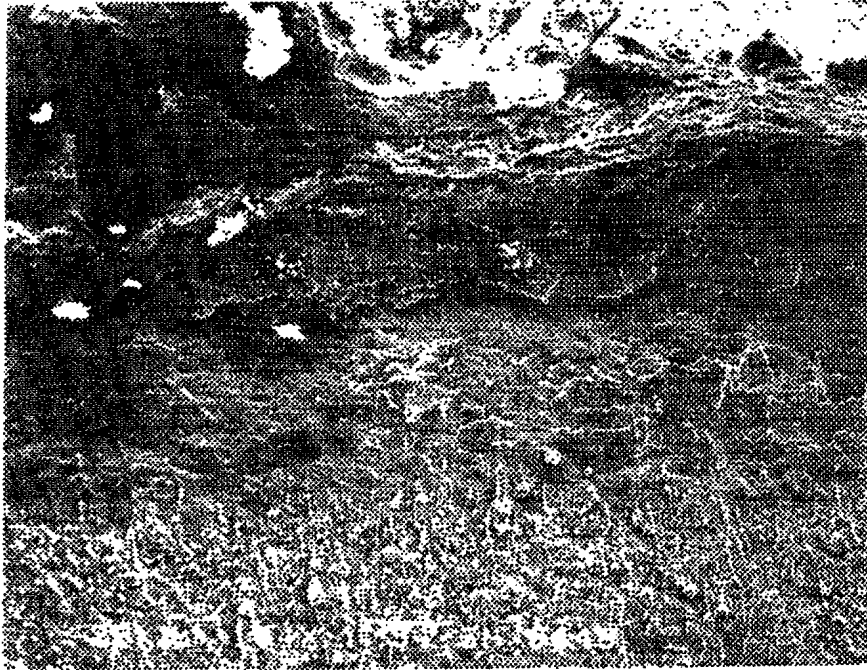


FIGURE A.39: Specimen 10, Position 3 (184 X).

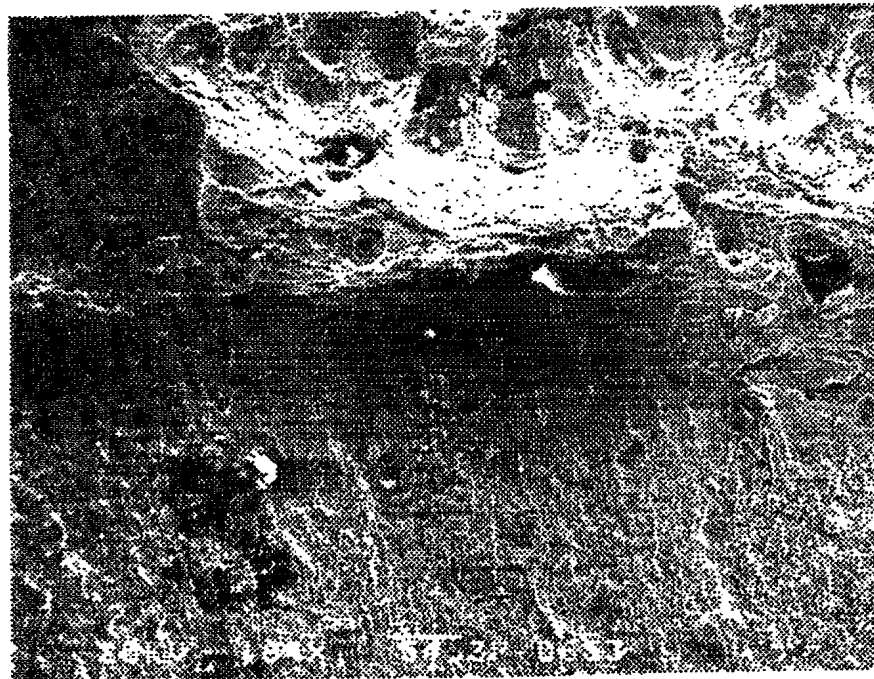


FIGURE A.40: Specimen 10, Position 4 (184 X).

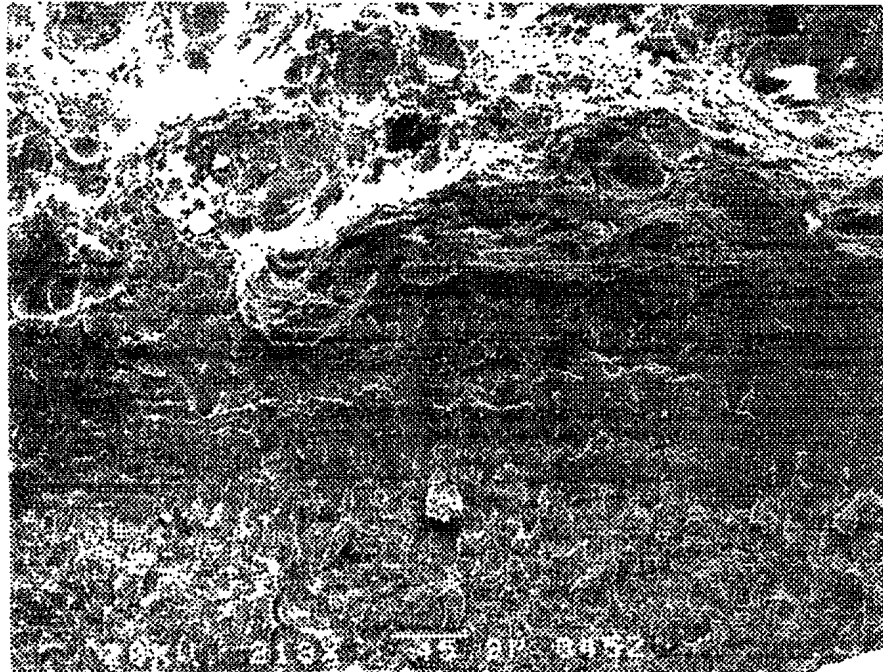


FIGURE A.41: Specimen 11, Position 1 (218 X).

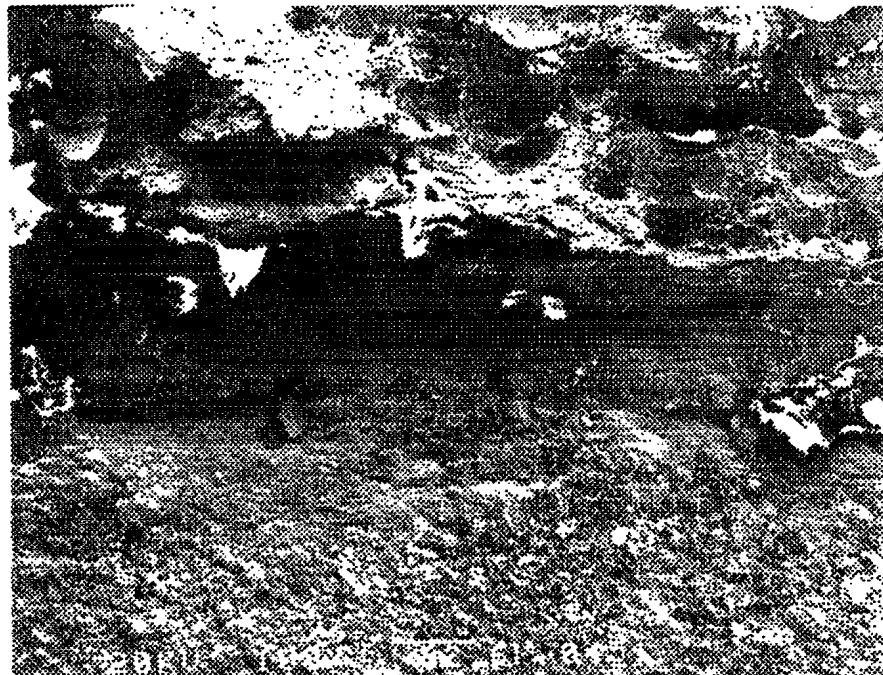


FIGURE A.42: Specimen 11, Position 2 (108 X).

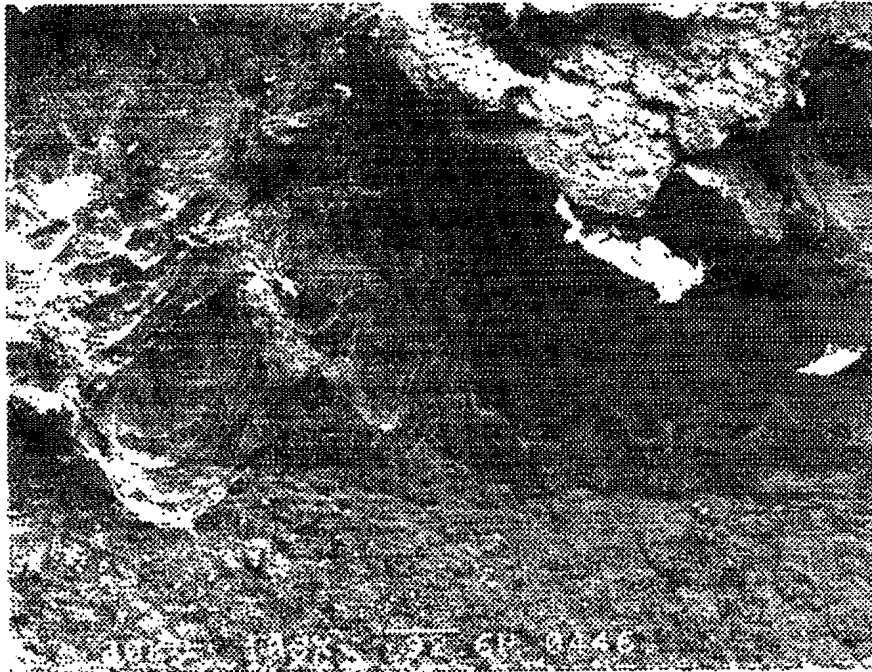


FIGURE A.43: Specimen 11, Position 3 (107 X).

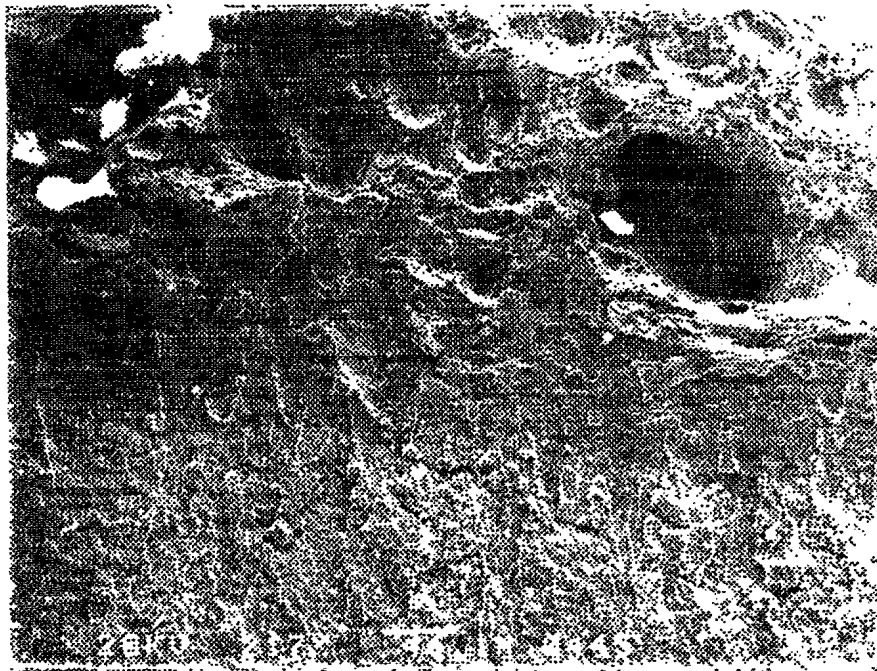


FIGURE A.44: Specimen 11, Position 4 (192 X).

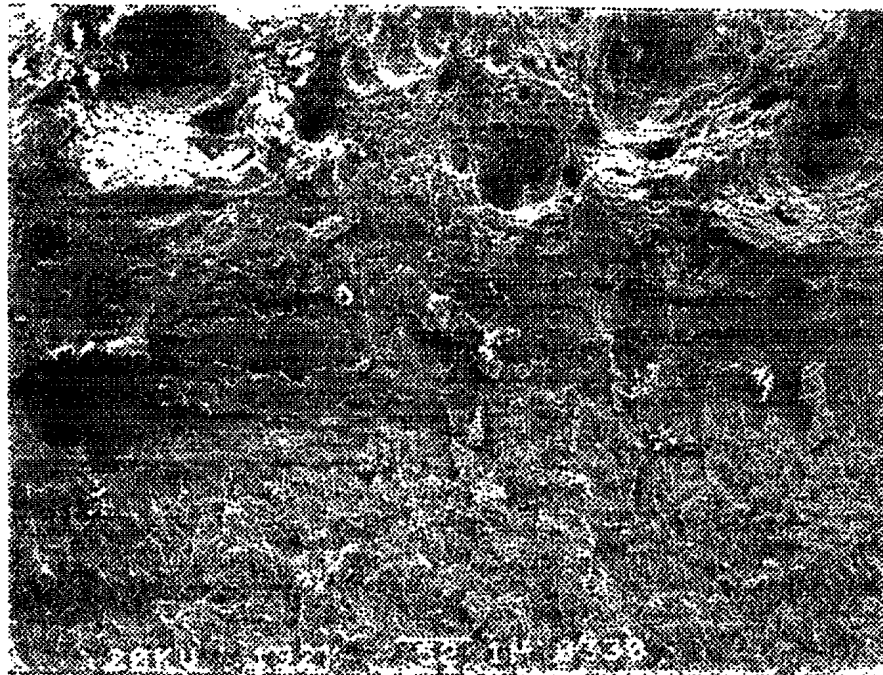


FIGURE A.45: Specimen 12, Position 1 (192 X).

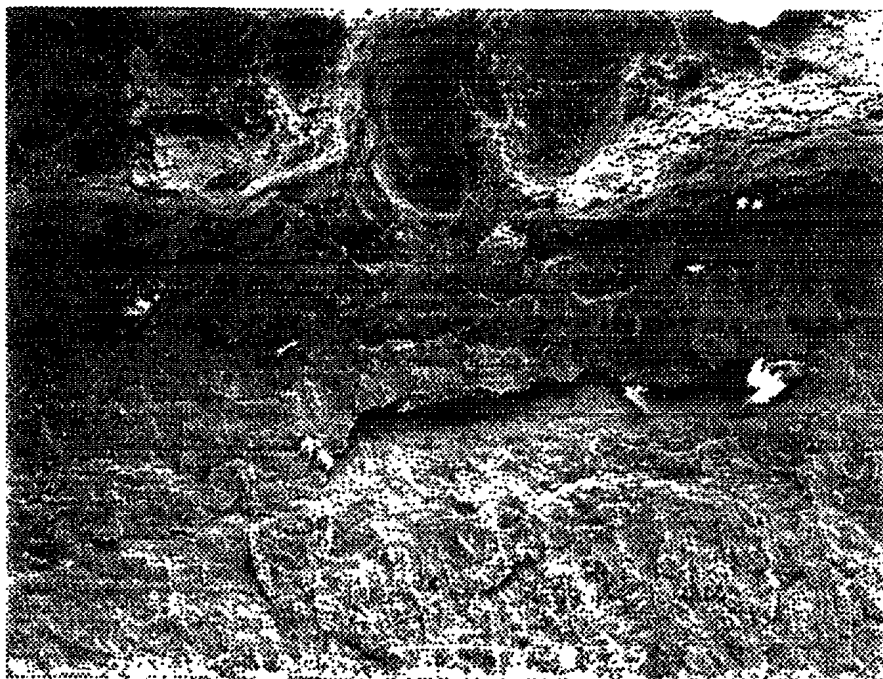


FIGURE A.46: Specimen 12, Position 2 (217 X).

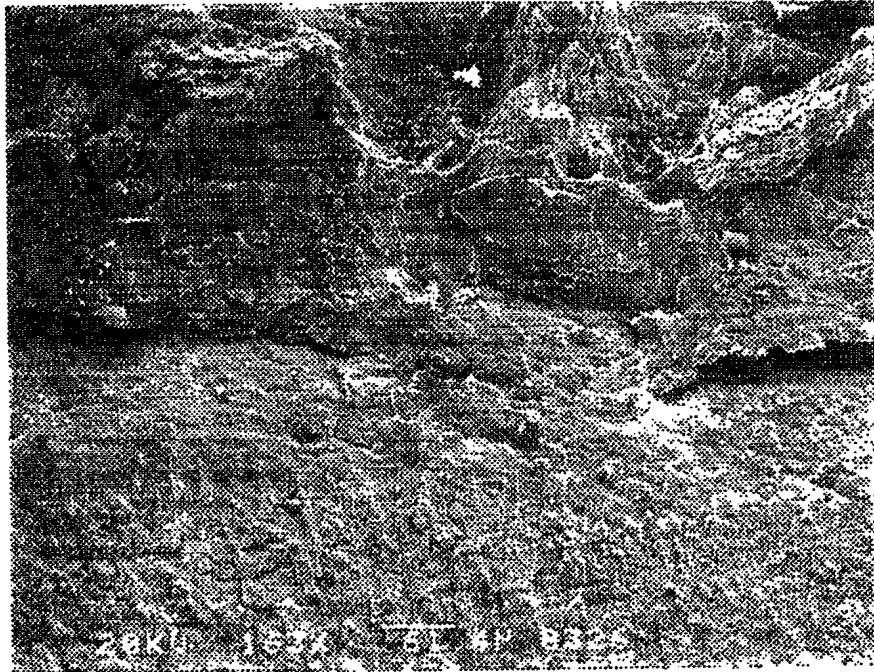


FIGURE A.47: Specimen 12, Position 3 (163 X).

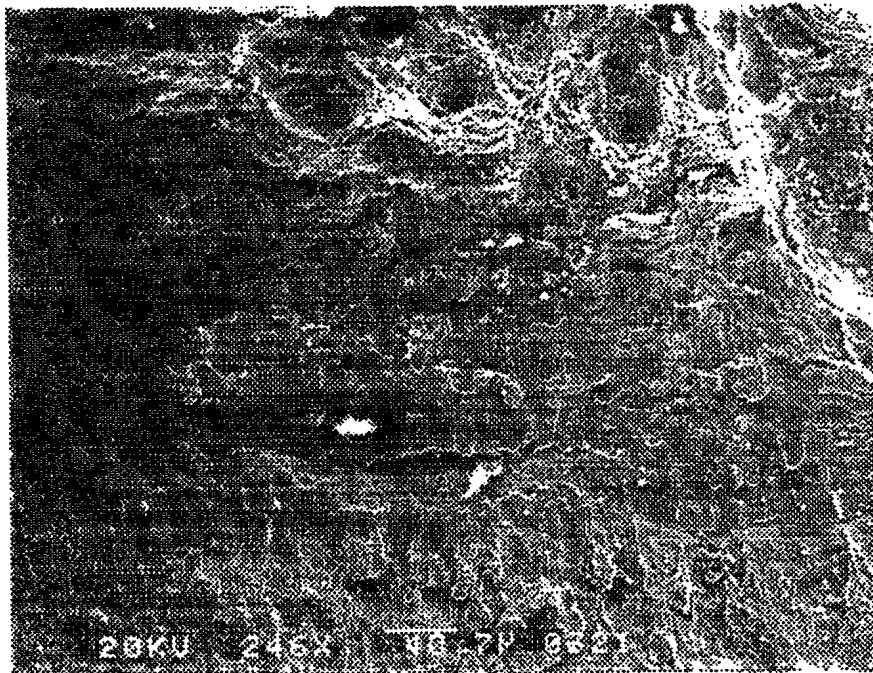


FIGURE A.48: Specimen 12, Position 4 (246 X).

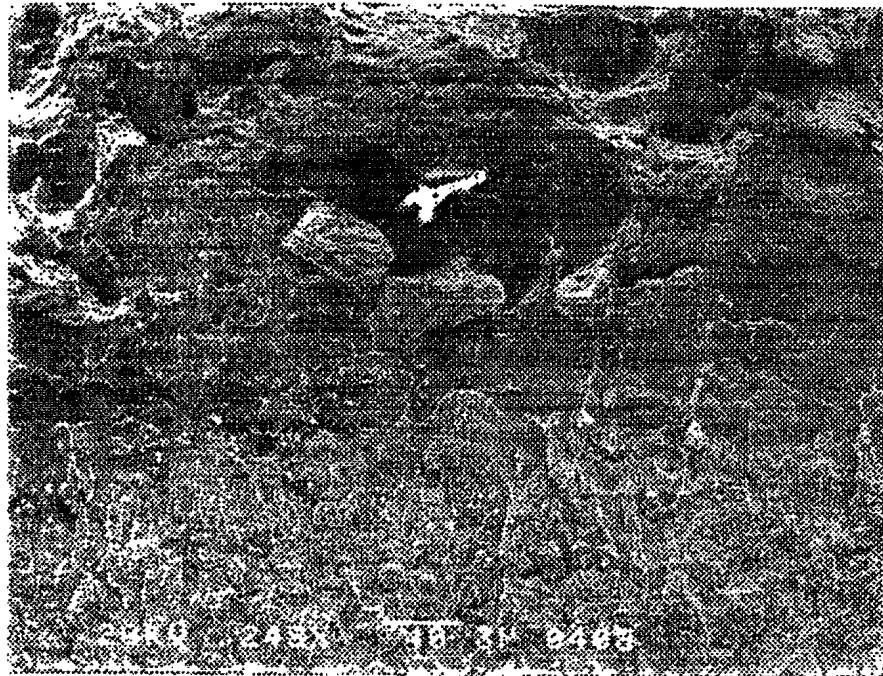


FIGURE A.49: Specimen 13, Position 1 (248 X).

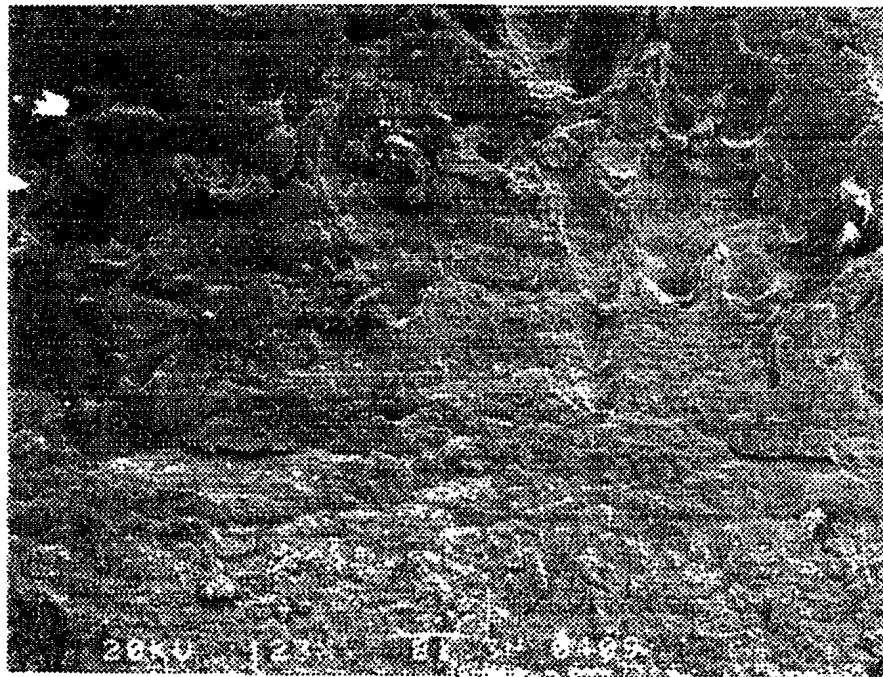


FIGURE A.50: Specimen 13, Position 2 (123 X).

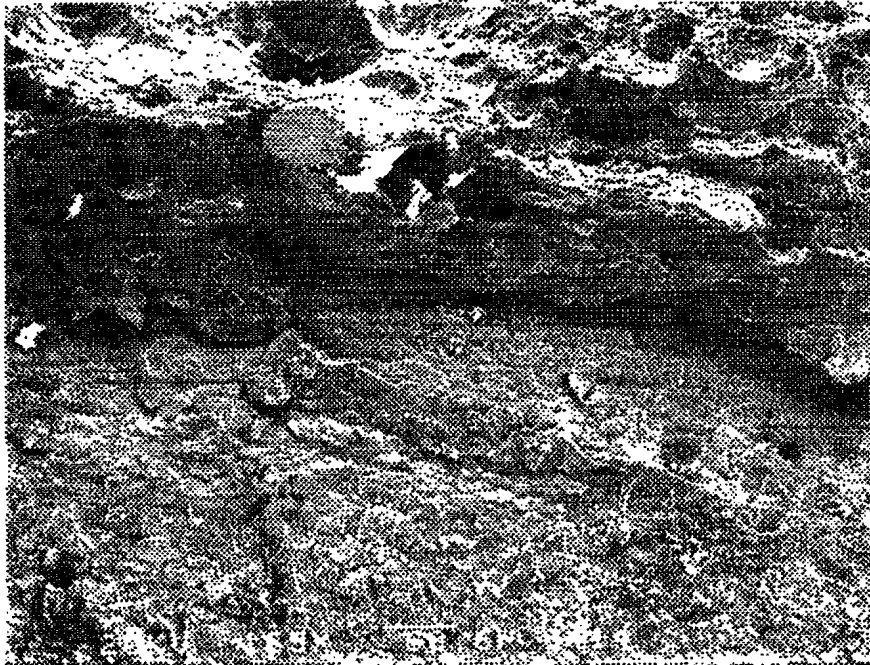


FIGURE A.51: Specimen 13, Position 3 (165 X).

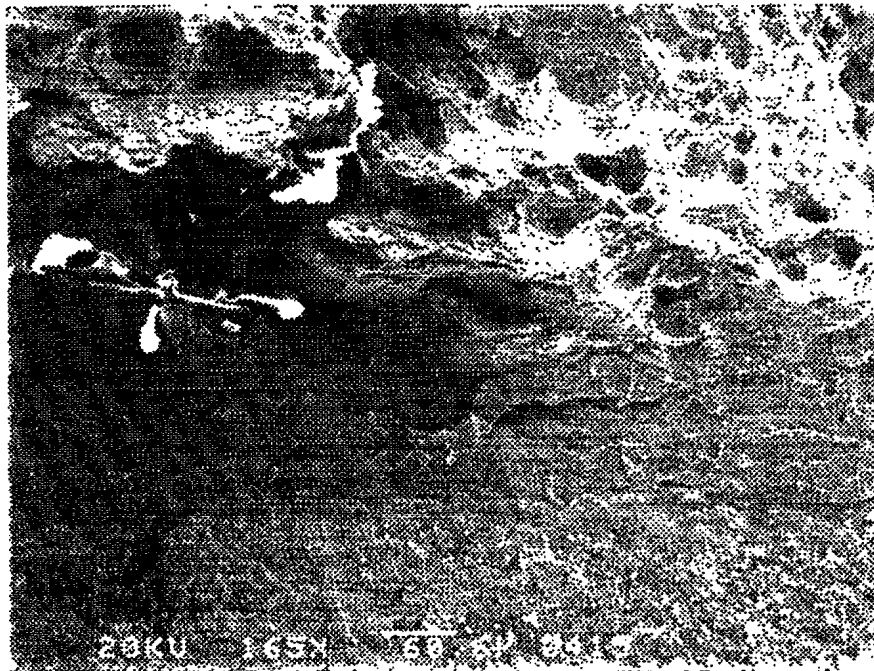


FIGURE A.52: Specimen 13, Position 4 (165 X).

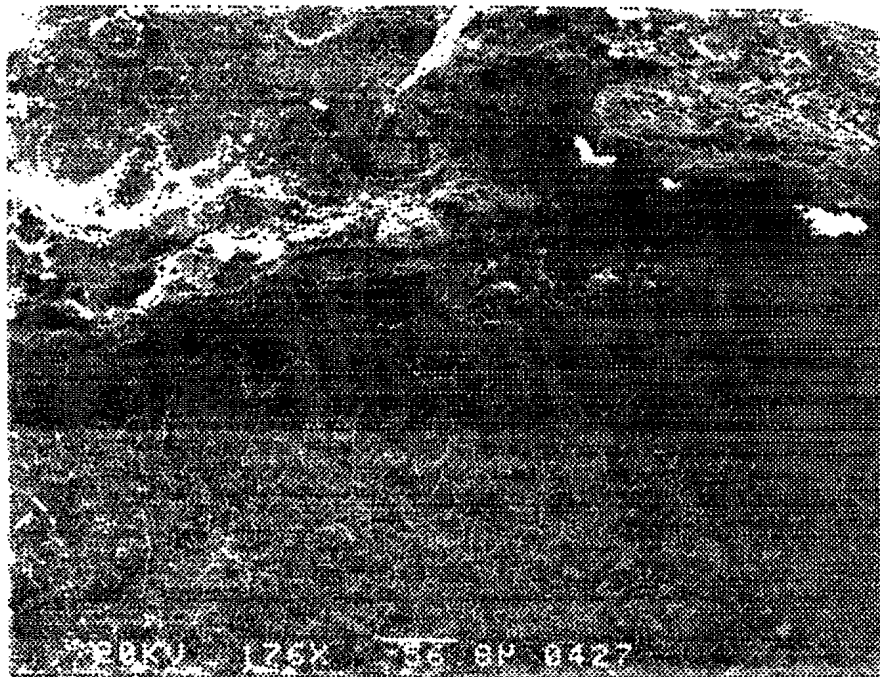


FIGURE A.53: Specimen 14, Position 1 (176 X).

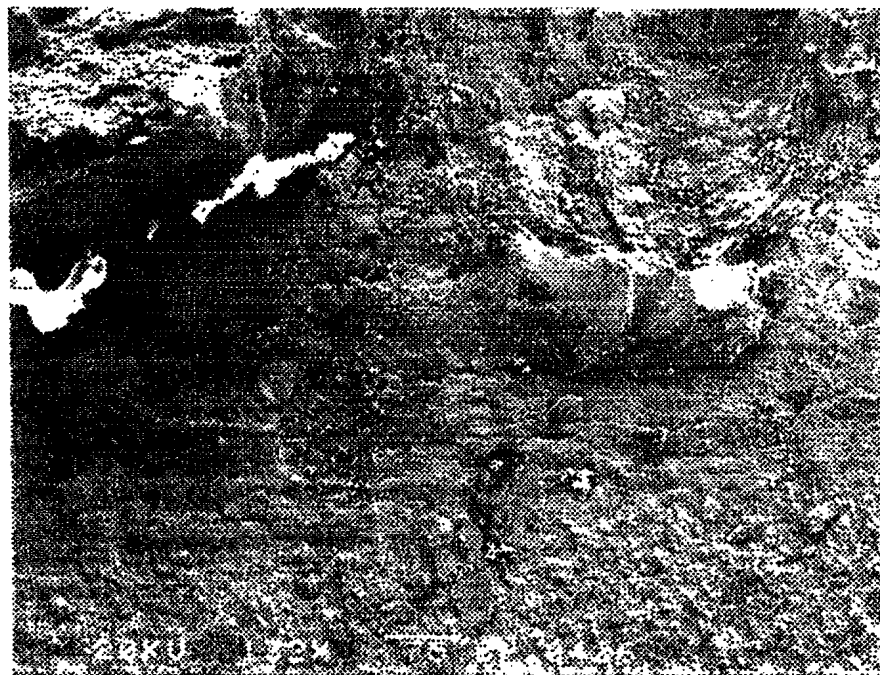


FIGURE A.54: Specimen 14, Position 2 (176 X).

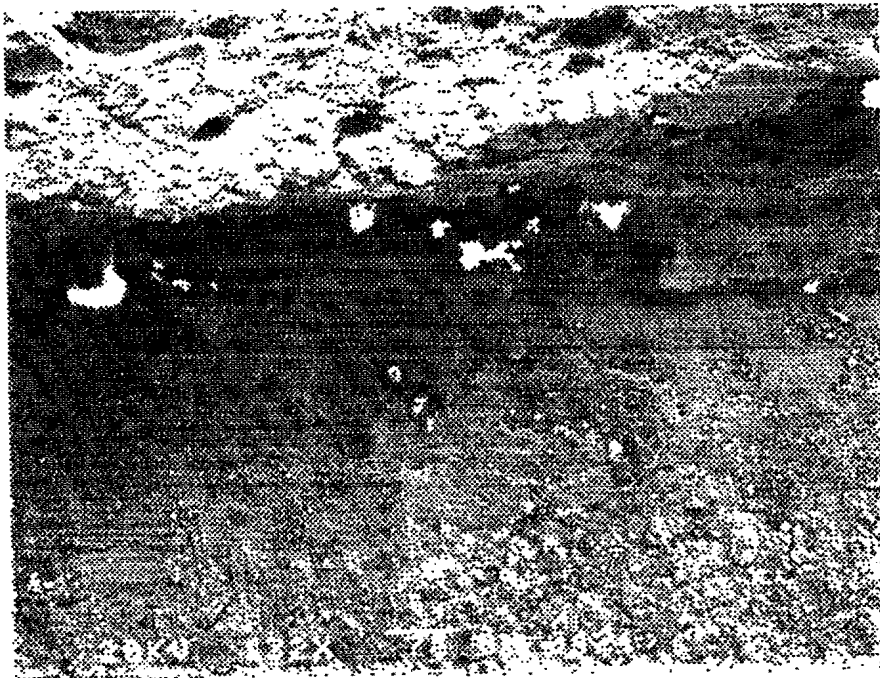


FIGURE A.55: Specimen 14, Position 3 (132 X).

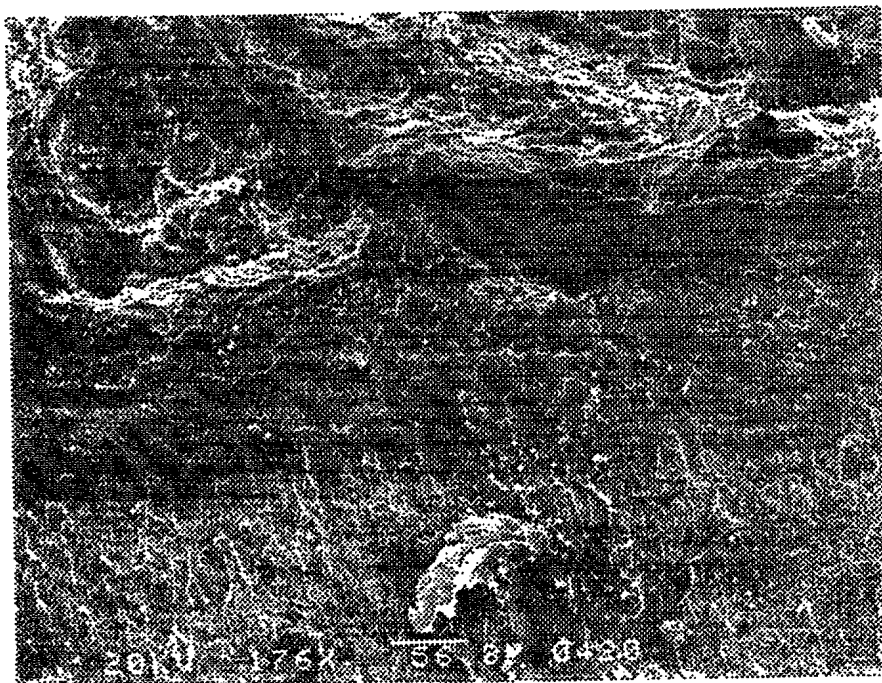


FIGURE A.56: Specimen 14, Position 4 (132 X).

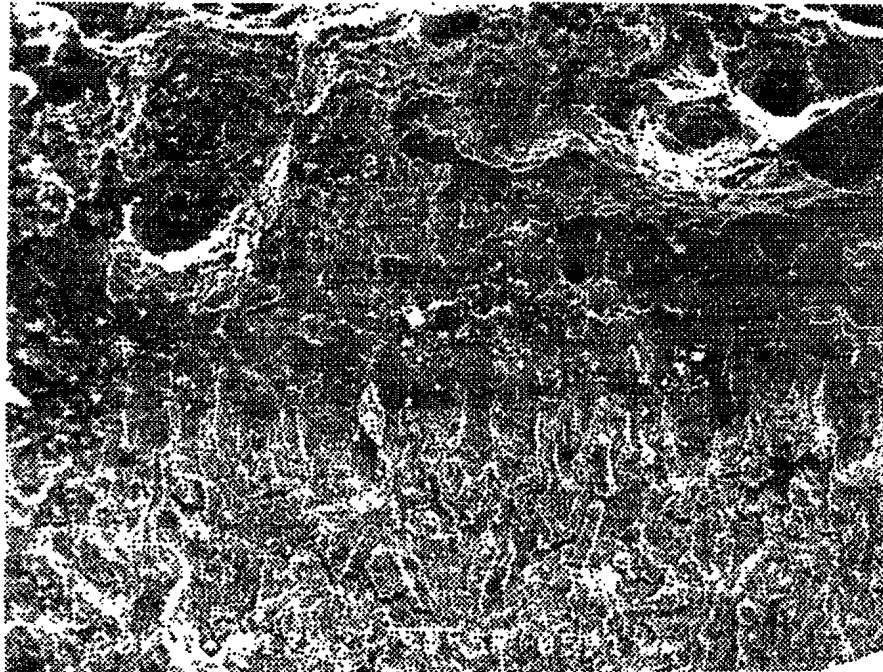


FIGURE A.57: Specimen 15, Position 1 (317 X).

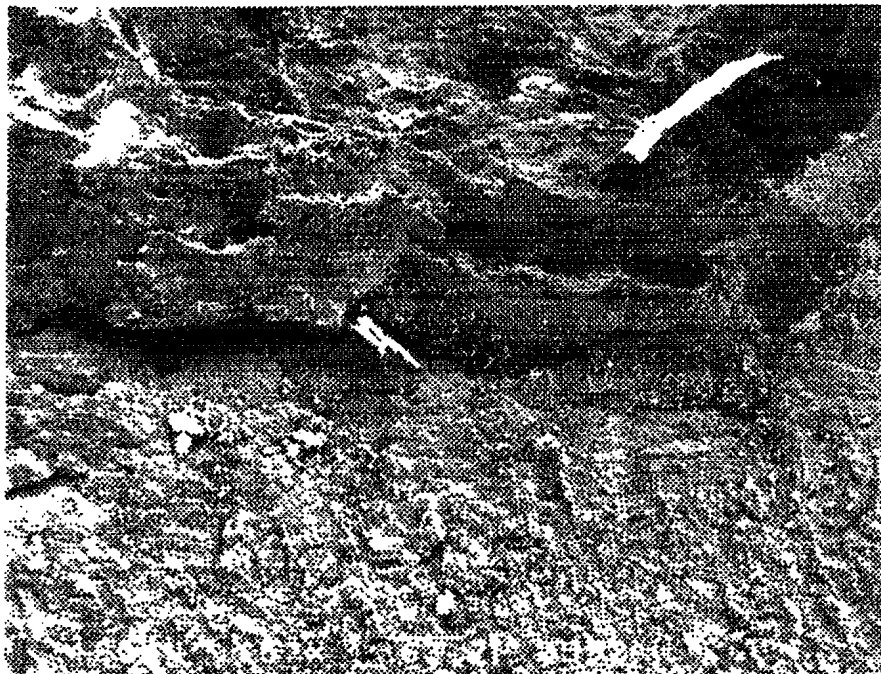


FIGURE A.58: Specimen 15, Position 2 (157 X).

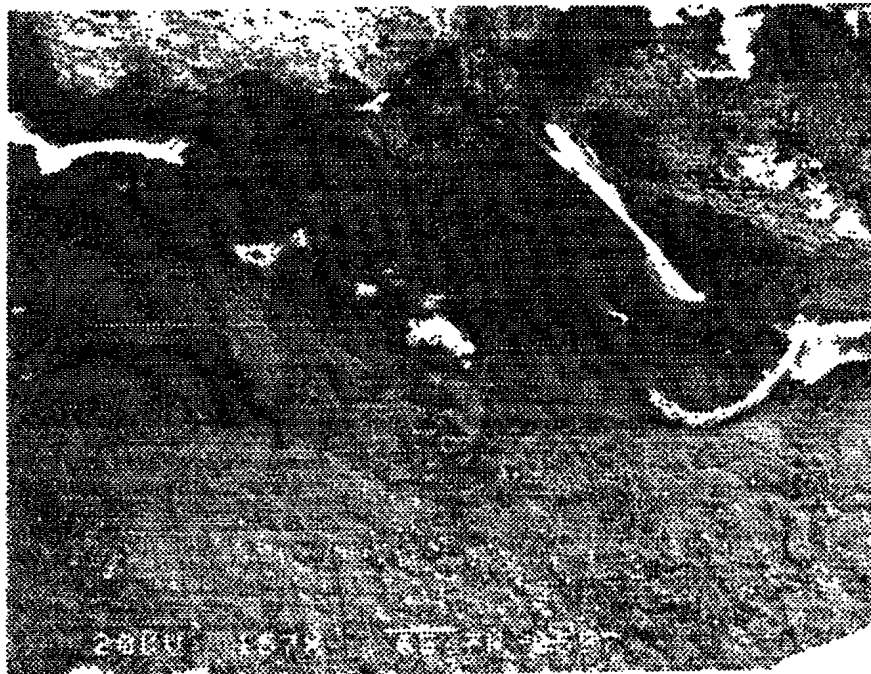


FIGURE A.59: Specimen 15, Position 3 (157 X).

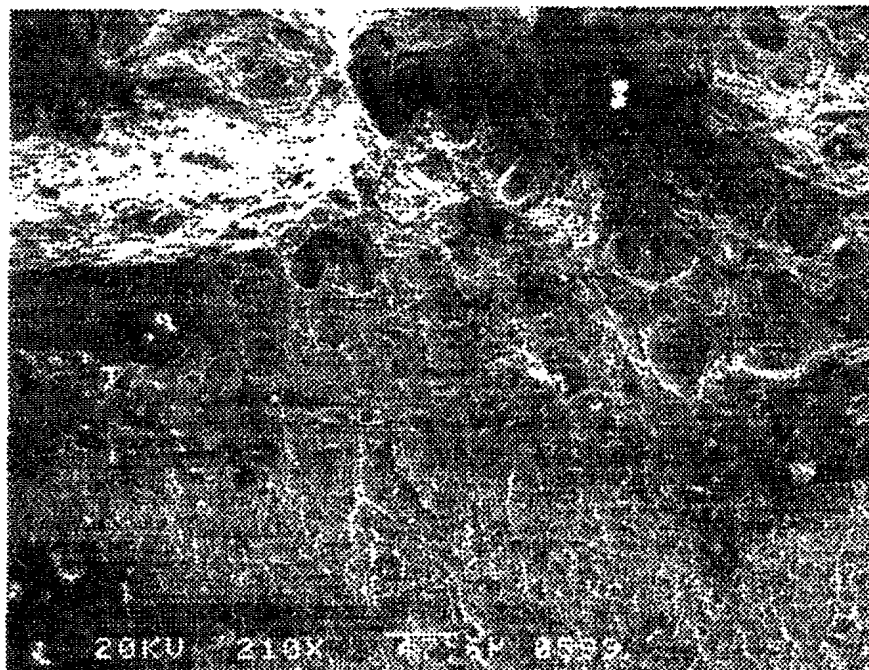


FIGURE A.60: Specimen 15, Position 4 (210 X).

FIGURE A.62: Specimen 16, Position 2 (260 X).

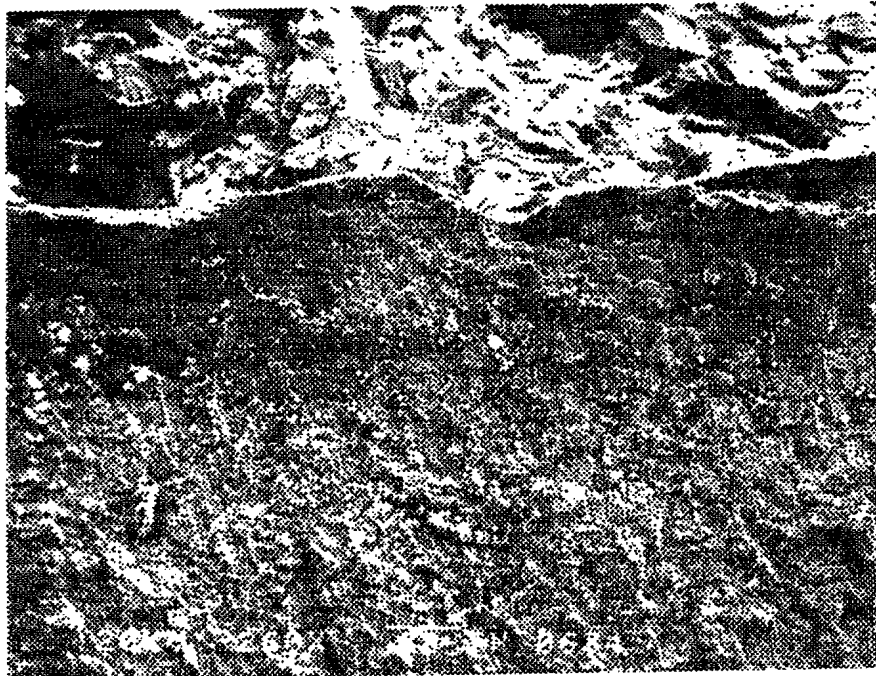


FIGURE A.63: Specimen 16, Position 3 (259 X).

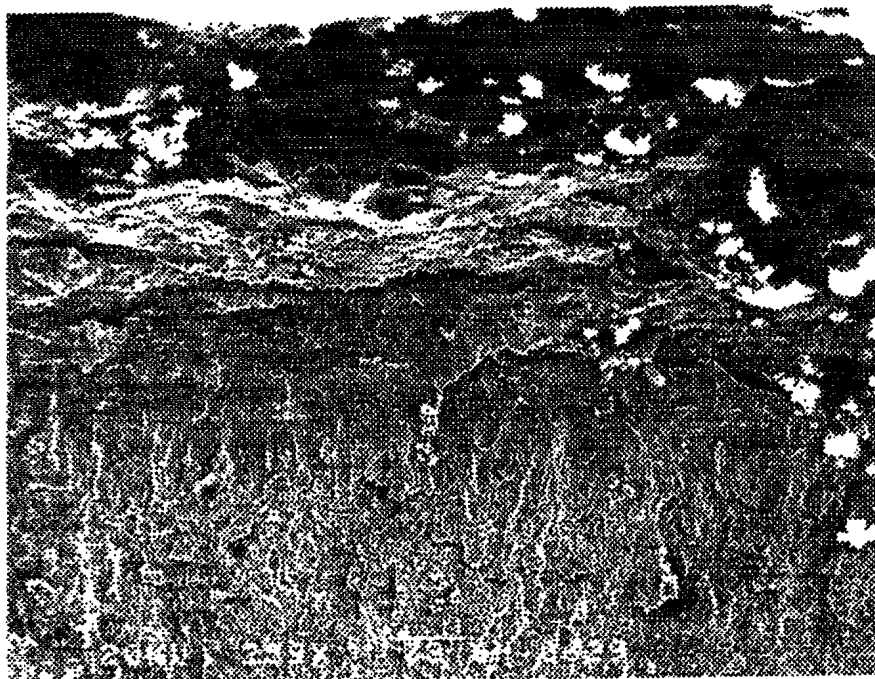


FIGURE A.64: Specimen 16, Position 4 (259 X).

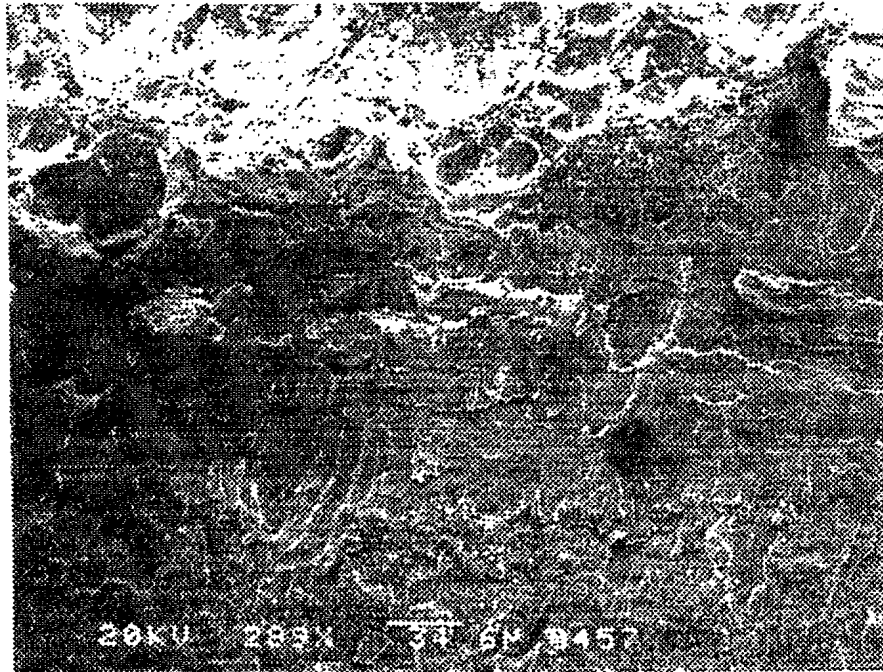


FIGURE A.65: Specimen 20, Position 1 (289 X).

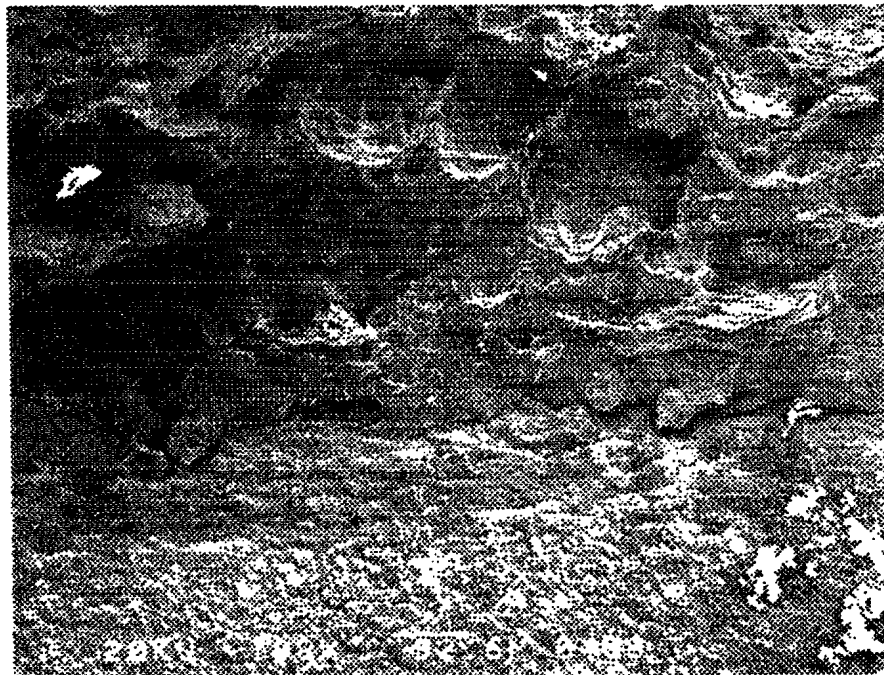


FIGURE A.66: Specimen 20, Position 2 (108 X).

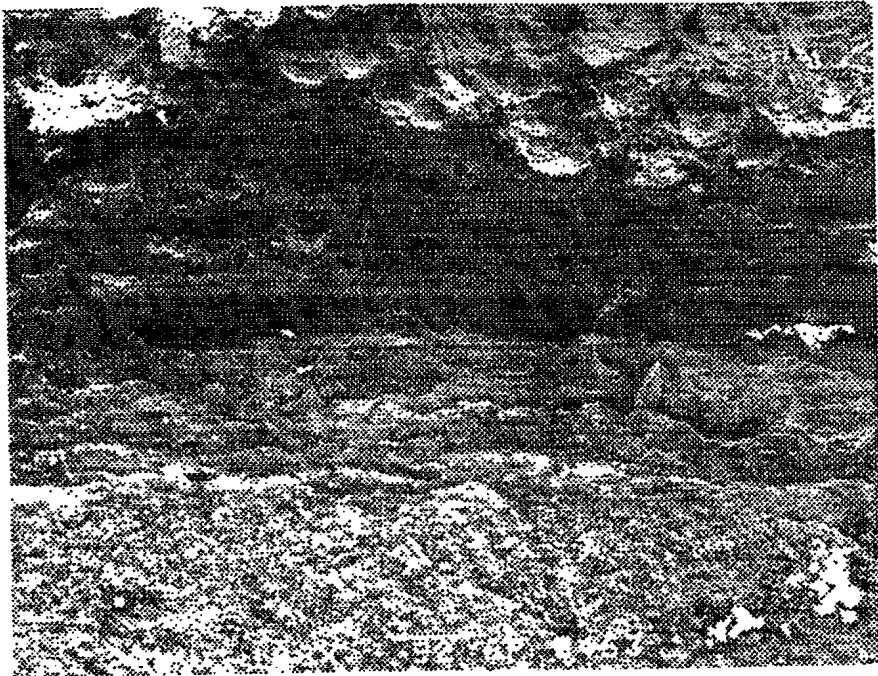


FIGURE A.67: Specimen 20, Position 3 (108 X).

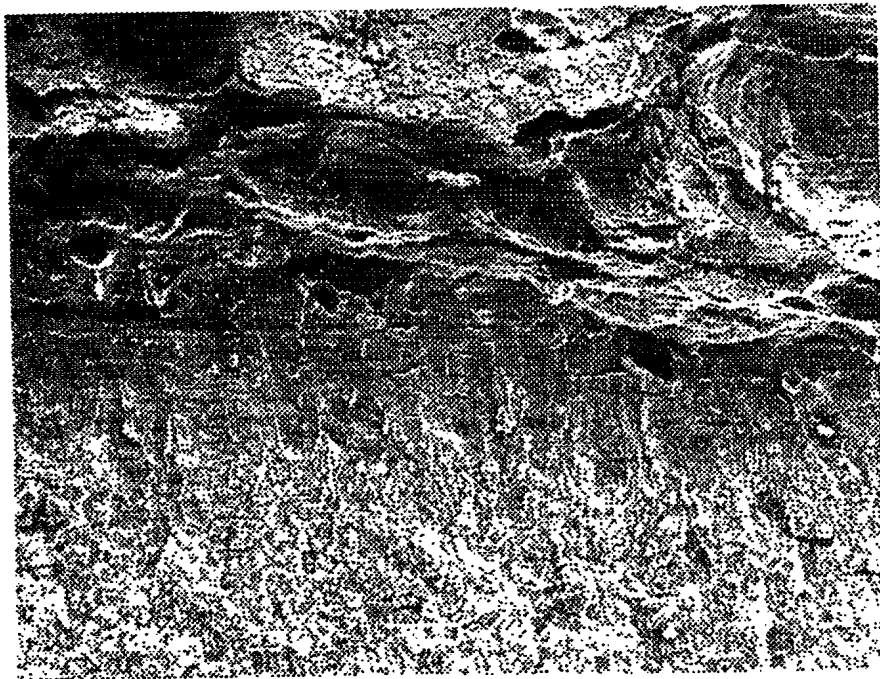


FIGURE A.68: Specimen 20, Position 4 290(X).

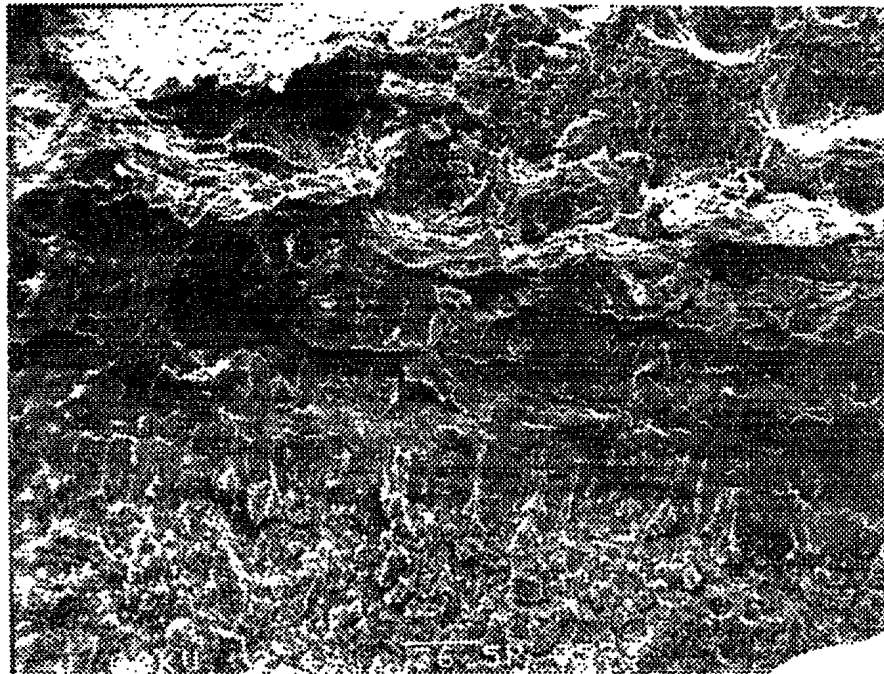


FIGURE A.69: Specimen 21, Position 1 (274 X).



FIGURE A.70: Specimen 21, Position 2 (180 X).

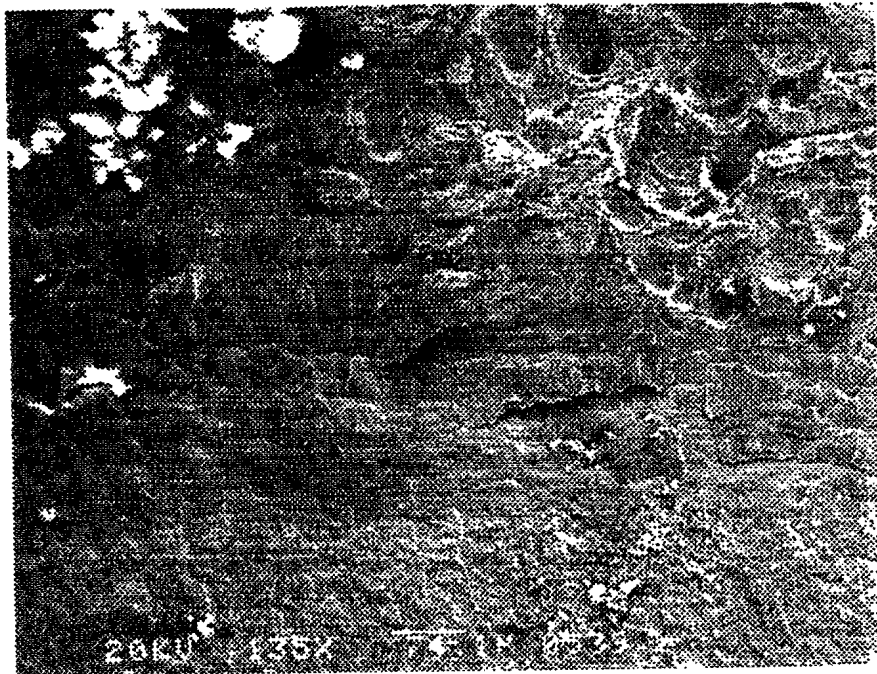


FIGURE A.71: Specimen 21, Position 3 (135 X).

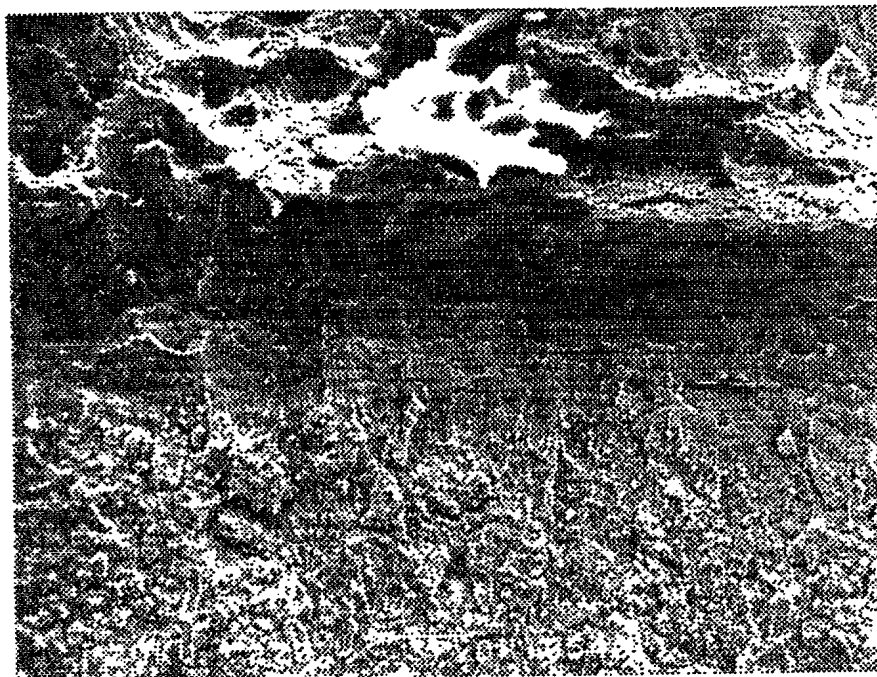


FIGURE A.72: Specimen 21, Position 4 (270 X).

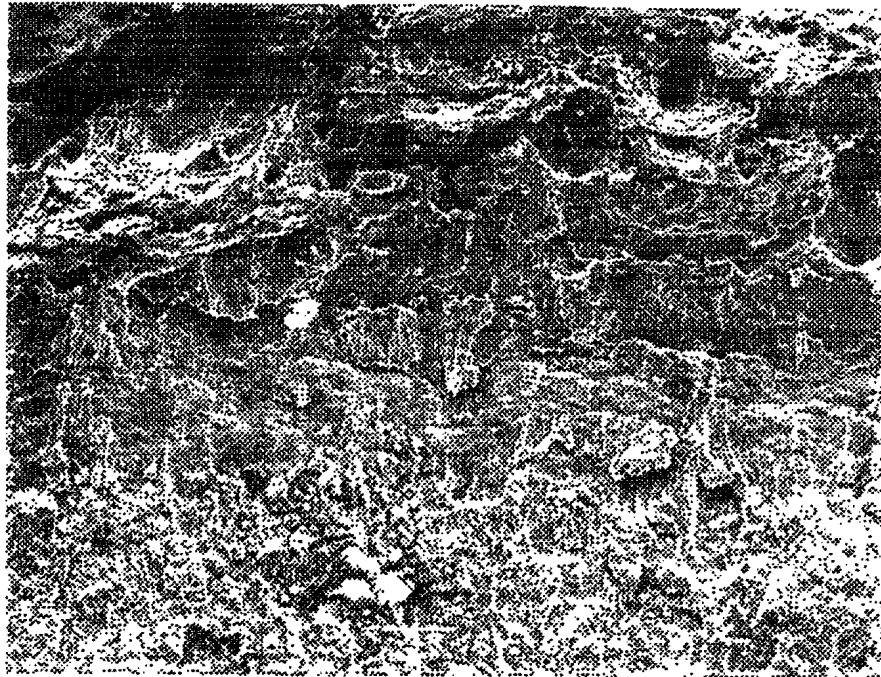


FIGURE A.73: Specimen 22, Position 1 (266 X).

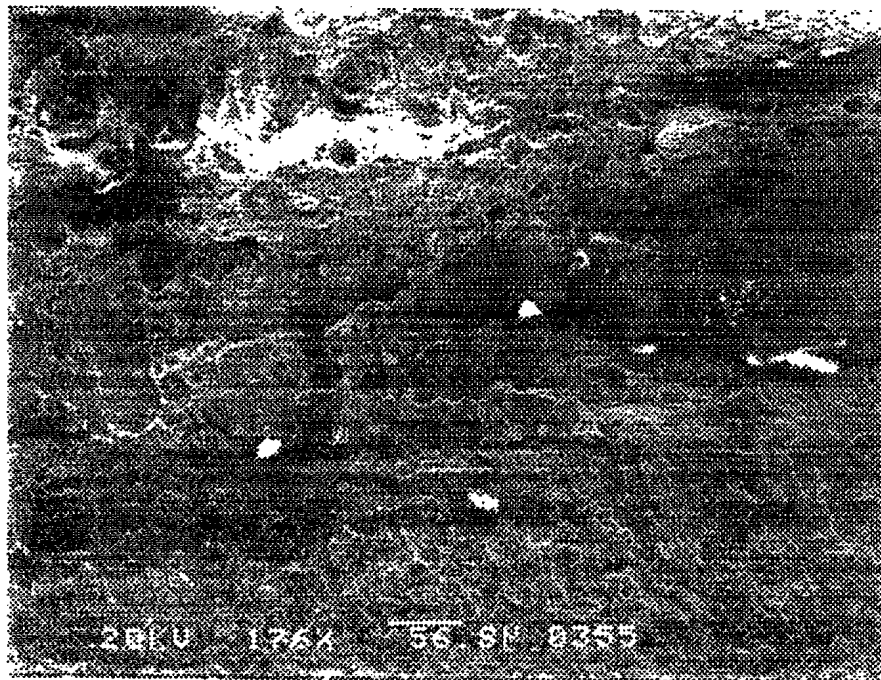


FIGURE A.74: Specimen 22, Position 2 (176 X).

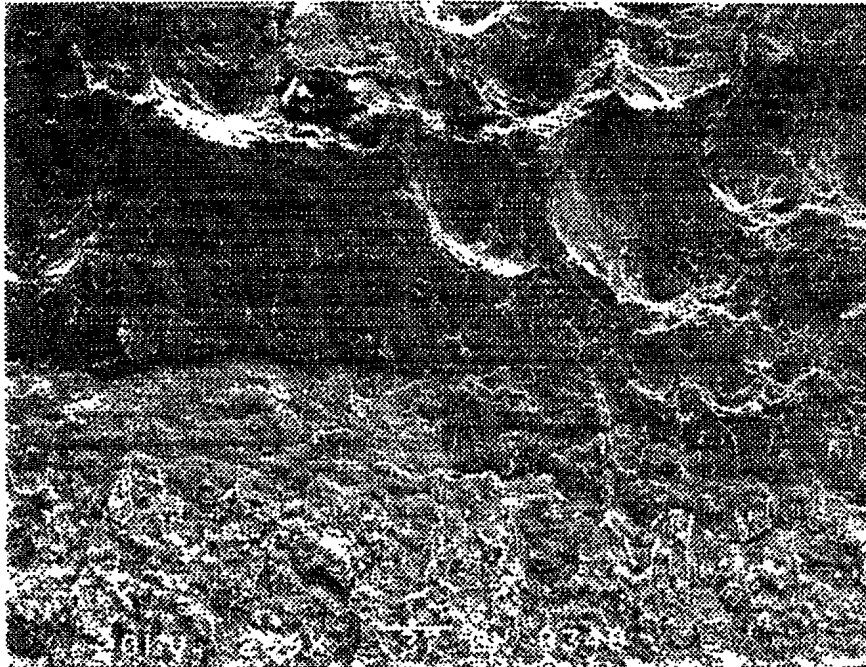


FIGURE A.75: Specimen 22, Position 3 (269 X).

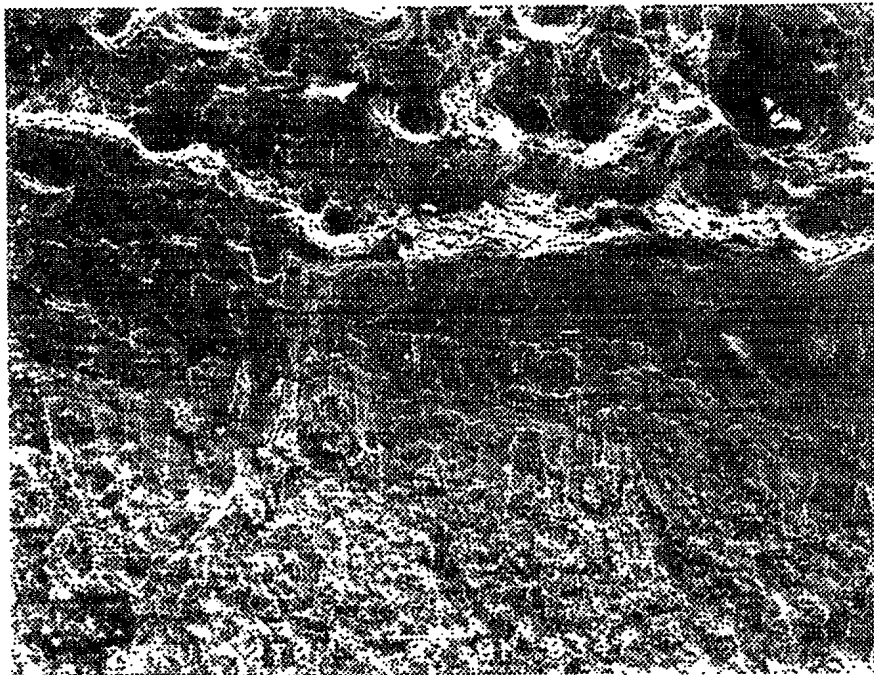


FIGURE A.76: Specimen 22, Position 4 (270 X).

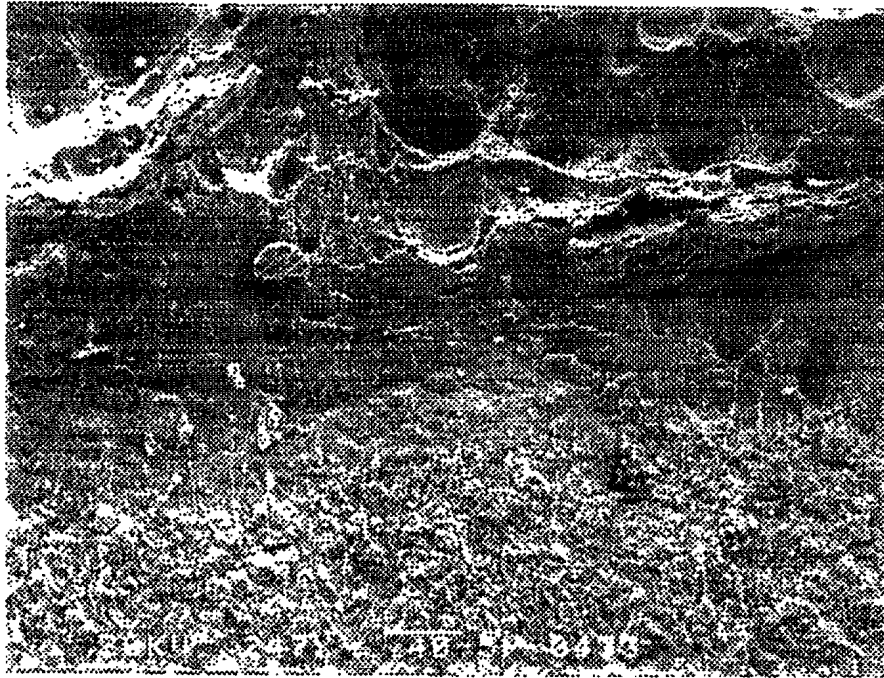


FIGURE A.77: Specimen 23, Position 1 (246 X).

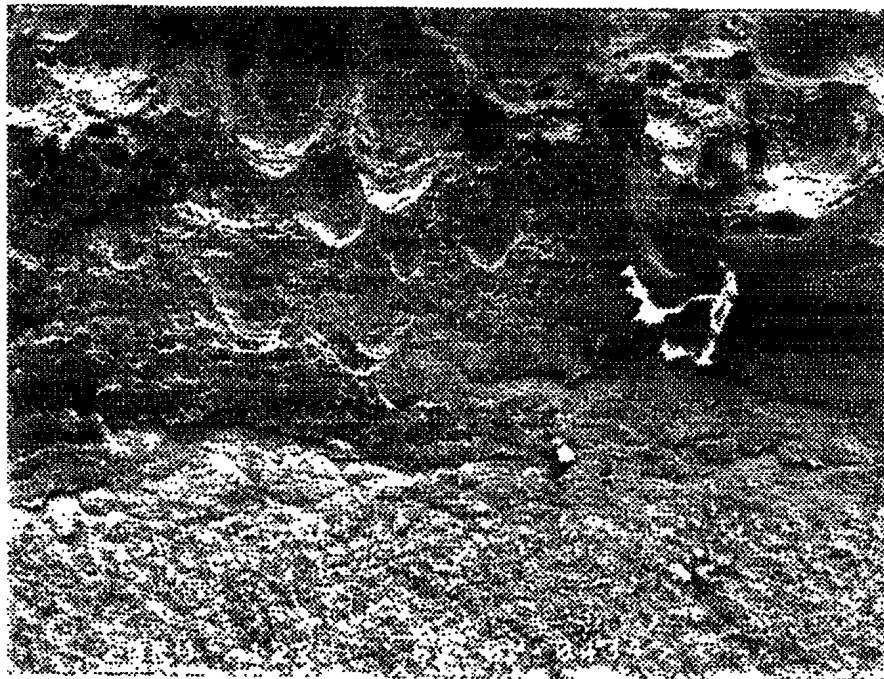


FIGURE A.78: Specimen 23, Position 2 (122 X).

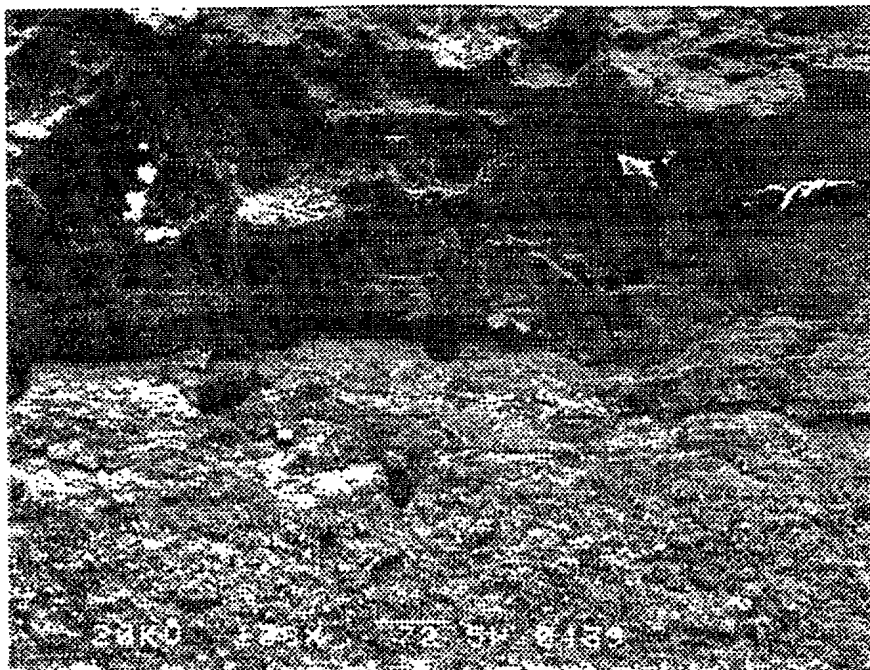


FIGURE A.79: Specimen 23, Position 3 (137 X).

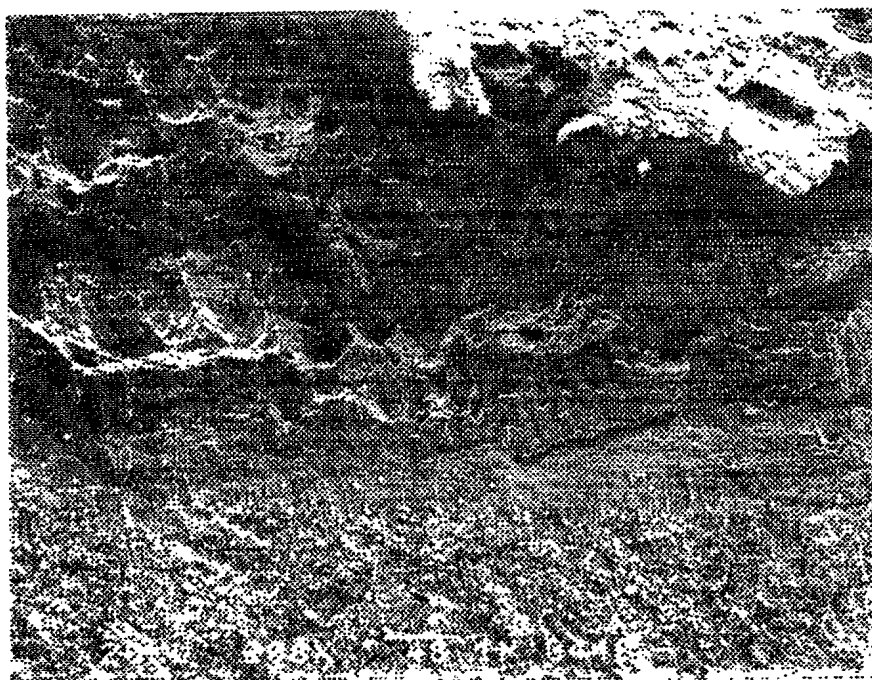


FIGURE A.80: Specimen 23, Position 4 (208 X).

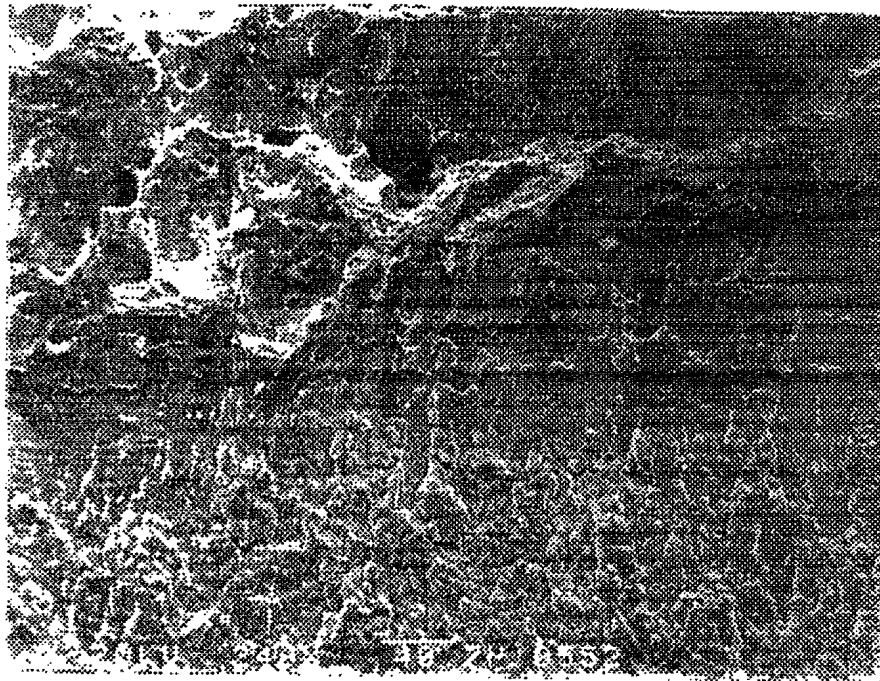


FIGURE A.81: Specimen 24, Position 1 (246 X).

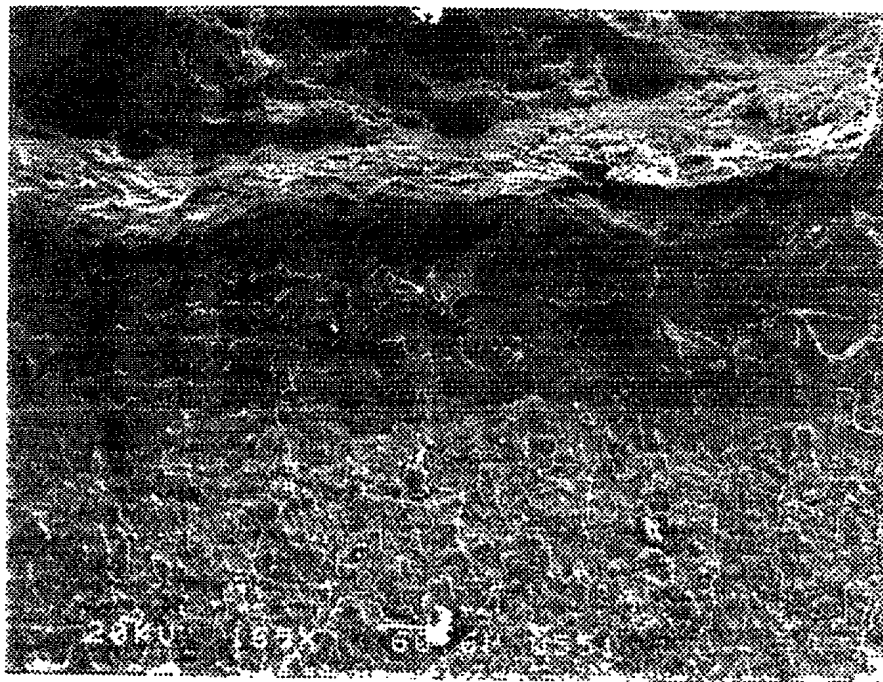


FIGURE A.82: Specimen 24, Position 2 (165 X).

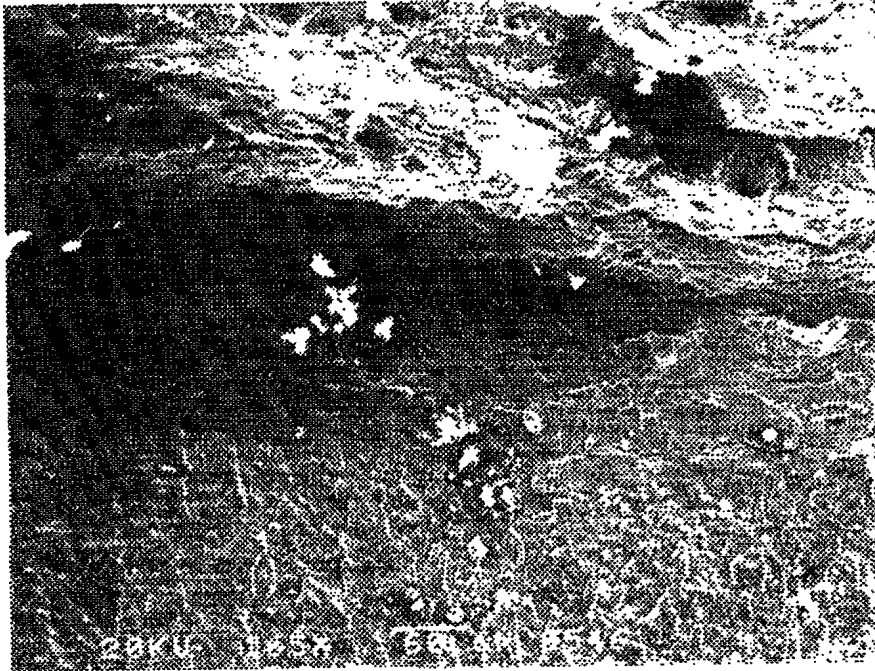


FIGURE A.83: Specimen 24, Position 3 (165 X).

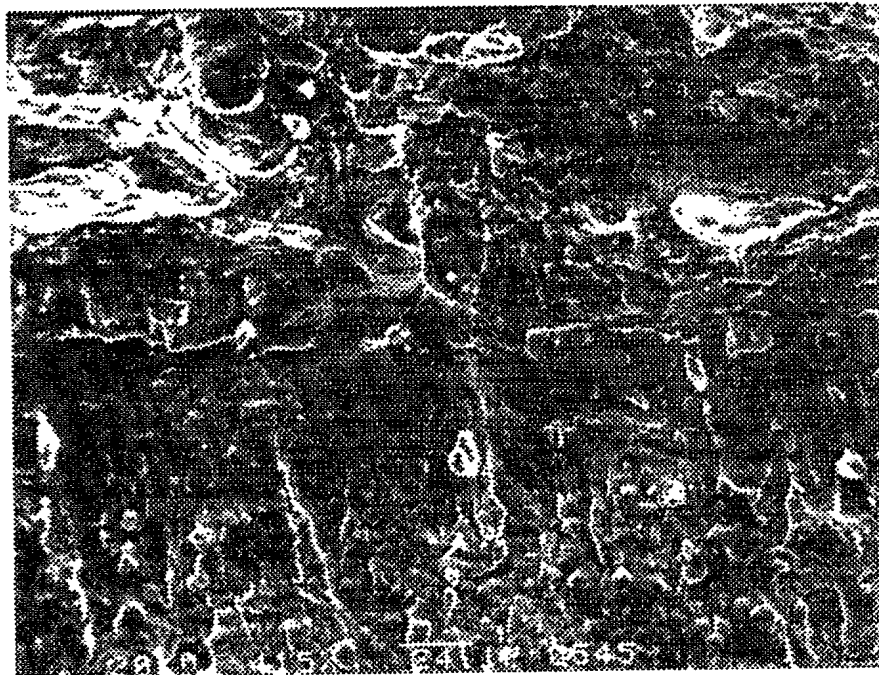


FIGURE A.84: Specimen 24, Position 4 (415 X).

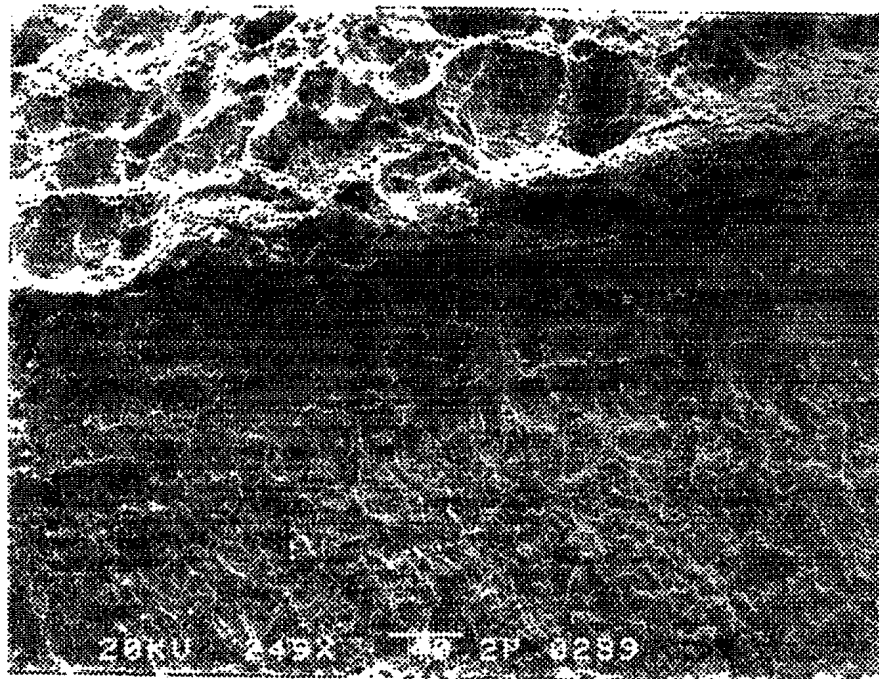


FIGURE A.85: Specimen 25, Position 1 (249 X).

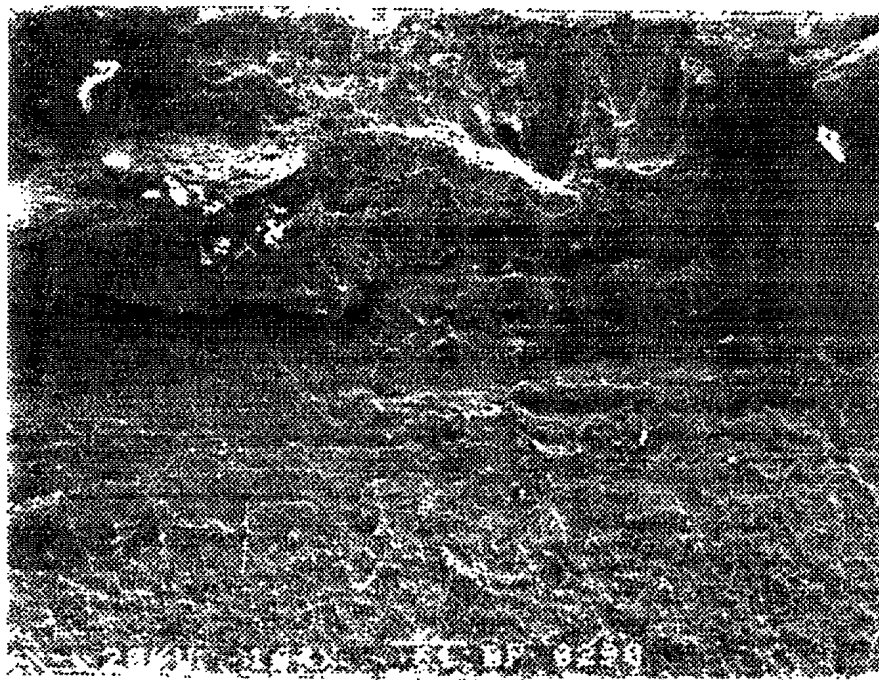


FIGURE A.86: Specimen 25, Position 2 (164 X).

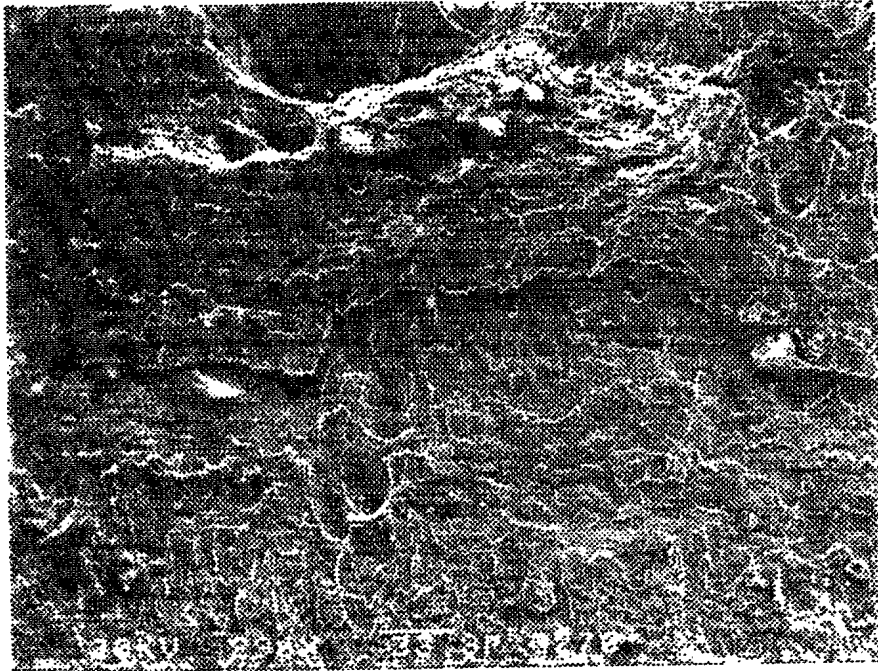


FIGURE A.87: Specimen 25, Position 3 (295 X).

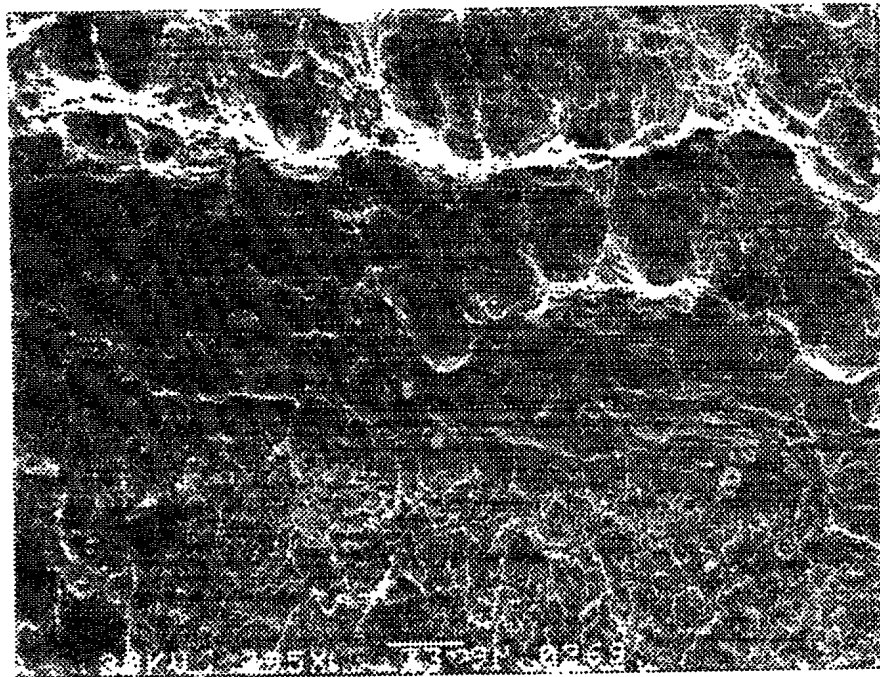


FIGURE A.88: Specimen 25, Position 4 (249 X).

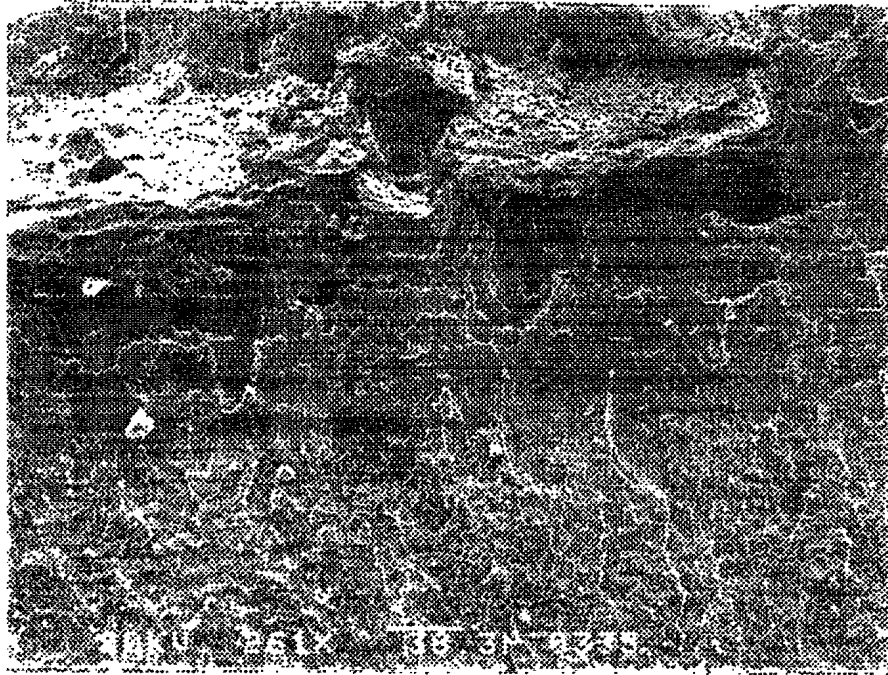


FIGURE A.89: Specimen 26, Position 1 (261 X).

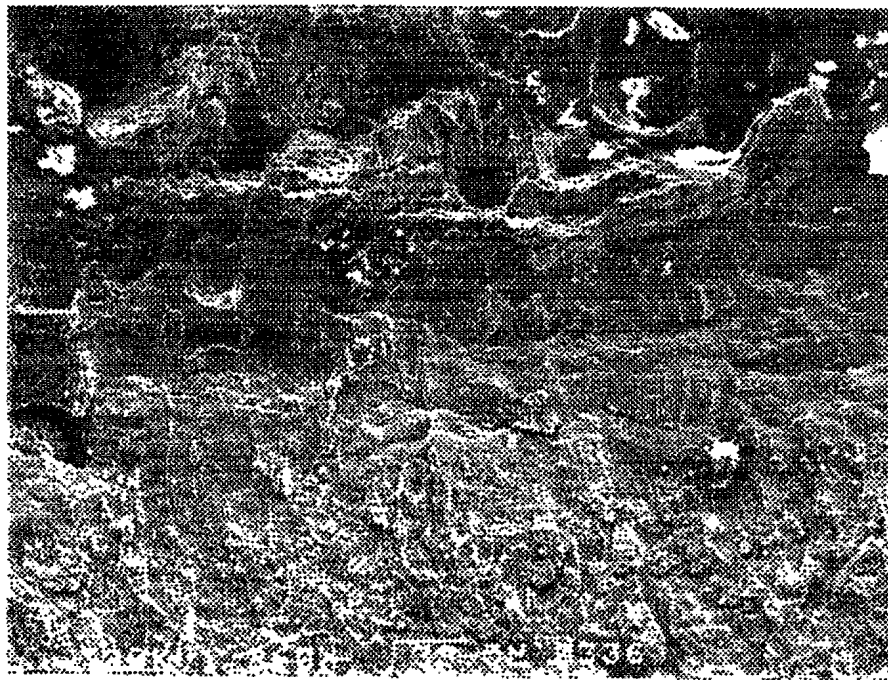


FIGURE A.90: Specimen 26, Position 2 (260 X).

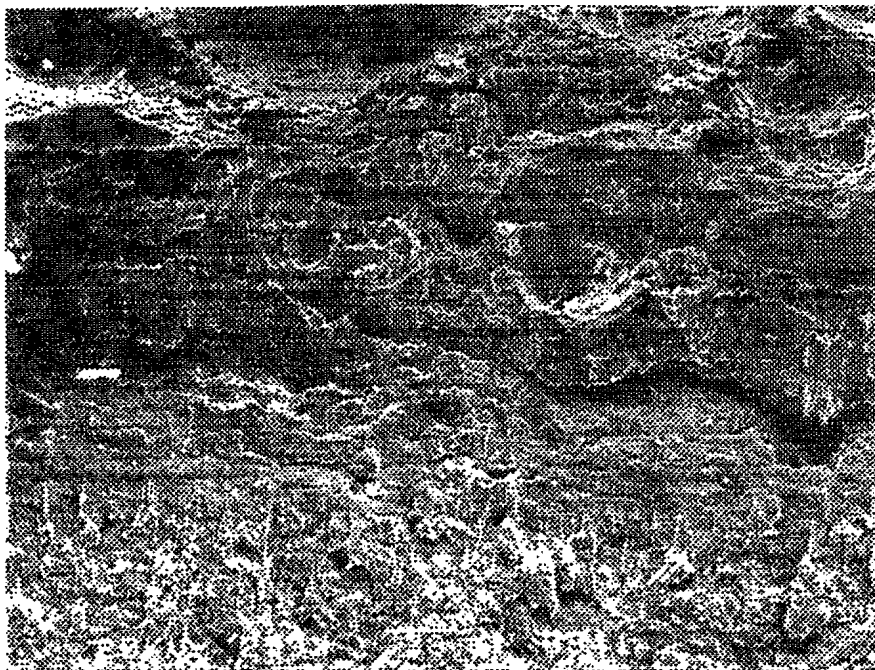


FIGURE A.91: Specimen 26, Position 3 (259 X).

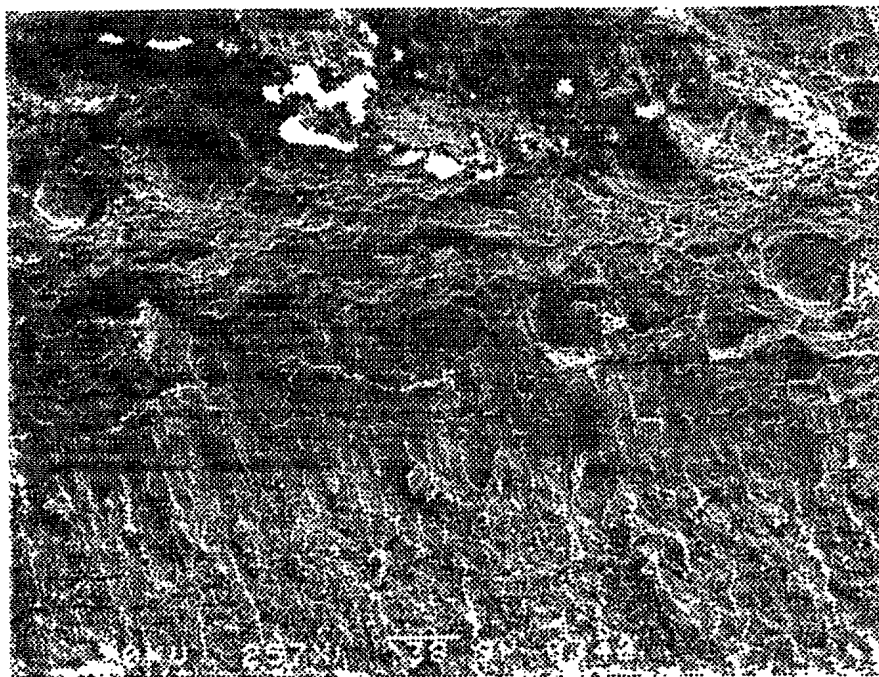


FIGURE A.92: Specimen 26, Position 4 (257 X).



FIGURE A.93: Specimen 27, Position 1 (700 X).

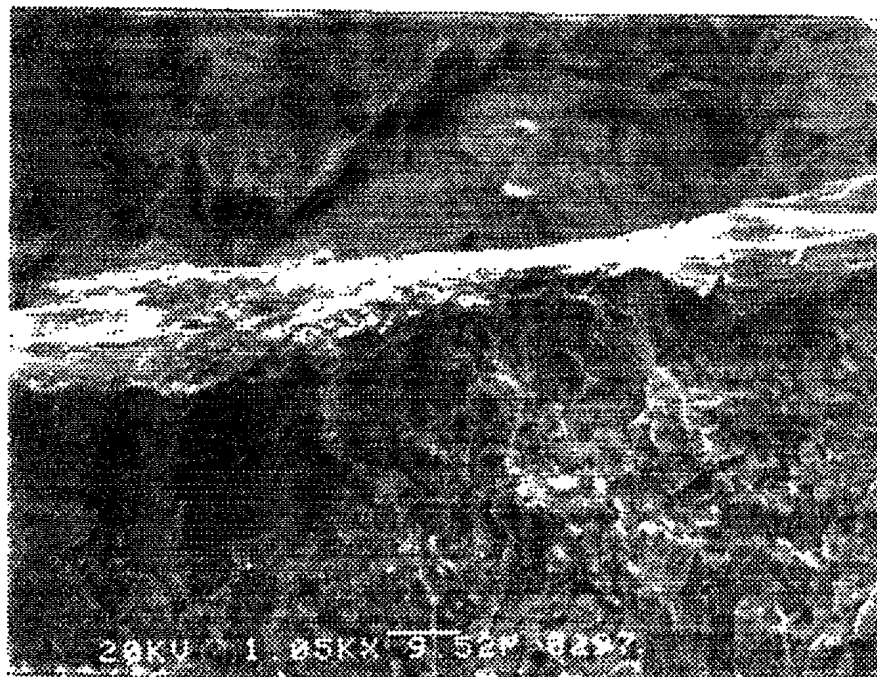


FIGURE A.94: Specimen 27, Position 2 (1050 X).

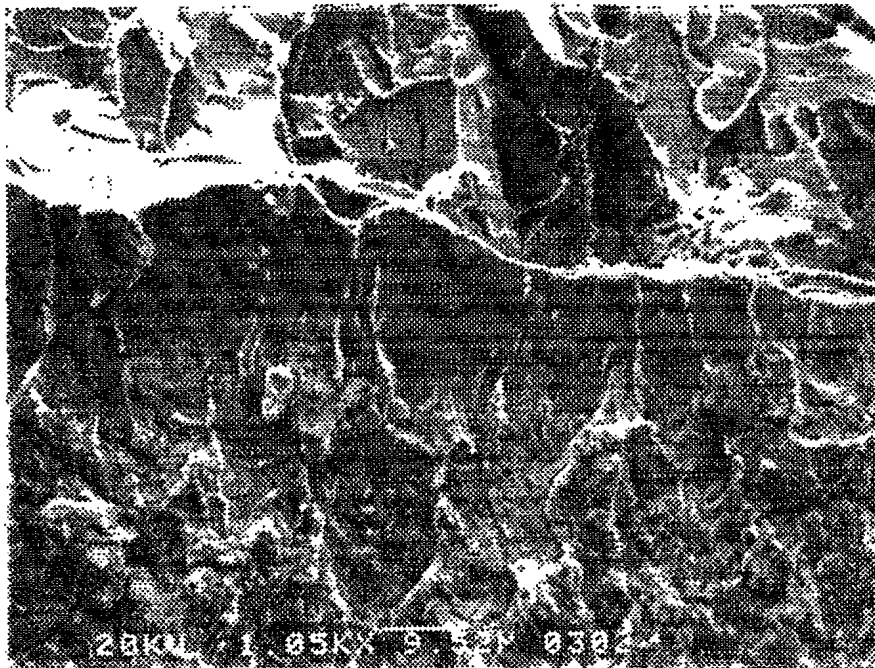


FIGURE A.95: Specimen 27, Position 3 (1050 X).

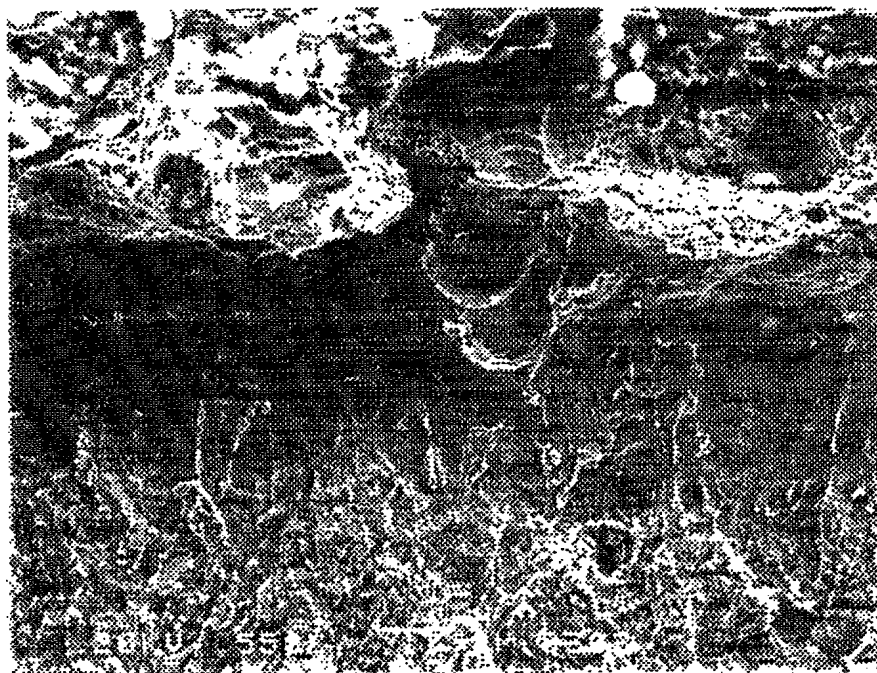


FIGURE A.96: Specimen 27, Position 4 (558 X).

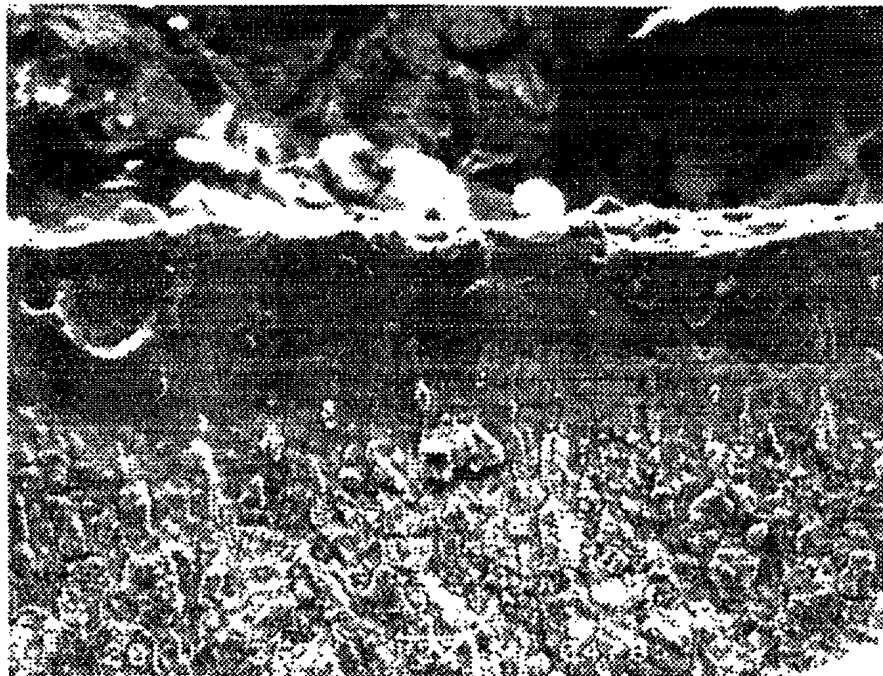


FIGURE A.97: Specimen 31, Position 1 (362 X).

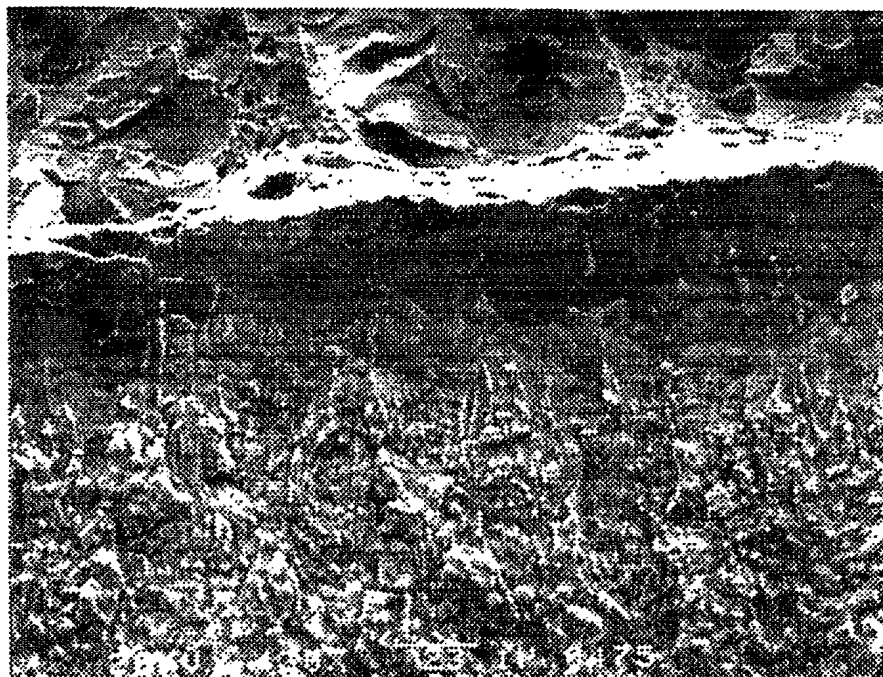


FIGURE A.98: Specimen 31, Position 2 (433 X).

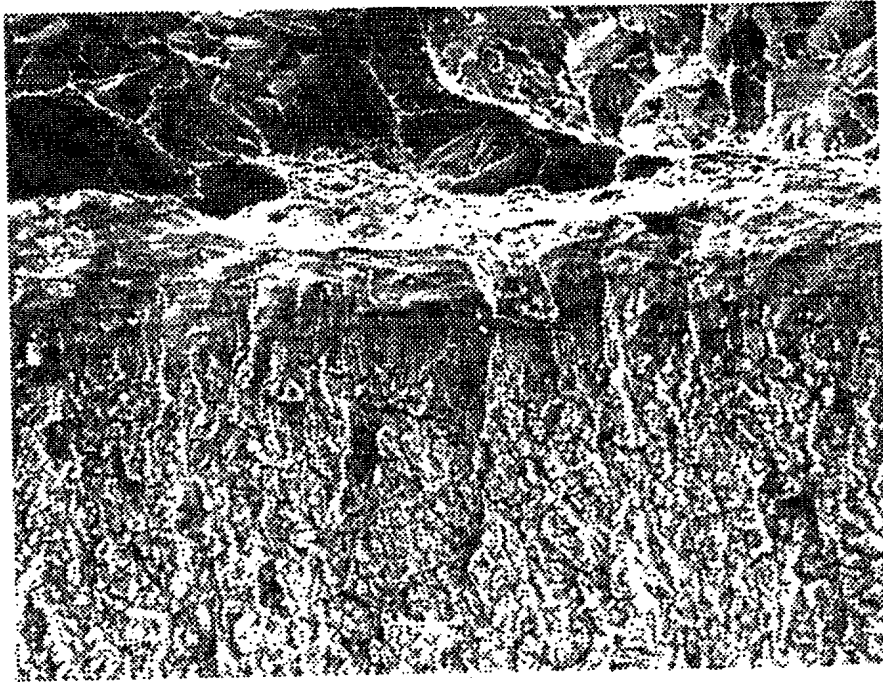


FIGURE A.99: Specimen 31, Position 3 (360 X).

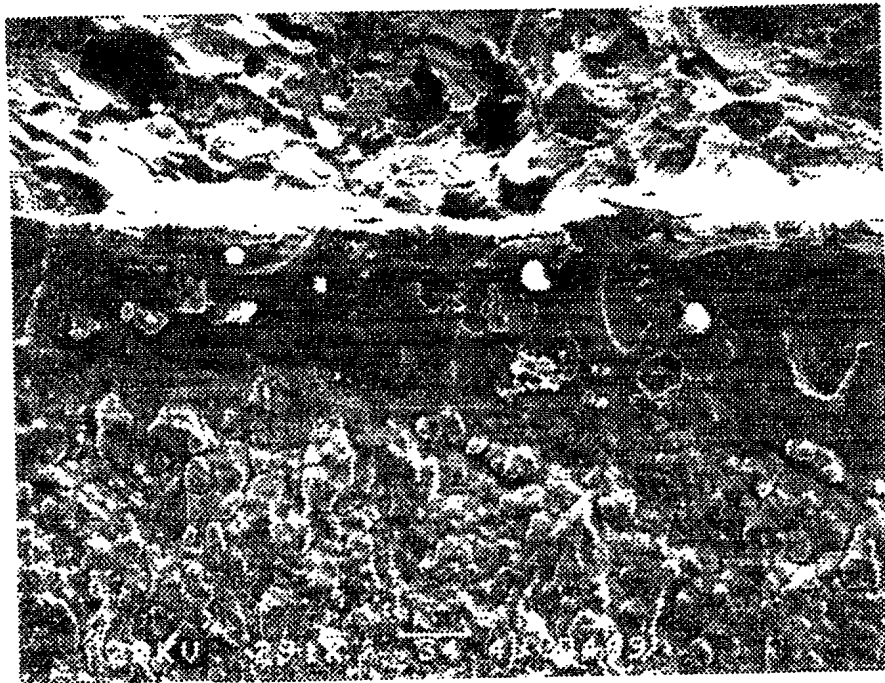


FIGURE A.100: Specimen 31, Position 4 (291 X).

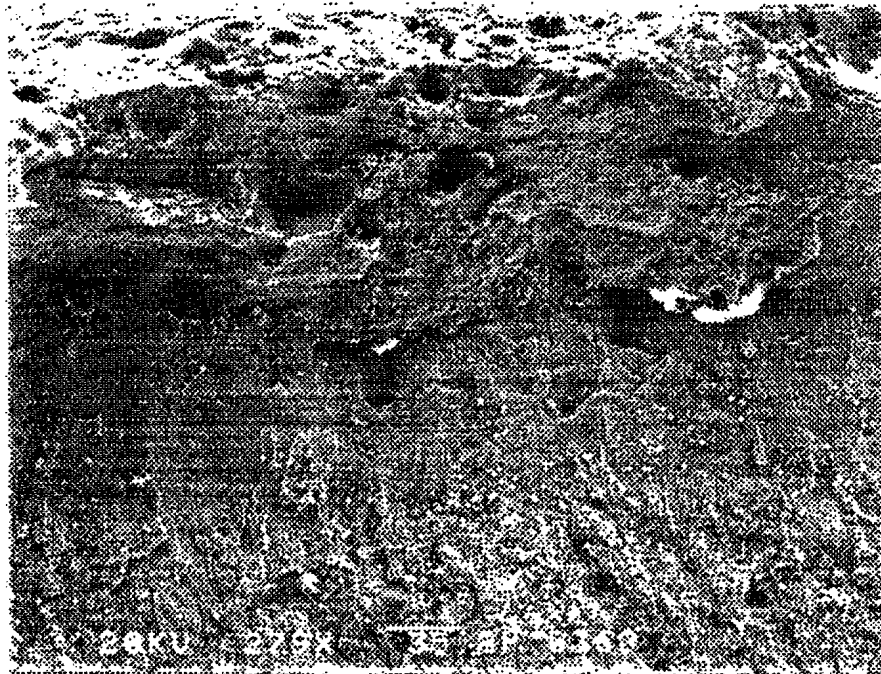


FIGURE A.101: Specimen 32, Position 1 (279 X).

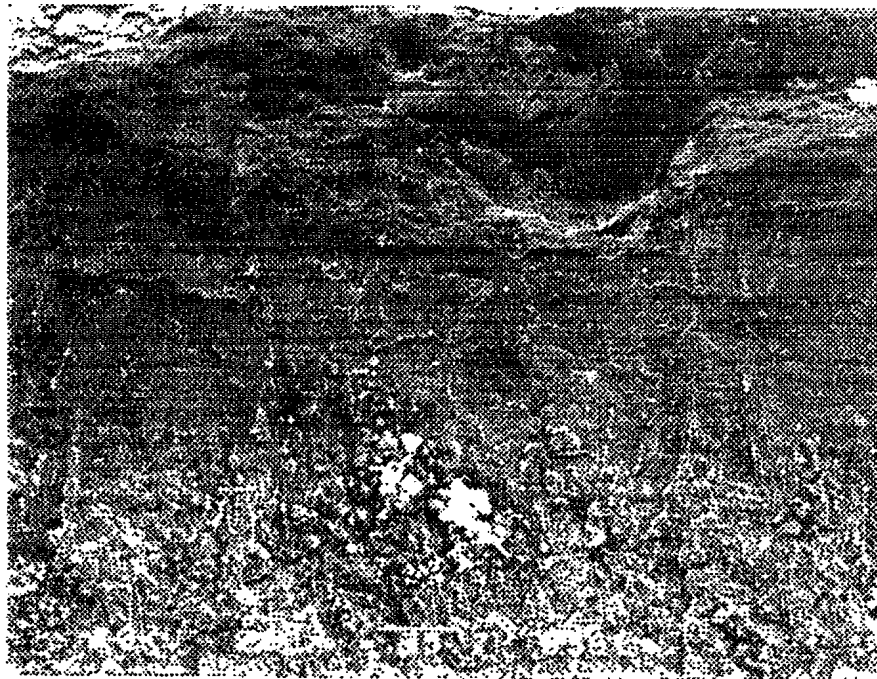


FIGURE A.102: Specimen 32, Position 2 (280 X).

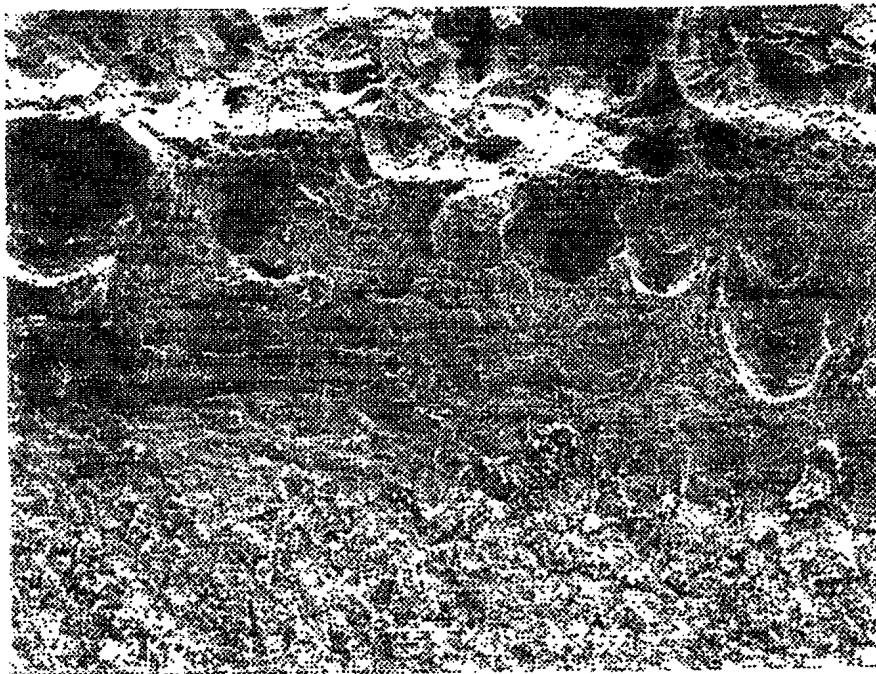


FIGURE A.103: Specimen 32, Position 3 (186 X).

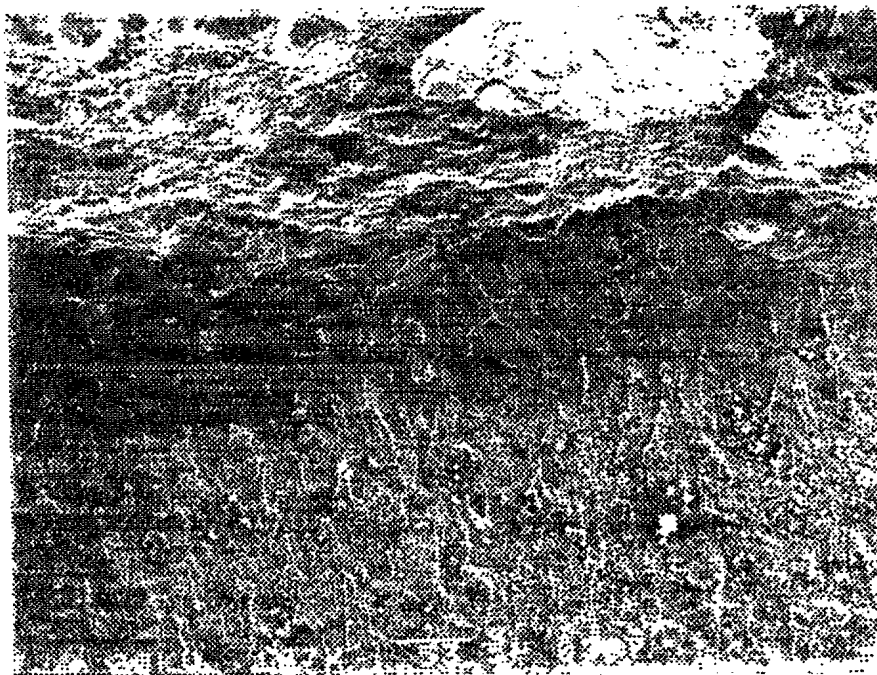


FIGURE A.104: Specimen 32, Position 4 (187 X).

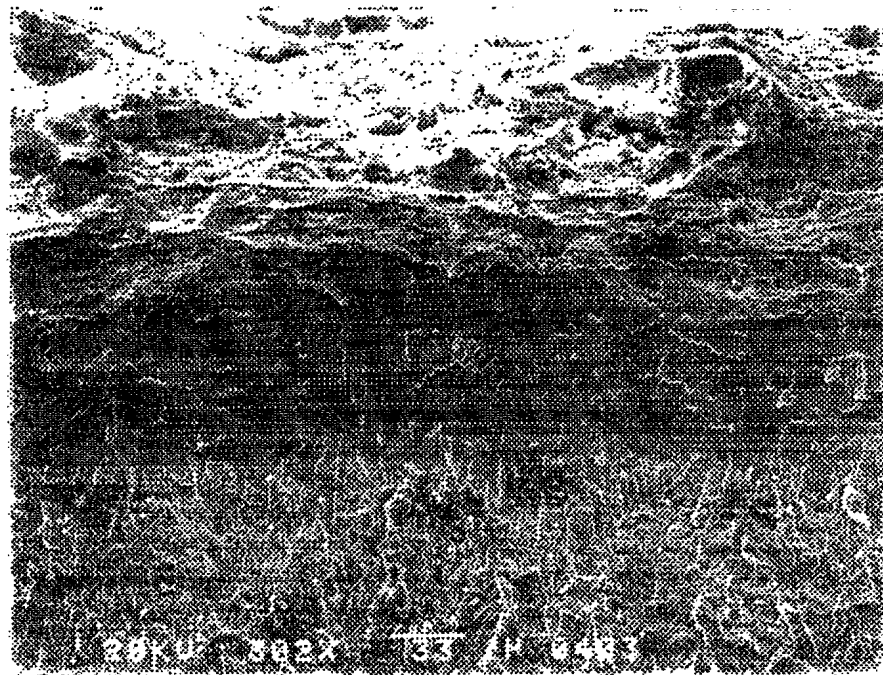


FIGURE A.105: Specimen 33, Position 1 (302 X).



FIGURE A.106: Specimen 33, Position 2 (302 X).

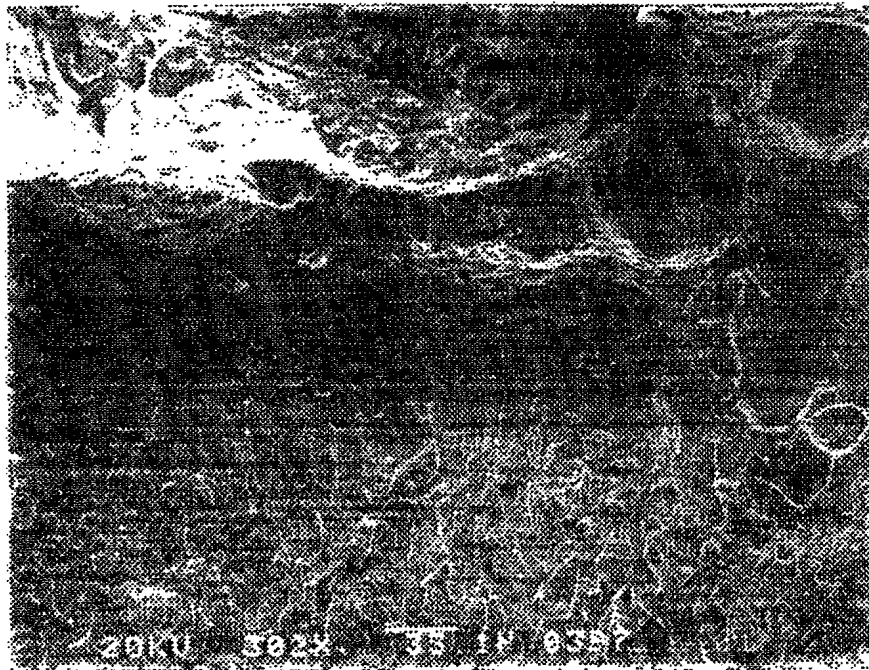


FIGURE A.107: Specimen 33, Position 3 (302 X).

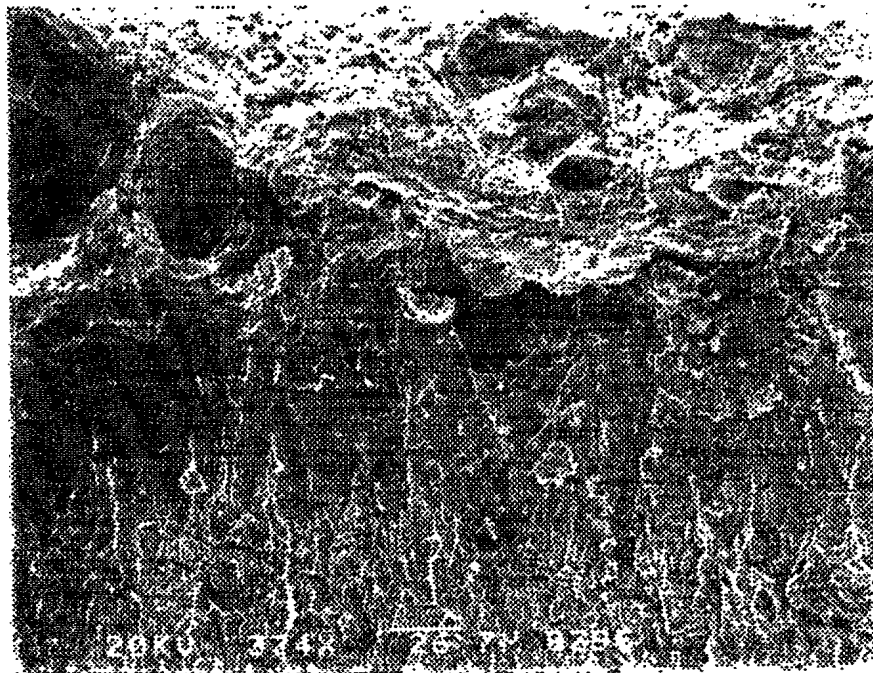


FIGURE A.108: Specimen 33, Position 4 (374 X).

UNCLASSIFIED
 SECURITY CLASSIFICATION OF FORM
 (highest classification of Title, Abstract, Keywords)

DOCUMENT CONTROL DATA		
(Security classification of title, body of abstract and indexing annotation must be entered when the overall document is classified)		
1. ORIGINATOR (the name and address of the organization preparing the document. Organizations for whom the document was prepared, e.g. Establishment sponsoring a contractor's report, or tasking agency, are entered in section 8.) Martec Limited 1888 Brunswick Street, Suite 400 Halifax, N.S. B3J 3J8	2. SECURITY CLASSIFICATION (overall security classification of the document including special warning terms if applicable). <div style="text-align: center; font-size: large;">Unclassified</div>	
3. TITLE (the complete document title as indicated on the title page. Its classification should be indicated by the appropriate abbreviation (S,C,R or U) in parentheses after the title). <div style="text-align: center; font-size: large;">Stretch Zone Measurement of Side-Grooved HSLA 80 Fracture Specimens</div>		
4. AUTHORS (Last name, first name, middle initial. If military, show rank, e.g. Doe, Maj. John E.) <div style="text-align: center; font-size: large;">K. MacKay and M.W. Chernuka</div>		
5. DATE OF PUBLICATION (month and year of publication of document) <div style="text-align: center; font-size: large;">Feb 1995</div>	6a. NO OF PAGES (total containing information include Annexes, Appendices, etc). <div style="text-align: center; font-size: large;">94</div>	6b. NO. OF REFS (total cited in document) <div style="text-align: center; font-size: large;">4</div>
7. DESCRIPTIVE NOTES (the category of the document, e.g. technical report, technical note or memorandum. If appropriate, enter the type of report, e.g. interim, progress, summary, annual or final. Give the inclusive dates when a specific reporting period is covered). <div style="text-align: center; font-size: large;">Contractor Report (final)</div>		
8. SPONSORING ACTIVITY (the name of the department project office or laboratory sponsoring the research and development. Include the address). Defence Research Establishment Atlantic P.O. Box 1012 Dartmouth, N.S. B2Y 3Z7		
9a. PROJECT OR GRANT NO. (if appropriate, the applicable research and development project or grant number under which the document was written. Please specify whether project or grant). <div style="text-align: center; font-size: large;">1AI</div>	9b. CONTRACT NO. (if appropriate, the applicable number under which the document was written). <div style="text-align: center; font-size: large;">W7707-4-2878/01-OSC</div>	
10a. ORIGINATOR'S DOCUMENT NUMBER (the official document number by which the document is identified by the originating activity. This number must be unique to this document). <div style="text-align: center; font-size: large;">DREA CR/95/406</div>	10b. OTHER DOCUMENT NOS. (Any other numbers which may be assigned this document either by the originator or by the sponsor). <div style="text-align: center; font-size: large;">N/A</div>	
11. DOCUMENT AVAILABILITY (any limitations on further dissemination of the document, other than those imposed by security classification) <div style="font-size: small;"> <input checked="" type="checkbox"/> Unlimited distribution <input type="checkbox"/> Distribution limited to defence departments and defence contractors; further distribution only as approved <input type="checkbox"/> Distribution limited to defence departments and Canadian defence contractors; further distribution only as approved <input type="checkbox"/> Distribution limited to government departments and agencies; further distribution only as approved <input type="checkbox"/> Distribution limited to defence departments; further distribution only as approved <input type="checkbox"/> Other (please specify): </div>		
12. DOCUMENT ANNOUNCEMENT (any limitation to the bibliographic announcement of this document. This will normally correspond to the Document Availability (11). However, where further distribution (beyond the audience specified in 11) is possible, a wider announcement audience may be selected). <div style="text-align: center; font-size: large;">Unlimited</div>		

UNCLASSIFIED
 SECURITY CLASSIFICATION OF FORM

DCD03 2/06/87-M

UNCLASSIFIED
SECURITY CLASSIFICATION OF FORM

13. **ABSTRACT** (a brief and factual summary of the document. It may also appear elsewhere in the body of the document itself. It is highly desirable that the abstract of classified documents be unclassified. Each paragraph of the abstract shall begin with an indication of the security classification of the information in the paragraph (unless the document itself is unclassified) represented as (S), (C), (R), or (U). It is not necessary to include here abstracts in both official languages unless the text is bilingual).

Stereoscopic imaging with a scanning electron microscope was used to measure stretch zone width on the fracture surfaces of side grooved HSLA 80 SENB fracture specimens which were tested over a range of temperatures (-42°C to 22°C) and loading rates (0.01 to 2710 mm/s). The data were examined to determine the relationship between stretch zone width and temperature at constant loading rate, and the relationship between stretch zone width and loading rate at constant temperature. Measurement error, the limited number of data points, and intrinsic variability collectively limit the confidence with which trends could be determined. For loading rates below 2 mm/s, the stretch zone width increased with temperature until a limiting temperature of -20°C was reached. Beyond this temperature the variation in stretch zone was less than the measurement error. At a loading rate of 2710 mm/s, the stretch zone width appeared to increase linearly with temperature over the range of -5°C to 15°C. The variation in stretch zone width with loading rate was less than the measurement error over the range of 0.01 to 60 mm/s. There appeared to be a decrease in stretch zone width when the loading rate was increased to 2710 mm/s. For specimens which exhibited stable crack growth after blunting, the stretch zone width was greater in the central region of the specimen than at the edges. For specimens which exhibited unstable (brittle) crack extension immediately after the stretch zone, the stretch zone width was essentially uniform across the specimen.


14. **KEYWORDS, DESCRIPTORS OR IDENTIFIERS** (technically meaningful terms or short phrases that characterize a document and could be helpful in cataloging the document. They should be selected so that no security classification is required. Identifiers, such as equipment model designation, trade name, military project code name, geographic location may also be included. If possible keywords should be selected from a published thesaurus, e.g. Thesaurus of Engineering and Scientific Terms (TEST) and that thesaurus-identified. If it not possible to select indexing terms which are Unclassified, the classification of each should be indicated as with the title).

Fracture, Elastic-Plastic, Stretch Zone, Rate Effects

UNCLASSIFIED
SECURITY CLASSIFICATION OF FORM

#152127

NO. OF COPIES NOMBRE DE COPIES	COPY NO. COPIE N°	INFORMATION SCIENTIST'S INITIALS INITIALES DE L'AGENT D'INFORMATION SCIENTIFIQUE
AQUISITION ROUTE FOURNI PAR		TC
DATE		09 Jun 75
DSIS ACCESSION NO. NUMÉRO DSIS		


 National Defence Défense nationale

PLEASE RETURN THIS DOCUMENT TO THE FOLLOWING ADDRESS:
 DIRECTOR
 SCIENTIFIC INFORMATION SERVICES
 NATIONAL DEFENCE
 HEADQUARTERS
 OTTAWA, ONT. - CANADA K1A 0K2

PRIÈRE DE RETOURNER CE DOCUMENT À L'ADRESSE SUIVANTE:
 DIRECTEUR
 SERVICES D'INFORMATION SCIENTIFIQUES
 QUARTIER GÉNÉRAL
 DE LA DÉFENSE NATIONALE
 OTTAWA, ONT. - CANADA K1A 0K2

DND 1153 (8-87)